論　文　主　題　目

Experimental study of solitary wave runup reduction by coastal
lagoon, coral reef and forest

（潟湖、サンゴ礁、海岸林による孤立波の遡上高減少量に関する実験的研究）

２０２１年３月

埼玉大学大学院理工学研究科（博士後期課程）

理工学専攻（主指導教員　田中　規夫）

Talpe Liyanage Chanaka Vinodh

EXPERIMENTAL STUDY OF SOLITARY WAVE RUNUP REDUCTION BY COASTAL LAGOON, CORAL REEF AND FOREST

by

Talpe Liyanage Chanaka Vinodh

A Dissertation

Submitted to the Department of Civil and Environmental Engineering

In partial fulfilment of the requirements for the degree of

Doctor of Philosophy in Civil Engineering

Hydraulic & Environmental Engineering Laboratory

Graduate School of Science and Engineering

Saitama University

Main supervisor: Professor Norio Tanaka

Co-supervisors: Associate Professor Junji Yagisawa

Professor Takeshi Fujino

Professor Ken Kawamoto

2021

To My Parents, Wife and Son

Declaration

The candidate confirms that the dissertation submitted is his own. The proper credit has been given where reference has been made to the others work.

Some parts of the work presented in this thesis have been published in the following articles:

Vinodh, T.L.C., Tanaka, N., 2018, Experimental study on the energy reduction of a solitary wave using a sand dune-coastal lagoon system, Journal of JSCE, Ser. B1 (Hydraulic Engineering), 74, 5, I_1231-I_1236. https://doi.org/10.2208/jscejhe.74.5_I_1231

Vinodh, T.L.C., Tanaka, N., 2018, Experimental study on the energy reduction of a solitary wave using a sand dune-coastal lagoon system, Proceedings of 12th International Conference on ISE, Tokyo, Japan

Vinodh, T.L.C., Tanaka, N., 2018, Experimental study on the energy reduction of a solitary wave using a sand dune-coastal lagoon system, Proceedings of 9th International Conference on ICSBE, 466, 111- 119

Vinodh, T.L.C., Tanaka, N., Takemura, T., 2019, Experimental study of runup reduction of solitary wave by emergent rigid vegetation on a slope, Journal of JSCE, Ser. B1 (Hydraulic Engineering), 75, 2, I_703-I_708. https://doi.org/10.2208/jscejhe.75.2_I_703

Vinodh, T. L. C., Tanaka, N., 2019, Review of existing coastal defence system in Sri Lanka against tsunami, Proceedings of the special session on Coastal and Lagoon Environment, 7th ACEPS2019, 84-91, 17th October 2019, Galle, Sri Lanka.

Vinodh, T.L.C., Tanaka, N., 2020, A unified runup formula for solitary waves on a plane beach. Ocean Engineering. 216, 108038. https://doi.org/10.1016/j.oceaneng.2020.108038

Acknowledgements

Abstract

EXPERIMENTAL STUDY OF SOLITARY WAVE RUNUP REDUCTION BY COASTAL LAGOON, CORAL REEF AND FOREST

The 2004 Indian Ocean Tsunami and the 2011 Great East Japan Tsunami emphasise the importance of Ecosystem-based Disaster Risk Reduction (Eco-DRR) to minimise the incredibly challenging impact of future tsunamis, to protect the living community, environment, and infrastructure.

As a preliminary study, a statistical and geospatial analysis was conducted for coastal lagoons in Sri Lanka that affected by tsunami using collected field surveying data, statistical data, DEM data and land use GIS data. The spatial variability of the settlement, forest and lagoon mouth was discussed. Influence by existing coast protective structures, drainage structures and the connection to the sea was investigated. The physical dimensions such as beach slope, dune height, barrier length, lagoon length in cross-shore and longshore direction and the area were investigated and how such parameters affect the damage ratio was illustrated.

Based on the statistical and geospatial analysis, it was found that the building located close to the lagoon mouth and on barrier land were found to be extremely vulnerable to tsunami wave. The presence of a narrow channel connecting to a lagoon observed high tsunami damage ratio. The lagoons with the closed mouth also exhibited more severe damage in the east part of Sri Lanka. The location of the forest does not make much difference in tsunami damage, but the dense mangrove could reduce the damage, whereas patchy, scattered and swamps did not reduce the tsunami damage. Existence of coast protective structures and the drainage structures did not exhibit an effect on impact to tsunami damage. The offshore bathymetry (i.e., fringing reef or reef lagoon) did not influence on tsunami damage ratios. When the length of barrier length in opening direction was less than 650 m, cause extensive damage, and the effectiveness of lagoon could not be observed. When the summation of lagoon length and barrier length reached beyond 750 m the damage in the upstream of the lagoon was minimised which implies that the distance to the coast is a major governing factor in evaluating damage ratio. The beach slope, barrier height and area of a lagoon is found to be less influence on the damage ratio.

Limitations of the statistical and geospatial analysis were presented. Hence the laboratory experiments were conducted at Saitama University to understand how a tsunami-like solitary wave vertical runup can be reduced in one horizontal dimension against the effects of the beach slope, dune height, depth and length of the lagoon in the cross-shore direction and also with and without forest. The rigid emergent circular cylinders in a staggered arrangement were used as the forest model for all wave conditions. The maximum runup of a compound slope was measured to investigate the influence of onshore slope and offshore slope. Besides, the solitary wave runup on coral reef system has been tested. The bathymetry of reef profile was tested as reef-flat, reef-lagoon and reef-crest. The rectangular strips at regular intervals representing the roughness of a more simplified coral reef system, along the cross-shore direction were tested for the case of reef-flat with roughness.

The solitary wave runup on a plane beach having the slopes of 1/4, 1/7 and 1/10 were tested. The compound slopes consist of 1/7 and 1/10 as the foreshore slopes and 1/4 as the onshore slopes were tested. The forest model on a sloping beach having slopes of 1/4 and 1/7 were investigated. The maximum runup of a lagoon by changing the foreshore slopes as 1/1, 1/2, 1/4, 1/7 and 1/10, dune height and lagoon inside depths, was measured. Also, the forest model was placed on a sand dune by changing the position (front, middle and back of sand dune) and investigated. A coral reef platform consists of the fore-reef slope of 1/7 and landward slope of 1/4 were tested.

The plunging breaking, surging breaking and nonbreaking type of waves were observed on the beach slope and the fore reef slope. The undulations with no breaking and leading wave breaking and turbulent bores were observed inside lagoon with the change of wave transmission height to lagoon water depth ratios. The multiple wave reflection and backwater rise could be observed with the introduction of forest model. The progressive and growing, progressive and dissipative, and resonant waves could be observed in coral reef platforms. The turbulent bores and spilling breaking on the reef flat, surging breaking (bore type) on the landward slope and nonbreaking waves were observed.

The resultant wave transmission height and maximum runup were measured varying incident wave characteristics as well as the dimensional physical properties of each model.

The wave height to depth ratio from 0.1 to 0.4 was used. The breaking criterion was discussed. The dimensional analysis was employed to pick up essential parameters for comparing the maximum runup effect. The present laboratory data and the previous researchers' work were also employed in the study. Hence the results of maximum runup were used in conjunction with previous research works to derive empirical formulas for solitary wave runup on a plane beach, forest on a sloping beach, sand dune coastal lagoon, reef flat and reef lagoon, individually.

The maximum runup found to be most sensitive to the bathymetry profile change and the location of wave breaking and then to the wave formation inside of the sand dune coastal lagoon or reef platform. At the near-breaking condition, the highest runup was observed. The runup effect corresponded to change of physical dimension was discussed in detail. In the case of the coral reef system, the length of reef-flat was found to be a dominant factor when it equals the one-fourth of the incident wavelength of a solitary gives the highest runup. The incident wave height to reef water depth ratio also found to be a determining parameter for estimating runup as it describes the breaking limit.

The forest on a sloping beach effectively reduces solitary wave runup from 4% to 28%. The higher runup reduction occurred on mild slopes with highly nonlinear waves. By increasing the forest width by twice, the runup reduction can be further increased from 6% to 27%. The runup on a sand dune coastal lagoon with a forest of finite width is reduced effectively by 17% to 45% depending on the slope parameter of front beach slope which is associated with the breaking phenomenon. At near-breaking condition, the effectiveness of coastal trees is found to be comparatively less. However, by introducing a larger forest width, the runup can be further reduced by 55% to 81%. The runup reduction by reef crest as compared to the reef flat was observed up to 31% and higher runup reduction was seen in shallow depths. In reef flat with dense roughness ('d' type) and shallow depths, runup was reduced up to 66%. In deep reef water depths, there was no reduction could be observed, and some cases runup with reef crest and reef flat with dense roughness was higher than in the case of the reef flat due to the resonance factor. For immediate roughness case ('k' type), the runup reduction was recorded between 3% to 81%. The highest runup reduction was observed in shallow water depths. However, the difference in the runup reduction by changing the ratio of spacing to roughness height (pitch ratio) among

intermediate roughness ('k' type) cases was not significant. The effect of runup reduction by the roughness of coral reef roughness was found to be less significant than the forest of finite width. The maximum runup on a reef lagoon was 5% to 59% higher than the reef flat case except for weakly nonlinear waves on deep water.

Thus, a coastal lagoon having larger dune and more considerable length in the cross-shore distance with a forest width helps to increase more resilience against tsunami attack even when energy reduction at the beach slope is not sufficient enough. A coral reef platform with wide width, shallow reef water depth and intermediate roughness can be considered as useful in tsunami energy dissipation but found to be not so effective compare to the sand dune coastal lagoon with coastal forest.

The most critical parameters which can be used to evaluate tsunami damage is highlighted in this study to design coastal landscapes based on Eco-DRR concept.

Keywords: solitary wave, runup, wave breaking, coastal lagoon, coral reef, forest

Contents

List of Figures

List of Tables

Nomenclature

In this thesis, all quantities are in SI-units, unless stated otherwise

Roman symbols

A	frontal area of vegetation
a_o	the length scale which is the half-excursion-length for a water particle
a,b	empirical parameters depend on beach slope, breaking condition and frictional effects
c	wave celerity
C_D	drag coefficient
C_I	an empirical coefficient for index I ($I = 1,2,3,..$)
C_R	agreement index (Willmott, 1981)
D	diameter of a cylinder
d_b	depth at wave breaking point
g	gravity acceleration
GX	wave gauge X (X=1,2,3,4)
H	Initial wave height
h	water depth
H_b	wave height at breaking point
H_{bst}	wave height at the toe of beach slope
H_{cr}	wave height at the reef ridge
h_D	sand dune height
h_L	initial lagoon inside depth
h_r	initial reef water depth
H_o	Initial wave height
h_o	initial water depth in the constant depth region
H_T	transmitted wave height

K	empirical coefficient (Chapter 3)
K	height of roughness element
k	wavenumber
KC	Keulegan Carpenter number
L	initial wavelength
l	tree height
L_b	length of the beach
L_L	length of the lagoon
L_o	initial wavelength
L_r	cross-shore distance of reef-flat
M_F	maximum momentum flux parameter (Hughes, 2004)
M_S	empirical coefficients (Hughes, 2004)
N	number of observations
N_S	empirical coefficients (Hughes, 2004)
R	maximum runup
R^2	Pearson coefficient of correlation
Re	Reynolds number
Re_{cr}	critical Reynolds number of transition to turbulence in the boundary layer of solitary wave (Sumer et al., 2010)
Re_o	solitary wave Reynolds number (Sumer et al., 2010)
Re_t	stem Reynolds number
R_{up}	maximum runup as per Madsen and Schaffer (2010)
R_{up}^{limit}	maximum runup limit as per Madsen and Schaffer (2010)
S	total stroke length
s	beach slope
s_1	foreshore slope

s_2	onshore slope/landside slope
S_o	surf-similarity parameter refer to Grilli et al. (1997)
t	time
T	wave period
T	entire time of the movement of the paddle in solitary wave generation
U_o	maximum orbital velocity in open water
VX	video camera X(X=1,2,3)
w	spacing of rectangular strips
W	width of forest
x	horizontal coordinate
X_o	near the toe of the beach slope
X_T	toe of the rearmost slope

Greek symbols

α	angle of back slope of the lagoon
β	angle of sloping beach in degrees
δ	coefficient used to express runup relationship
η	free surface displacement of a solitary wave
ξ	surf-similarity parameter
ξ_{ir}	Irribaren number (Battjes, 1974)
ξ_{KK}	surf-similarity parameter (Kobayashi and Karjadi, 1994)
ξ_{Lo}	surf-similarity parameter (Lo et al., 2013)
ξ_{MS}	surf-similarity parameter (Madsen and Schaffer, 2010)
ξ_s	surf-similarity parameter (Synolakis, 1987, Lo et al., 2013)
π	3.142
ρ	density of water

σ dimensional number concerning frequency (Kajiura, 1984)

v kinematic viscosity of water

χ_{break} parameter refers Madsen and Schaffer (2010)

χ_{elev} parameter refers Madsen and Schaffer (2010)

Ω angular frequency

ϕ the proportion of volume occupied by the solid canopy

Other symbols

ΔS spacing between cylinders

Abbreviations

1HD   one horizontal dimension

BP   breaking point

BS   breaking at final slope

BT   geometric form of breaking at beach slope

CO   convex slope

ComDam   completely damaged houses

DCS   Department of Census and Statistics

DTotalT   total number of damages

Eco-DRR   Ecosystem-based Disaster Risk Reduction

FR   breaking at fore reef slope

GEBCO   General bathymetric Chart of the Oceans

GEJT   Great East Japan tsunami

GIS   Geographic Information System

GN   Grama Niladhari

GPS   Global Positioning System

IOT   Indian Ocean Tsunami

LES	Large-eddy simulation
LG	breaking at lagoon inside
LLg-OD	lagoon length in opening direction
LLn-OD	barrier length in opening direction
MAE	mean absolute error
N/A	not applicable
NOAA	National Oceanic and Atmospheric Administration
ParDamU	Partially damaged but usable houses
ParDamUn	Partially damaged and unusable houses
PL	plunging breaking
RANS	Reynolds averaged Navier-Stokes equation
RC	reef-crest
RF	reef-flat
RFRw/K	reef-flat with roughness w/K
RL	reef-lagoon
RMSE	root-mean-square error
RT	breaking at reef crest
SCI	scatter index
SRTM	Shuttle Radar Topography Mission
SU	surging breaking
TR	trapezoidal shape
WLg-CD	Width of lagoon in longshore direction/perpendicular to opening direction

Chapter 1

Introduction

Part of this chapter has been published as:

1.1 Background

The 2004 Indian Ocean Tsunami (IOT) has brought to the attention of the issue of coastal frontline protection in Sri Lanka (Pomonis et al., 2006; Vinodh and Tanaka, 2019). Conventional coastal engineering, such as sea walls, breakwaters and embankments, is widely recognised as the ultimate solution to tsunami risks. However, the structures including breakwaters, sea walls and tidewater control forests were not designed for the massive tsunami like the 2011 Great East Japan Tsunami (GEJT) resulting many were destroyed and could not mitigate the tsunami as expected (Raby et al., 2015; Suppasri et al., 2013). The hard structural defences are seriously questioned in many locations as their repetitive and costly maintenance, as well as their reinforcing and widening to keep up with the increasing tsunami risk, are becoming unsustainable (Temmerman et al., 2013). Although often effective in lowering tsunami damage, these costly hard structural solutions have some significant shortcomings, including negative habitat changes (Martin et al., 2005) and degraded beaches and increased downdrift erosion (Basco, 2006).

Ecosystem-based Disaster Risk Reduction (Eco-DRR) is so vital and becoming a more widespread trend as it is sustainable, conservation and restoration of ecosystems to reduce disaster risk, to achieve sustainable and resilient development (Renaud et al., 2013). The schematic figure of the concept of Eco-DRR is shown in Fig. 1-1. In contrast to conventional engineering solutions such as sea walls or embankments, Eco-DRR provides numerous benefits for humankind regardless of a disaster event. Eco-DRR involves comparatively low-cost construction and maintenance where ecosystems are healthful and adequately managed. In this regard, Eco-DRR is a cost-effective and no disappointment in investing (Barbier, 2016).

1
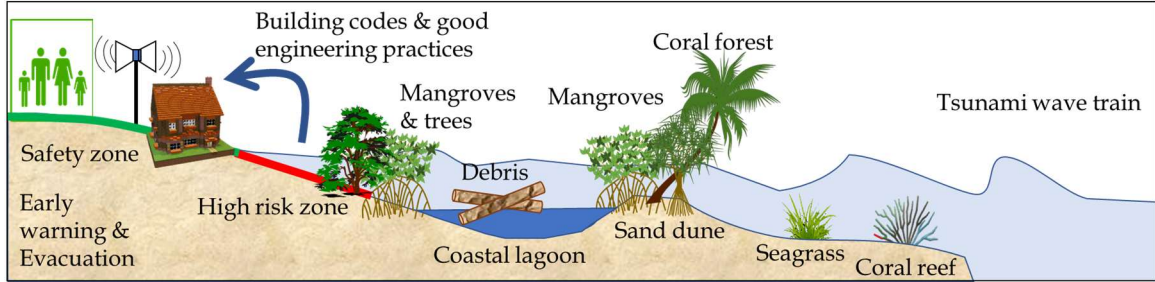
Figure 1-1 Ecosystem-based disaster risk reduction (Modified after Vinodh and Tanaka, 2019).

The protective role of coastal forests and mangroves in the tsunami mitigation unexpectedly became a questioned topic in the aftermath of the 2004 IOT. It could be observed that nearby the lagoon the tsunami impact was low during the post-tsunami field surveys of 2004 IOT (Dahdouh-Guebas et al., 2005a) and 2015 Chile Tsunami (Contreras-López et al., 2016), and behind the dune (Mascarenhas and Jayakumar, 2008; Tanaka et al., 2007). Gedan et al. (2011) explained that the evidence that coastal lagoons can mitigate tsunami impacts is more questionable because, due to the sudden and catastrophic nature of tsunami events, the testimony tends to be unreliable. Kerr and Baird (2007) showed that the significance of coastal vegetation in mitigating tsunami remains an open-ended question because of the lack of proper studies, and more data and more potent approaches may well find a link.

It is essential to recognise that ecosystems also have limits in protecting against hazards (Alongi, 2008; Cochard et al., 2008; Shuto, 1987; Tanaka, 2009). Chatenoux and Peduzzi (2007) suggested that the potential protective role of vegetation was determined by its spatial arrangement and should be considered as an essential consideration. Many projects around the world were invested in an ecosystem without any systematic and scientific collection of evidence on the role of vegetation and coral reef in protecting populations against the tsunami waves, ended with disappointing results (Cochard, 2011). Besides the loss of human victims and properties, severe beach erosion, coastal water bodies filled with debris and driftwood, and destroyed agricultural lands were some of the aftershock environmental consequence. Thorough knowledge of wave phenomena

occurred nearby coastal ecosystems is essential in effective coastal landscape planning by considering the scarcity of resources (Tanaka et al., 2011).

Hybrid defence system which consists of structural solutions like embankments, moats and natural solutions like forests have been studied in mitigating tsunami impact (Igarashi and Tanaka, 2018; Kimiwada et al., 2020; Zaha et al., 2019).

The developing countries like Sri Lanka consist of lagoons, sand dunes, coral reefs and mangroves at the oceanfront and hardly seen any hard structural solutions to cater to the tsunami mitigation problem primarily. The application of new hard structural solutions for Sri Lanka seems complicated due to allocating enough budgets for their high capital cost and the technology incurred. Hence Eco-DRR concept can be recommended to adapt for tsunami mitigation with other precautionary measures like an early warning and evacuation strategies (Vinodh and Tanaka, 2019). Investing in ecosystems cannot be viewed as a single solution to risk reduction. Ecosystem-based precautions could be part of a broader disaster risk management strategy, and it would always be paired to other essential risk management measures, such as early warning systems and evacuation plans (Dengler and Preuss, 2003). Eco-DRR, like all disaster risk reduction activities, diminishes the risk but does not remove the risk comprehensively.

When a tsunami wave reaches the coast, the bathymetry influence tsunami behaviour and shoaling, reflection and combined refraction and diffraction could cause both converging and diverging of tsunami energy. Due to the shoaling effect, the tsunami wave height can be increased up to several meters. During all the tsunami cases, the detailed shape of the incoming tsunami wave remains unknown. Tsunami characteristics (i.e., wave height and wavelength or wave period) are either pre-computed using different hydrodynamic models or estimated from the captured satellite images or detected wave measurements by DART buoys. Due to the time-consuming nature of tsunami simulation, timely processing is unfeasible if calculation is started after an earthquake occurs. Tsunami runups based on empirical models, numerical models and analytical models, therefore, need to be used to analyse in advance with a variety of earthquake scenarios, locations, and magnitudes to determine arrival times and wave heights for particular coastal areas. Based on the past field surveys (Pomonis et al., 2006), satellite images analysis (Hayashi, 2008),

tide gauge measurements in the ocean (Rabinovich and Thomson, 2007) and seismic inversion models (Ammon et al., 2005), the tsunami wave propagation characteristics and tsunami heights have been studied for tsunamis in the past. Nevertheless, the features of the tsunami wave nearshore were found to be challenging to forecast because it is being affected by the bathymetry, coastal topography, large roughness effect caused by vegetation and buildings, amount of entrained debris and density of habitation in its path.

The most challenging phase of the dynamics of tsunami flows to deal with breaking as they close to the shore. This stage depends significantly on the bottom bathymetry and the coastal topography. At the transition of breaking severe damages may occur. Then the tsunami inundation is progressed slowly and can last for several minutes, causing structural damages. The path of these currents and their velocity is quite unpredictable in the final stages as they are changed with abrupt changes in the topography, the collapse of buildings, and accumulation of driftwoods.

The hydrostatic forces like lateral fluid pressure, vertical buoyancy effects; hydrodynamic forces like bore impact, drag force, impact from large water-borne objects (e.g., vehicles, driftwoods, building fragments), increase in flow viscosity/density due to accumulated debris and sediment, damming, foundation effects like scouring, overturning and sliding, can be identified as the primary cause of failure modes (Applied Technology Council and Federal Emergency Management Agency (FEMA), 2012; Shuto, 2019). However, it is difficult to predict or conduct real-time simulations as the tsunami may form in different scale and shapes, and the phenomena are complicated. Under these circumstances, as an approximation to the reality and initial estimate, it will be still useful to conduct physical modelling tests to identify the basic knowledge of maximum runup.

The runup is defined as the maximum elevation attained by seawater (on/along the beach) above the still water level, and as such defines the extent of wave action. The estimation of solitary wave runup on plane beaches has been studied in the study of tsunamis generated by rockfalls, landslides, snow and ice avalanches, caving of glaciers and earthquakes (Fuchs and Hager, 2015; Li and Raichlen, 2001; Synolakis, 1987). Solitary wave runup solutions are useful for experimental investigations and calibration of runup modules in numerical models. Despite being widely used to represent tsunamis, Madsen et

al. (2008) showed that both the length and time scales of an actual tsunami could not be tied with solitary waves. Larsen and Fuhrman (2019) demonstrated that undular bores with several shorter waves developed at the front of the tsunami did not influence the overall runup of the tsunamis. Therefore, they concluded that solitary wave runup solutions could not be used to evaluate the tsunami impact. Although solitary waves cannot be viewed as representative of tsunamis, the research performed is still valid for the physics of solitary waves, and the methods developed have also, to some degree, been used as an inspiration in more recent tsunami research. Furthermore, solitary waves can also be beneficial in terms of model validation.

1.2 Objective of the thesis

During 2004 IOT, Sri Lanka was vastly affected, resulting in many victims and structural damages. This research is mainly focused on Sri Lanka and the experience related to tsunamis by Japan and other countries.

This research aims to study how a tsunami-like solitary wave transformation occurs based on the physical characteristics of a sand dune coastal lagoon, coral reef and forest in one horizontal dimension (1HD) to identify the optimum mitigation measure on the surrounding area.

1.3 Outline of thesis

The Dissertation analyses the tsunami behaviour in coastal areas. Experimental results are reported in view of solitary wave transmission and the maximum runup on the slope. It improves the understanding of the main variables which affect tsunami runup by using solitary wave transformations. The adverse effects caused by the 2004 IOT and the 2011 GEJT along the coastline motivated the author to study on tsunami mitigation as his future career relies on coastal engineering field. The present thesis consists of 8 chapters. The first chapter gives a brief overview of the tsunami research after the events in 2004 and 2011. The analysis of the bathymetry effect and the different roughness aspects of tsunami propagation and runup is the main study of this thesis. The statistical and geospatial analysis was carried out to evaluate the vulnerability of tsunami-affected lagoons in Sri Lanka, and the findings and the limitations of the study are elaborated in the second chapter. To overcome the limitations from the statistical and geospatial analysis, the laboratory

experiments were conducted for further investigations. Chapter 3 has been published in a journal *Ocean Engineering*, which was based on solitary wave runup on plane beaches. Chapter 4 discusses the runup on compound slopes and the applicability of derived empirical runup equation on solitary wave runup on plane beaches to the case of runup on compound slopes. Chapter 5 illustrates the solitary wave runup behaviour concerning the forest of finite width on a sloping beach. Chapter 6 examines solitary wave runup along sand dune lagoon against the variation of physical dimensions. How solitary wave interact with different roughness and coral reef bathymetry profiles which can be categorised as reef flat, reef lagoon and reef crest are considered in Chapter 7. Finally, conclusions drawn from each chapter are summarised, and future direction has been explained in Chapter 8.

Chapter 2

Vulnerability analysis for coastal lagoons in Sri Lanka

2.1   Introduction

Coastal lagoons can be considered as transitional zones between land and sea, and it is characterised by shallow depths typically detached from the sea by a barrier. It may be connected to the sea by one or more channels which remain open or closed occasionally (Kjerfve, 1994). Coastal lagoons are driven to a significant extent by the high density of hard structures such as buildings, sluice gates and breakwaters and mass exchanged with the surrounding ecosystems. The coastal lagoons have complex morphological variations and highly diverse. The effectiveness of such coastal lagoon in dissipating tsunami energy is debated after 2004 IOT based on past field surveys and laboratory experiments (Dahdouh-Guebas et al., 2005b; Inoue et al., 2007; Vinodh and Tanaka, 2019; Wijetunge, 2006). There are many kinds of research conducted to derive vulnerability functions and fragility curves. The investigations regard to Sri Lanka is discussed here.

Choi et al. (2006) investigated on the measured tsunami runup heights in the region of Indian Ocean, and they derived a lognormal distribution (i.e., density distribution function) confirming the theoretical model based on the randomness character of the coastal topography.

Peiris and Pomonis (2005) derived vulnerability functions for the building damage in relationship with the distance to the coast for the south and west coast of Sri Lanka. They found that the total damage ratio shows a reduction with distance from the coast. Miura et al. (2005) by using high-resolution satellite IKONOS images captured after tsunami event occurred in Batticaloa, have identified the damage distribution near the coastline by visual detection method. Leelawat et al.(2016) carried out a statistical analysis to investigate the influential parameters in tsunami-damaged areas and found that the inundation depth and the structural materials were the significant parameters in the evaluation of tsunami impact to the building. Dias et al. (2009) derived vulnerability curves for completely damaged houses using statistical data based on Divisional Secretariat divisions in Sri Lanka and Monte Carlo simulations to replicate the curves obtained from field observations. They found that the percentage of houses with permanent walling materials has a significant

effect on the vulnerability curves. Rosetto et al. (2007) based on the water level measured during field survey conducted by Pomonis et al. (2006), derived a tsunami intensity scale and emphasised the importance of acceptable engineering practices in the construction sector.

Chatenoux and Peduzzi (2007) conducted a spatial and statistical analysis to investigate the effect of morphological and ecosystem configurations such as mangroves forest, seagrass and coral and found that the inundation influenced by the distance to fault lines as well as inclination and length of the proximal slope. Furthermore, they have found that areas behind seagrass beds were less impacted, whereas areas behind coral reefs were severely affected. Satyanarayana et al. (2017) used ground-truth data and remote sensing analyses and based on the professional judgement; they derived vulnerability index maps for the all-around coastline of Sri Lanka. They found that among the coastal sites, Trincomalee, Yala and Puttalam are less vulnerable and the Kaluvanchikudy to Komari area and Jaffna are vulnerable areas. The reason for the less vulnerable areas was found as sand dunes, and multi-species mangrove and dense vegetation are suggested to tsunami mitigation.

Wijetunge (2009a) found that the measured inundation distance along the south coast of Sri Lanka can be expressed in terms of the ground slope. Wijetunge (2014) conducted a multi-scenario deterministic analysis using four seismic zones capable of generating tsunamis which can affect to the southwest coast of Sri Lanka and found that event similar to 2004 IOT can be considered as the worst-case scenario.

Dahdouh-Guebas et al. (2005b) evaluated the characteristics of the pre-tsunami extent of the first 500 m front mangrove, the extent of mangroves already destroyed before the tsunami, the mangrove status in terms of the presence or absence of cutting activities and of cryptic ecological degradation, tsunami damage to the front mangrove, and tsunami damage to lives and properties behind the mangroves. They classified the coastal lagoons based on a cluster analysis of the 24 mangrove sites in Sri Lanka that they have investigated, signifying the status of the mangroves and the impact of the tsunami. They concluded that the status of mangroves is the crucial factor in disaster risk reduction by a coastal lagoon.

Vinodh and Tanaka (2018a, 2018b, 2018c) conducted laboratory experiments using solitary waves to investigate the runup reduction by a sand dune coastal lagoon and found that a lagoon of a large sand dune, considerable lagoon length in cross-shore direction with a finite forest width can effectively reduce the runup.

Mizoguchi et al. (2018) discussed the importance of categorising coastal lagoons in terms of its potential on Eco-DRR based on the morphological and hydraulic properties in and around lagoons.

The research mentioned above is mainly focused on a limited area and either they are based on building materials or ecosystem configurations and or morphological variations only. However, the concept of Eco-DRR of lagoons is often either not clearly understood or not appropriately applied. As tsunami is in high energetic form and subjected to many morphodynamically changes and combined refraction, diffraction and reflection, a comprehensive study to evaluate major influential parameters is necessary. In this study, the statistical and geospatial analysis is employed to the field data as well as existing data in the literature to identify the main drivers in the tsunami energy dissipation in a coastal lagoon.

2.2 Materials and Methods

A typical coastal lagoon generally consists of complex morphological form, the various spatial distribution of buildings and coastal protective structures in and around lagoon mouth. For simplicity in this study, a coastal lagoon can be classified concerning opening of lagoon mouth (i.e., centre (OpCe), not centre (OpNoCe) and closed (Cl)), the position of forest patch (i.e., front (FoFro) and far (FoFar)), location settlements (i.e., front (BuFro), far (BuFar) and all-around (BuAll)), link to the sea by channel (i.e., connected by channel (Ca) and directly opened to the sea (CaNo) and coastal structures nearby lagoon (i.e., bridge, causeway, groyne, breakwaters and natural condition, etc.), as illustrated in Fig. 2-1. The critical parameters that affect tsunami mitigation can be identified as land/barrier length in opening direction (LLn-OD), length of the lagoon in opening direction (LLg-OD) and width of the lagoon in the longshore direction/perpendicular to opening direction (WLg-CD), as shown in Fig. 2-2.
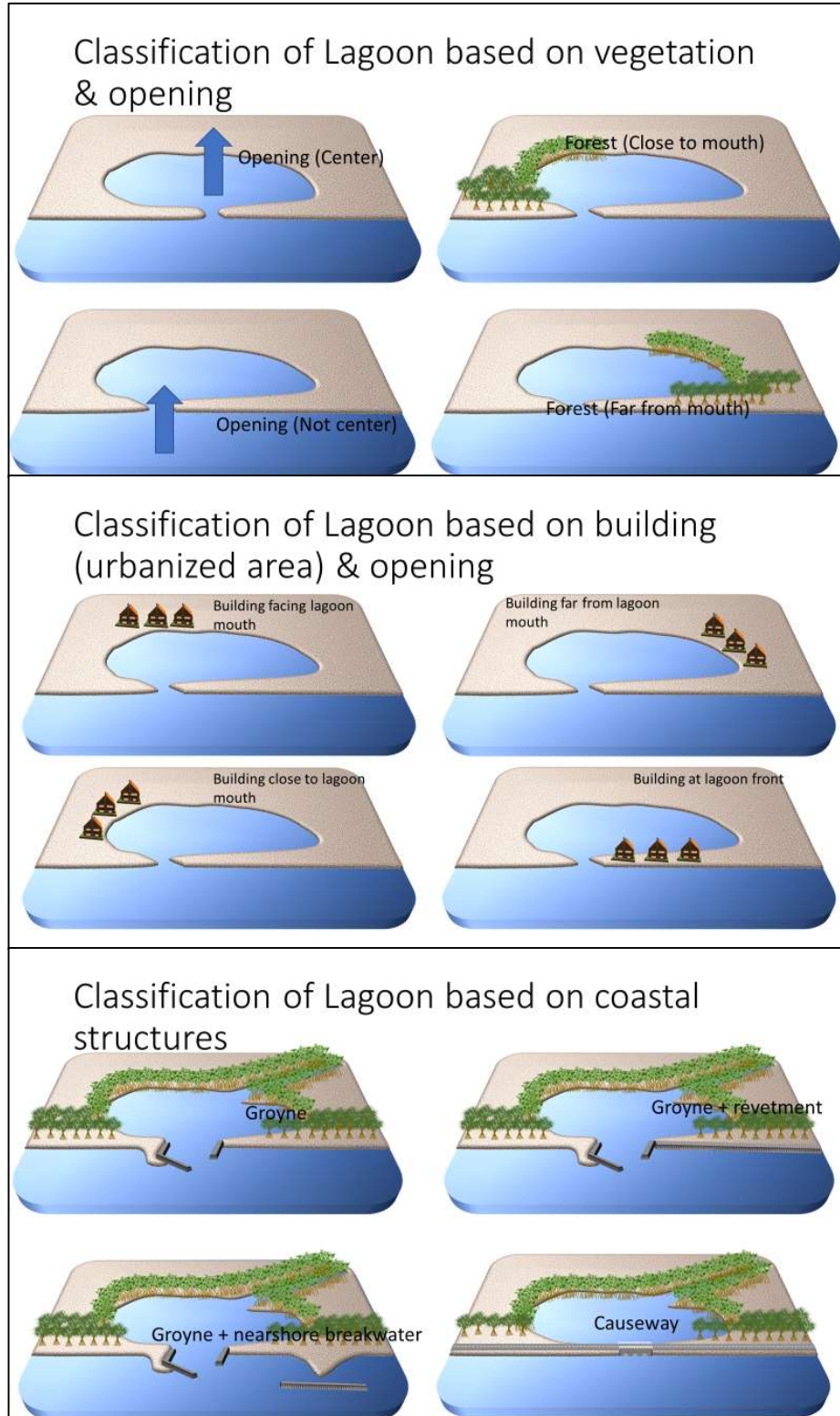
Figure 2-1 Classification of coastal lagoons based on (a) forest and opening, (b) settlement area and (c) coastal structures.
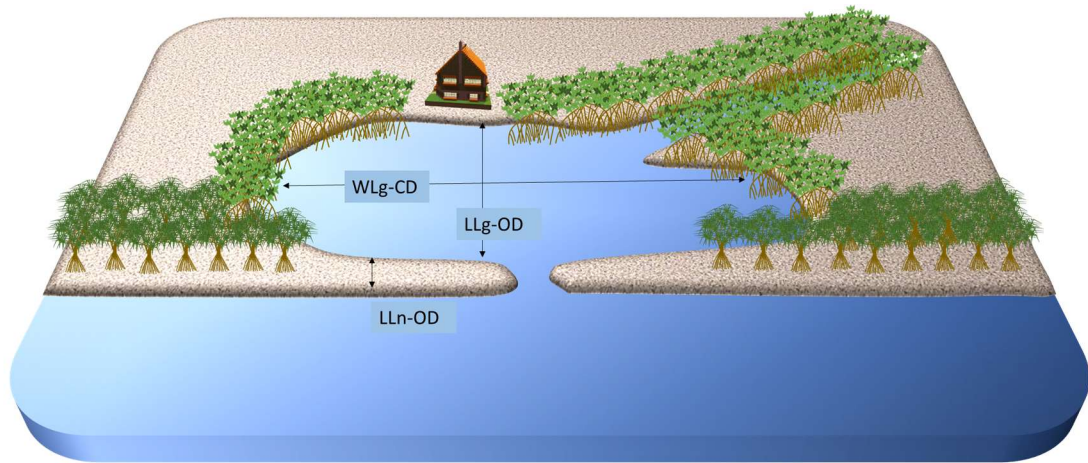
Figure 2-2 Dimensions of coastal lagoons. LLn-OD is land/barrier length in opening direction, LLg-OD is length of the lagoon in opening direction and WLg-CD is width of the lagoon in longshore direction /perpendicular to opening direction.

Besides, physical dimensions of beach slope (Slope), sand dune height (h_D), area of a coastal lagoon (Area) and the condition of the offshore bathymetry (i.e., fringing reef or reef lagoon) were investigated. The classification of mangrove forest can be identified as dense, few, fringe, patchy, scattered and swamps and the data were obtained from Silva et al. (2013).

Field surveying was conducted in lagoons around the tsunami-affected area to obtain the lagoon bathymetry data, to observe the current situation of lagoon opening and the existing drainage structures, the coastal structures nearby them and other relevant data which are supposed to be considered as essential to propose modifications for lagoon surroundings. Bathymetry data were collected using a handheld Global Positioning System (GPS) and a sonar depth meter. Tsunami heights along the coastline during 2004 IOT were obtained from NOAA tsunami historical database. Data on tsunami damaged houses, collected and compiled by the Department of Census and Statistics (DCS), Sri Lanka and Geographic Information System (GIS) data obtained from Surveying Department, Sri Lanka, were used to analyse the vulnerability of Sri Lankan lagoons.

Eighty-seven lagoons (see Figure 2-3) that experienced tsunami inundation were tested. The numbering of the lagoon is as per Table 2-1.

Table 2-1 – Tsunami affected lagoons in Sri Lanka

1. Negombo	44. Kunukala
2. Lunawa	45. Solambe
3. Bolgoda	46. Panakala
4. Katukurunda/Ingrilli Ganga	47. Panama
5. Thalan/Silliya Ganga	48. Arugam
6. Madu Ganga	49. Urani/Potuvil-Ureni
7. Madampa	50. Hidayapuram
8. Telwatte Ganga	51. Paladi/Murugetena
9. Hikkaduwa	52. Komari
10. Rathgama	53. Sangamankanda/Thimbutu
11. Koggala	54. Thirukkovil/Korai complex
12. Garanduwa	55. Periya
13. Dondra	56. Pulputti
14. Mawell	57. Arasady
15. Rekawa	58. Sainthamatuthu
16. Kahandamodara	59. Kalmunai
17. Ranna/Tillawatana	60. Kaluvanchikudy
18. Kunukalliya	61. Batticaola
19. Lunama-Kalametiya	62. Valachchennai
20. Mahasittarakala	63. Nasiwanthieve
21. Hambantota harbor/Karagan Lewaya	64. Pasikuda
	65. Uppar
22. Koholanka Maha Lewaya	66. Lanka Patuna/Ullakkalie
23. Malala Ambilikala	67. Tiruconamalai
24. Bundala	68. Tiruconamalai 2
25. Kirinda Lewaya	69. Tiruconamalai 1
26. Kirinda	70. Mutur/Illakkantai
27. Palatupana Maha Lewaya	71. Thambalagamuwa
28. Gode	72. Uppuveli
29. Yala	73. Irrakkakandi/Sinnakarachchi
30. Butawa	74. Kumburupiddi/Kuchchaveli
31. Gonalabbe	75. Puduwa-kattu
32. Uda Potana	76. Arisimale/Pulmudai
33. Pahal Potana Lewaya	77. Pilmoddai
34. Etheliwela	78. Kokkilai
35. Uda Gajaba Eliya	79. Nayaru
36. Yakkala	80. Vannakukam
37. Kumana/Itikala	81. Nanthikadal
38. Andaraka	82. Vadduvakallu
39. Barura/Bagura	83. Chalai
40. Okanda	84. Chundikulam
41. Tillanwala	85. Thalayadi/Thondamannaru
42. Uvanthai	86. Nithanapuri/Uppu Aru
43. Okandawara/Helawa	87. Palali/Jaffna complex
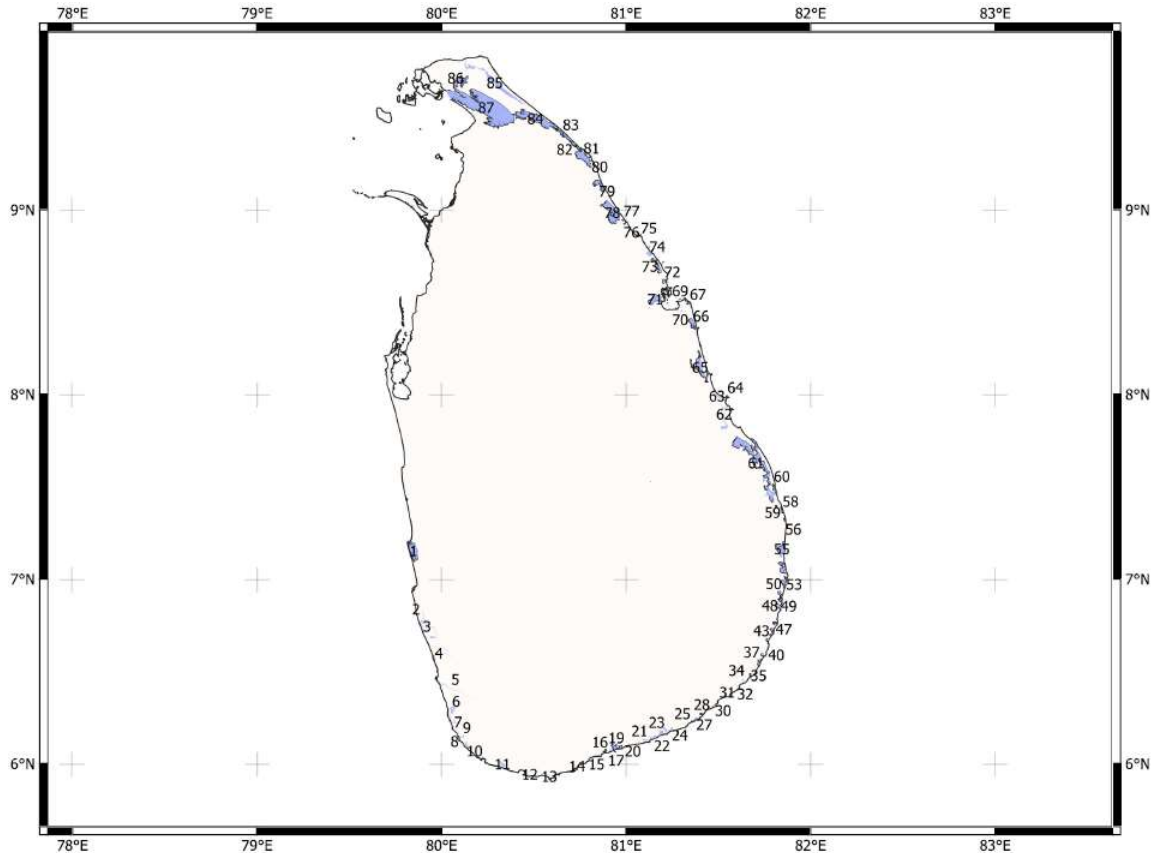
Figure 2-3 Tsunami affected lagoons in Sri Lanka. The numbering refers to Table 2-1.

Some lagoons have many names, and all are mentioned in Table 2-1. It also should be noted that Karagan Lewaya (No. 21) in the list has now been converted to a harbour. Therefore, the pre-tsunami status of the lagoon was considered in the damage analysis. Digital Elevation Model (DEM) data obtained from SRTM (Shuttle Radar Topography Mission) with 30 m resolution for the land in conjunction with GEBCO (General bathymetric Chart of the Oceans) bathymetry data with 500 m resolution for the ocean were also analysed to obtain the beach slope. The barrier height (h_D) was estimated by Google Earth image analysis. The dimensions of the coastal lagoons (i.e., LLn-OD, LLg-OD and WLg-CD) were found by both GIS data and Google Earth image analysis. Identification of land use pattern was extracted from the GIS data obtained from the Surveying Department. The land-use GIS data and the damaged house data were compiled in QGIS software to analyse geospatially for the vulnerability analysis of the coastal lagoons.

The study focused on completely damaged (ComDam), partial damaged which were usable (ParDamU) and unusable (ParDamUn) in Sri Lanka for the vulnerability analysis. The damage ratio was calculated from the collected data from DCS for Grama Niladhari (GN) division which is the smallest administrative division, and the data covered all tsunami-affected area in Sri Lanka. The damaged location along the cross-shore direction was not identified in DCS data. Hence, the damage ratio was defined in this study as completely damaged houses over a summation of all damaged housing units. The damaged data for a lagoon was obtained from summing up all the damaged data in GN divisions which were close to the lagoon. The extent of all damaged housing units implies the extent of the dangerous zone of a tsunami. On the other hand, the number of total damaged houses indicate the severity of the incoming tsunami. Hence the damage ratio calculated as above provides a good indicator of vulnerability. The categorised data were plotted in graphs for each parameter mentioned above.

2.3 Results and Discussion

The overview of field data collection in the present study can be seen as in Fig. 2-4. During the bathymetry survey conducted in both Rekawa lagoon (No.15) and Malala Ambilikala lagoon (No.23), it was found that the lagoon inside depth varied between 1 m to 3 m. Near to the lagoon mouth, the depths were gradually becoming more in-depth and then suddenly become shallower due to natural closure by accumulated sand that transported from the sea. In SRTM DEM data, the depth of water bodies was not captured perfectly and found that it was difficult to obtain. Since the variation of the lagoon inside depths was found minor in Sri Lanka and they are shallow, the effect of the lagoon inside depth was not taken into the present study. The land use pattern and the damaged ratio were analysed for all the lagoons. A typical sample of the analysis done for Rekawa lagoon (No. 15) is shown in Fig. 2-5. The lagoons of number 17, 20, 23, 24, 26 to 46, 50, 52, 56 to 61, 63, 64, 67 to 71 and 75 were found as undamaged area. Aforementioned lagoons are situated in either with low settlement area or located in the forest reserve area. The lagoons from 76 to 87 which are in the Northern province of Sri Lanka were found to be difficult to compare as the data obtained from DCS were missing in some GN divisions.
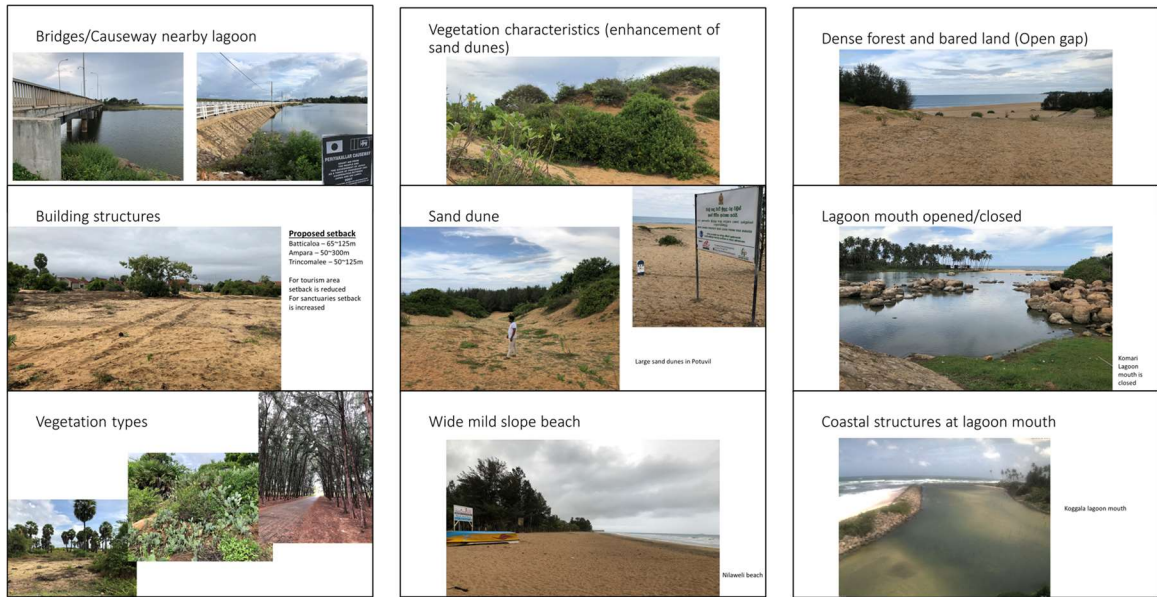
Figure 2-4 Identified features of the coastal lagoons during the field survey.
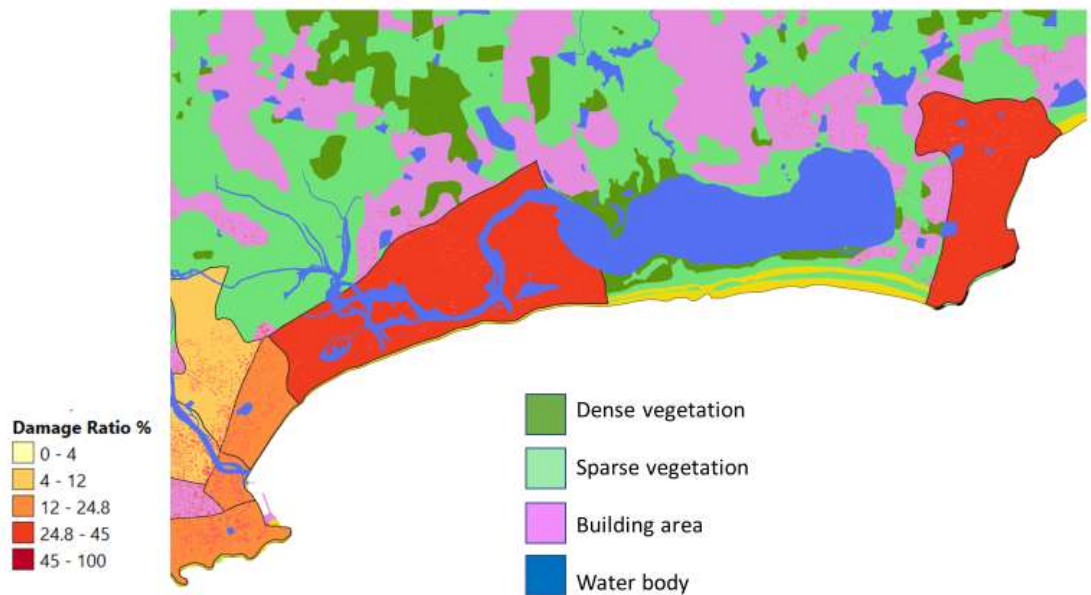
Figure 2-5 Damage ratio and the land use pattern in Rekawa lagoon (No.15).

2.3.1   Effect of settlement area in the lagoons from West to South

In this section, the effect of opening, the location of settlement area and forest area, links to the coast and the existence of structures is explained for the lagoons from Negombo lagoon (No. 1) to Dondra lagoon (No. 13). The results of the damage ratio were plotted in

the aspect of building location and the condition of lagoon mouth in Fig. 2-6. The definition of the symbols is as per Section 2.2.

It can be seen that building located at the front are subjected to higher damage ratio than in the case of the building area located at far from lagoon mouth. The buildings in the barrier land face the direct impact of the tsunami wave, and it can be expected severe damage in the frontline of building area. Even the damage ratio indicates the severity of the incoming tsunami; there are some instances, such as a zone with a smaller number of buildings, the defined damage ratio may become ineffective. The houses in low settlement area may become vulnerable to be destroyed entirely for comparatively less energetic tsunami waves than in the case of dense settlement. Better detail regarding damaged houses along a cross-shore direction by either satellite image analysis of captured image after the event of tsunami occurred, or post field surveying may provide better confident results.

The opening condition of the lagoon mouth does not show much effect in reducing tsunami damage. This may be that in the west and south coast are generally subjected to river flood and in need of mouth to be opened when a flood occurred. Therefore, the sand accumulation at the lagoon mouth is restricted, and as a result, the difference between a closed mouth and opened mouth is harshly identifiable as an obstruction to the inflow of tsunami.
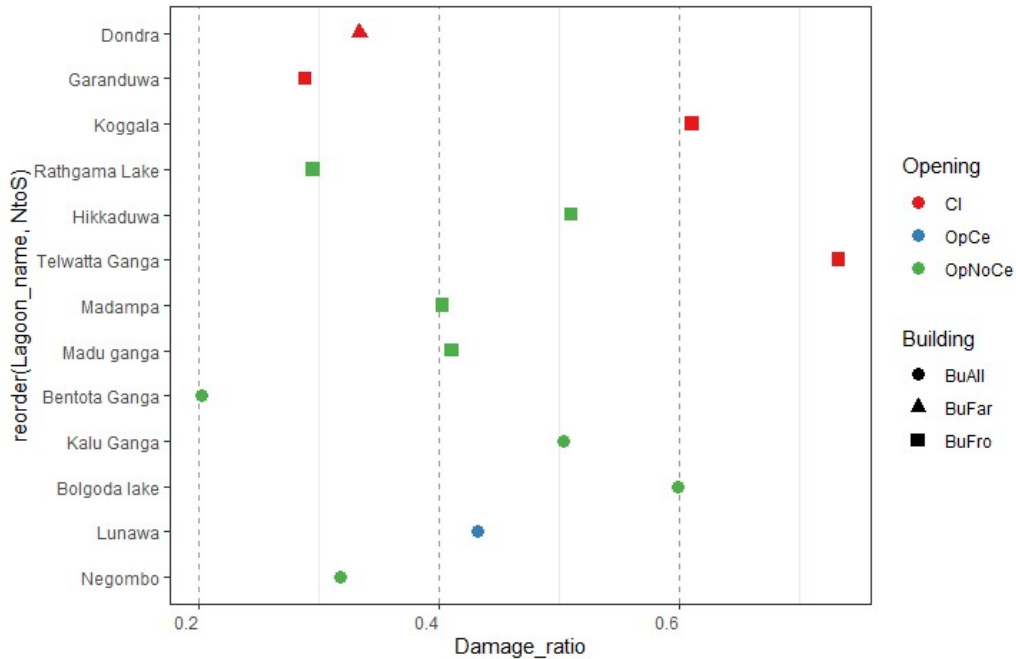
Figure 2-6 The effect of the condition of lagoon mouth and the settlement area. The colours indicate the opening condition and the shapes indicate the location of the building area. The definition of symbols is referred to as Section 2.2. Lagoon names are in order from North to South.

Figure 2-7 shows the effect of the link to the lagoon from the sea. The data were appeared as scattered and could not be separated into distinct zones. Nevertheless, based on the majority of plots lying in the graph, it can be found that the lagoons that have a link to the sea by channel cause greater damage than the lagoons that are directly open to the sea. When there is a narrow channel, it causes a funnelling effect which enables a tsunami inflow to converge energy and produce severe damage near the lagoon mouth. The lagoons that are directly opened to the sea managed to absorb the tsunami energy causing less energy transfer to the adjacent area.
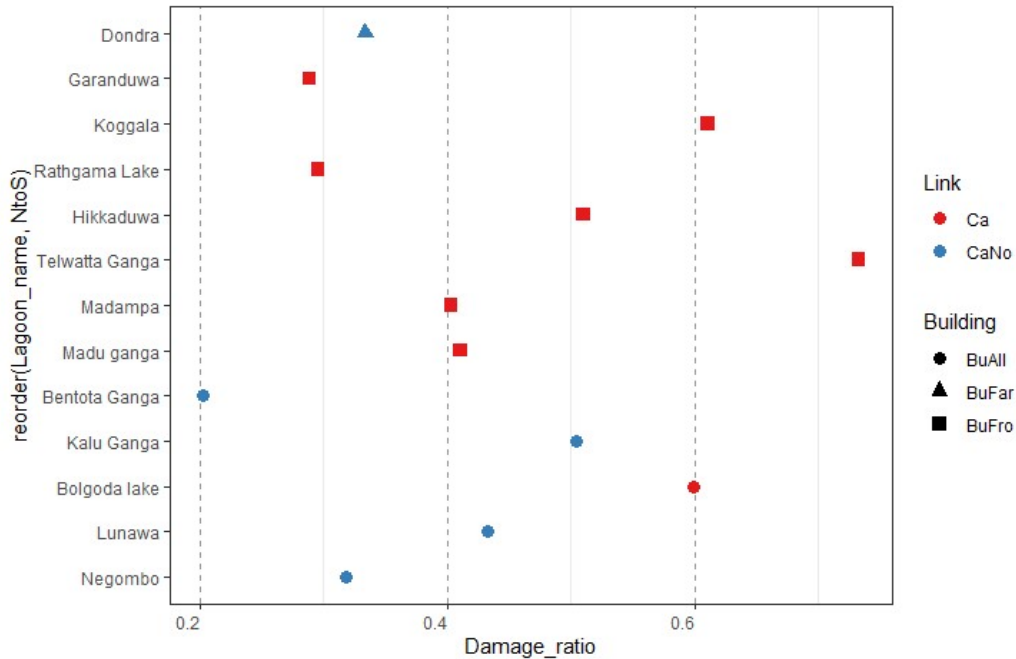
Figure 2-7 The effect of the condition of link to the lagoon from the sea and the settlement area. The colours indicate the link type and the shapes indicate the location of the building area. The definition of symbols is referred to as Section 2.2. Lagoon names are in order from North to South.

The effect of the forest area in a lagoon in tsunami mitigation can be found from the Fig. 2-8. There is no clear evidence of the damage reduction by the existence of coastal forest in a lagoon. This may be due to the west and south part of Sri Lanka is urbanised and hardly found a coastal forest belt that may cause a significant impact in tsunami energy dissipation. Mostly, the coastal trees and mangroves can be found as either patchy, or they exist in the sheltered area towards further inland. Since the damage ratio used in this study, did not interpret the location of damage along a cross-shore direction, it was hard to find the connection of the mitigation effect by the forest, with the available data.

18
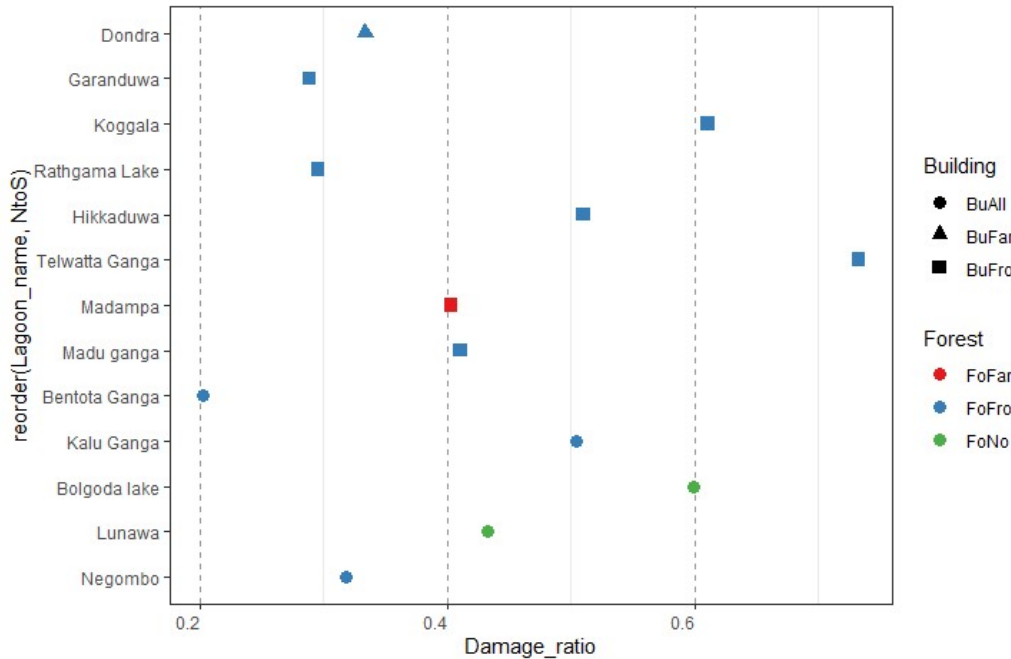
Figure 2-8 The effect of the location of the forest area in a lagoon. The colours indicate the location of the forest and the shapes indicate the location of the building area. The definition of symbols is referred to as Section 2.2. Lagoon names are in order from North to South.

There are no hard structures designed in Sri Lanka to mitigate tsunami energy as in Japan. Instead, they are designed to protect the coastline from erosion, for ports and harbours. The bridges, causeways and sluice gates can be found nearby the lagoon mouths to function the drainage facility. It can be found from Fig. 2-9 that the existence of coastal structure regardless of the structure type, showed higher damage ratios. When there are no hard structures that are naturally operated, the damage ratio is appeared to be less. This implies that the existence of a coastal protective structure nearby a lagoon in west and south part of Sri Lanka does not affect reducing the tsunami damage.

The offshore bathymetry of Sri Lanka in west and south part generally exhibit a fringing reef type. Therefore, the effect of fringing reef and reef lagoon in tsunami mitigation cannot be distinguished in this region, as seen in Fig. 2-10. A better-detailed analysis regarding high-resolution bathymetry incorporating numerical analysis might provide confident results in damage analysis with respect to offshore bathymetry.
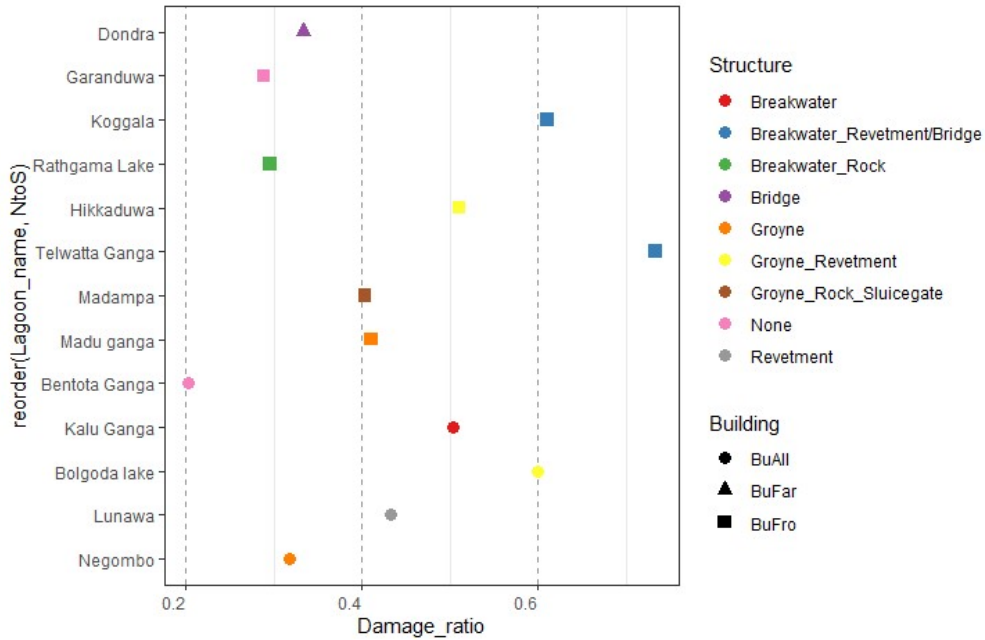
Figure 2-9 The effect of the hard structures in a lagoon. The colours indicate the structure type and the shapes indicate the location of the building area. The definition of symbols is referred to as Section 2.2. Lagoon names are in order from North to South.
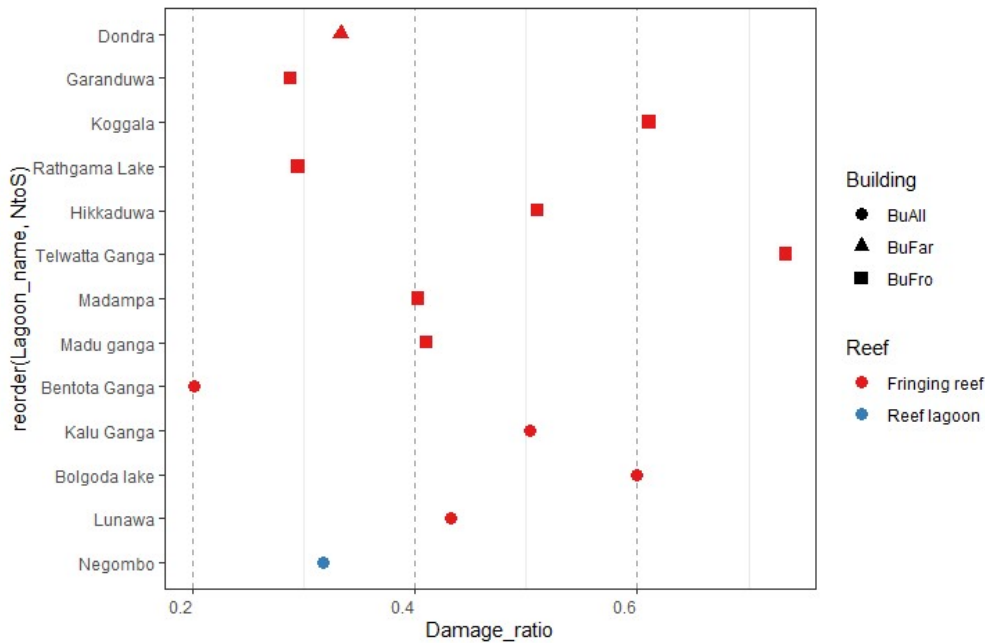
Figure 2-10 The effect of the offshore bathymetry in a lagoon. The colours indicate the reef type (i.e., fringing reef or reef lagoon) and the shapes indicate the location of the building area. The definition of symbols is referred to as Section 2.2. Lagoon names are in order from North to South.

2.3.2   Effect of settlement area in the lagoons from South to East

The effect of opening, the location of settlement area and forest area, link to the coast and the existence of structures is explained for the lagoons from Mawella lagoon (No. 14) to Arisimale lagoon (No. 76). The results of the damage ratio were plotted in the aspect of building location and the condition of lagoon mouth in Fig. 2-11. The definition of the symbols is as per Section 2.2. The results showed that the lagoons which have closed mouth, cause high damage ratio. Most of the lagoons in the south to north via east are found as closed mouth lagoon. This area is in the dry zone, and the expected rain is comparatively lesser than in the west and south part of Sri Lanka. The accumulated sand nearby the lagoon mouth is found to be higher than west and south. Due to the closed mouth, there is a restriction of incoming tsunami energy and the energy absorption capability of a lagoon may reduce. It is hard to distinguish the difference between a lagoon with an opened mouth at the centre and a lagoon with an opened mouth not located at the centre. However, unlike the lagoons in the west and south part, in this region, there is clear evidence of opened lagoon will reduce the damage ratio. The location of the building area did not exhibit a clear trend. Due to the existence of low lying lands in the east part of Sri Lanka, tsunami energy penetrated farther than west and south part (see (Wijetunge, 2009b, 2009a). Therefore, the houses were damaged irrespective of the location in a lagoon. The variation of damage ratio along a cross-section with either inundation depths might provide better analysis and produce confident results.

Almost all the lagoons existed in the south to north via east section, consist of a forest at front. There are lagoons with the forest at front experienced higher damage ratios as seen by Fig. 2-12. Even the coastal forests protected the houses behind them; the energy may convey from open gap among forest causing the damage. In this study, it was found difficult to compare the effectiveness of the forest width in mitigating tsunami impact, as the damage ratio was compared based on GN division as the data were compiled to a particular larger area. The present results provide an overall effect on the damaged area and not specific to a location where forest existed or not. Detail investigations like Miura et al. (2005) may help in damage analysis in relationship with a coastal forest belt.
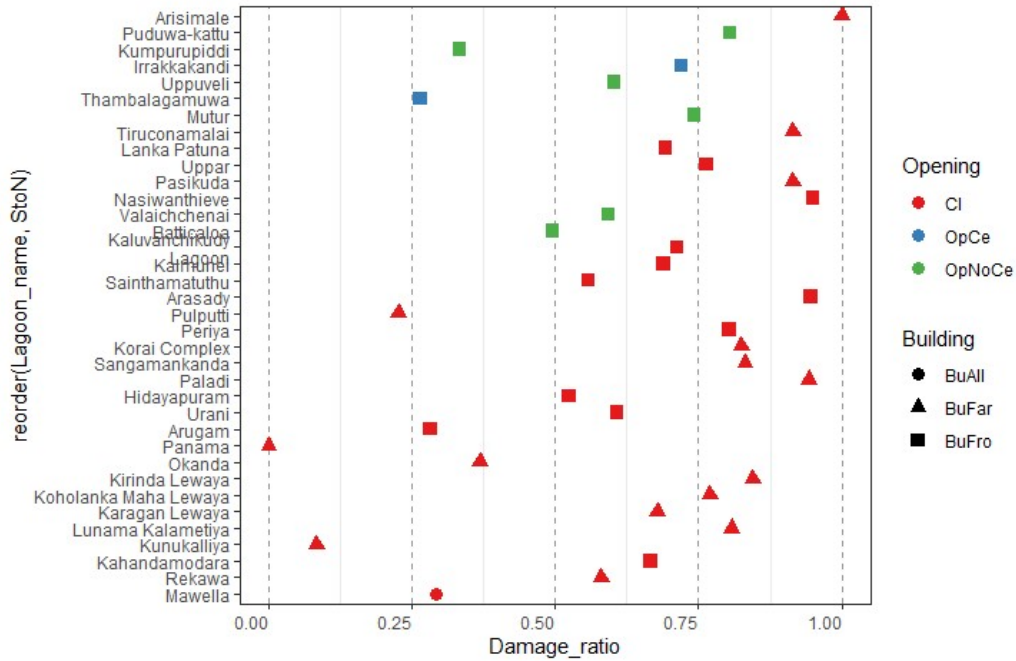
Figure 2-11 The effect of the condition of a lagoon mouth. The colours indicate the condition of the lagoon mouth and the shapes indicate the location of the building area. The definition of symbols is referred to as Section 2.2. Lagoon names are in order from South to North.
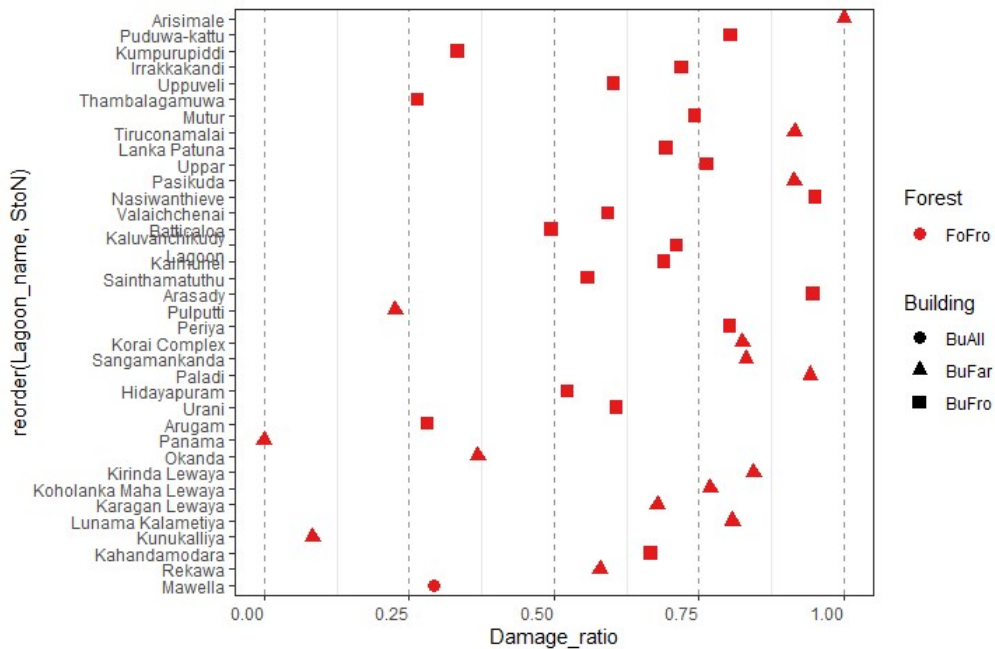
Figure 2-12 The effect of the location of the forest area in a lagoon. The colours indicate the forest condition and the shapes indicate the location of the building area. The definition of symbols is referred to as Section 2.2. Lagoon names are in order from South to North.

The effect of structures was investigated as detailed in Fig. 2-13. From the south to north via east, there were no coast protective structures near the lagoon mouths except the breakwaters constructed in Hambantota harbour (i.e., Karagan Lewaya (No. 21). The conversion to harbour occurred after the tsunami. Hence in this study, the pre-tsunami status was considered in the analysis. During the field survey up to Nilaweli, it was observed that many drainage structures were damaged and replaced in the tsunami rehabilitation projects. The data appeared to be mixed, and there was no clear evidence to express the effect of bridge or causeway in tsunami mitigation.
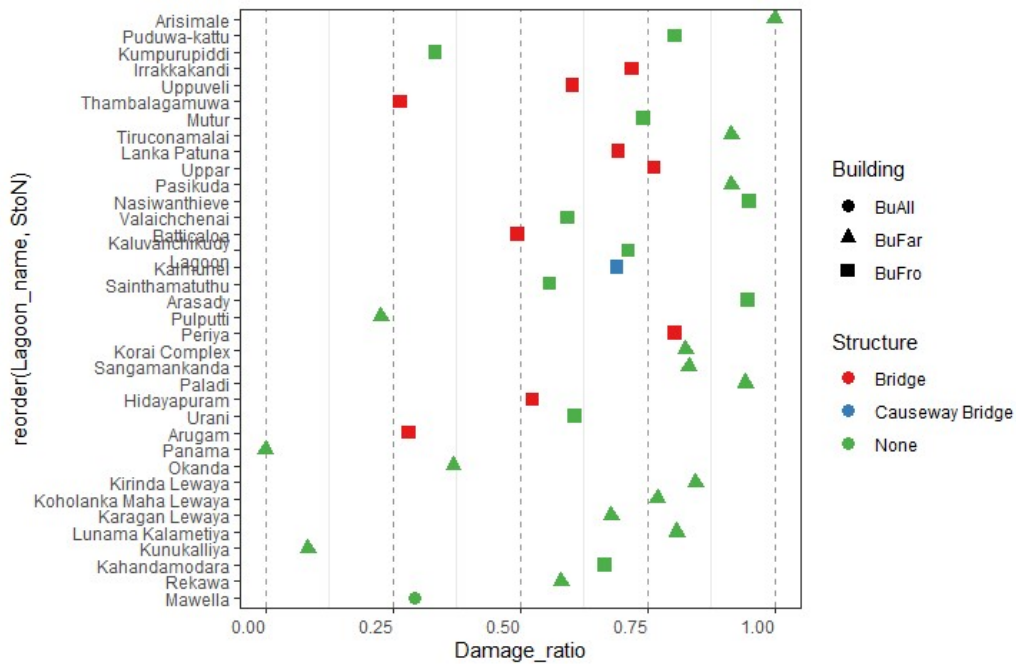
Figure 2-13 The effect of the structures nearby a lagoon. The colours indicate the structure type and the shapes indicate the location of the building area. The definition of symbols is referred to as Section 2.2. Lagoon names are in order from South to North.

Unlike the west and south part of Sri Lanka, the south and east part exhibited no significant difference in tsunami damage reduction regarding the link connected to the sea, as observed in Fig. 2-14. As seen by Wijetunge (2009b), due to low lying area, the tsunami penetrated farther into the land in the east of Sri Lanka. Onshore topography in the east, appeared to the dominant factor in the estimation of damage to the building. The offshore topography was found to be less significant in evaluating damage ratio as witnessed by Fig. 2-15.
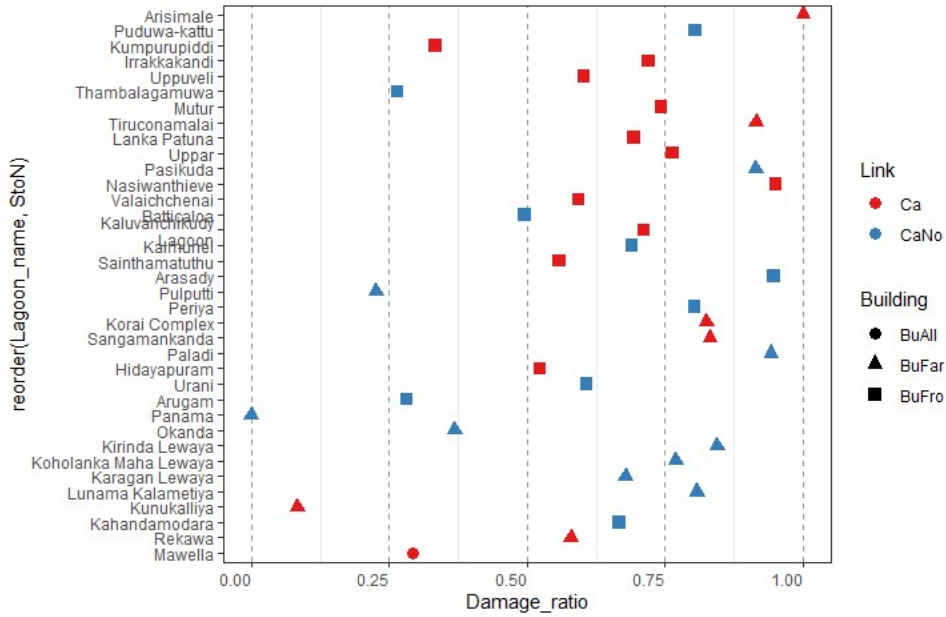
Figure 2-14 The effect of the link from a lagoon to the sea. The colours indicate the condition of the link, and the shapes indicate the location of the building area. The definition of symbols is referred to as Section 2.2. Lagoon names are in order from South to North.
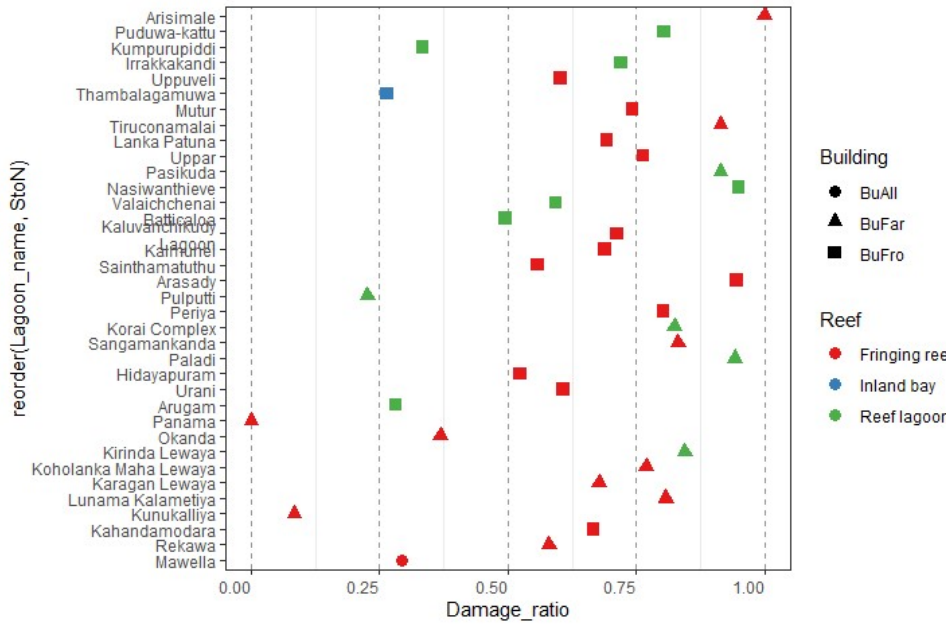
Figure 2-15 The effect of the offshore bathymetry near a lagoon. The colours indicate the reef type (i.e., fringing reef or reef lagoon) and the shapes indicate the location of the building area. The definition of symbols is referred to as Section 2.2. Lagoon names are in order from South to North.

2.3.3 Effect of mangrove

According to the classification made by Silva et al. (2013), the lagoons around Sri Lanka were investigated as depicted by Fig. 2-16. In general, dense mangrove showed less damage ratio. Scattered and Patchy mangroves and swamps showed higher damage ratio. Besides, there are instances where the existence of dense forest could not mitigate tsunami energy. However, tsunami waves can overwhelm the attenuation effect of vegetation as a sufficiently large width of forest in need to reduce the tsunami energy (Mazda et al., 1997). In this study, the mangrove area was not taken into consideration, and the location of damage along the cross-shore direction was not investigated. The results may deviate from the present study if both mangrove condition as well as area together are taken into account for evaluating the effect of damage ratio.
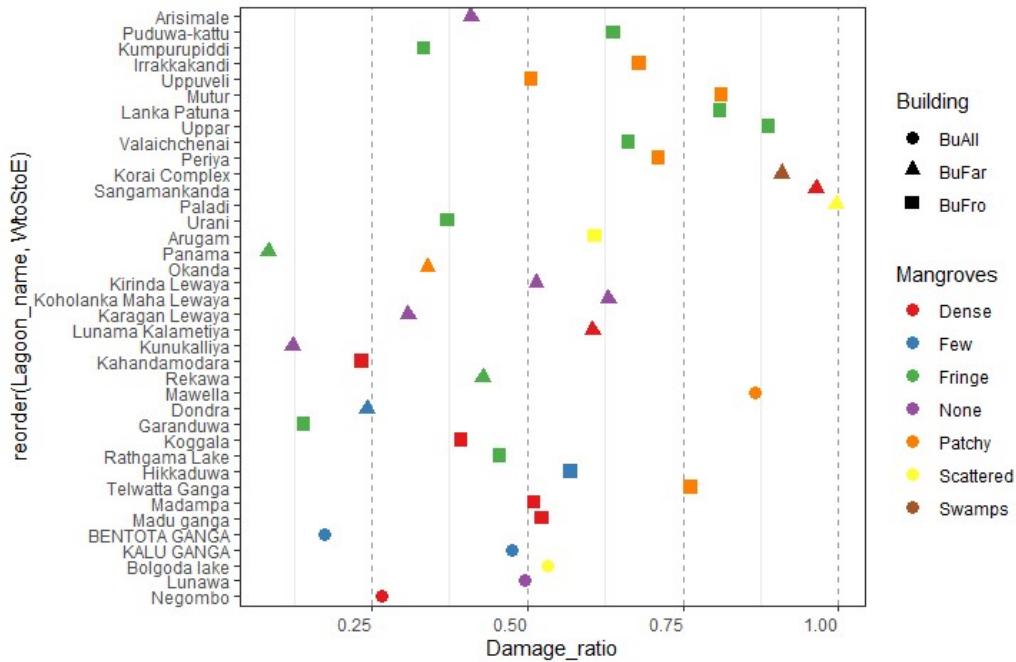
Figure 2-16 The effect of the mangroves in a lagoon. The colours indicate the mangrove condition and the shapes indicate the location of the building area. The definition of symbols is referred to as Section 2.2. Lagoon names are in order from South to North.

2.3.4 Effect of land/barrier length in the opening direction

As seen in Fig. 2-17, the scatterplot of damage ratio against the barrier length in opening direction (LLn-OD) is with much noise; it is hard to see a dominant pattern. Each plot is

labelled with its lagoon number regarding Table 2-1. When barrier length (LLn-OD) < 650 m, damage ratio decrease with decreasing LLn-OD. When LLn-OD < 150 m, the damage ratio was extremely high for many lagoons in both east and south of Sri Lanka. However, in the west part, there was no clear trend that can be identified. The results showed that the distance to the coast is important as many damaged houses can be found in the barrier area and close to the shoreline. Nevertheless, the increment of barrier length induces the energy dissipation by a lagoon to be less effective.
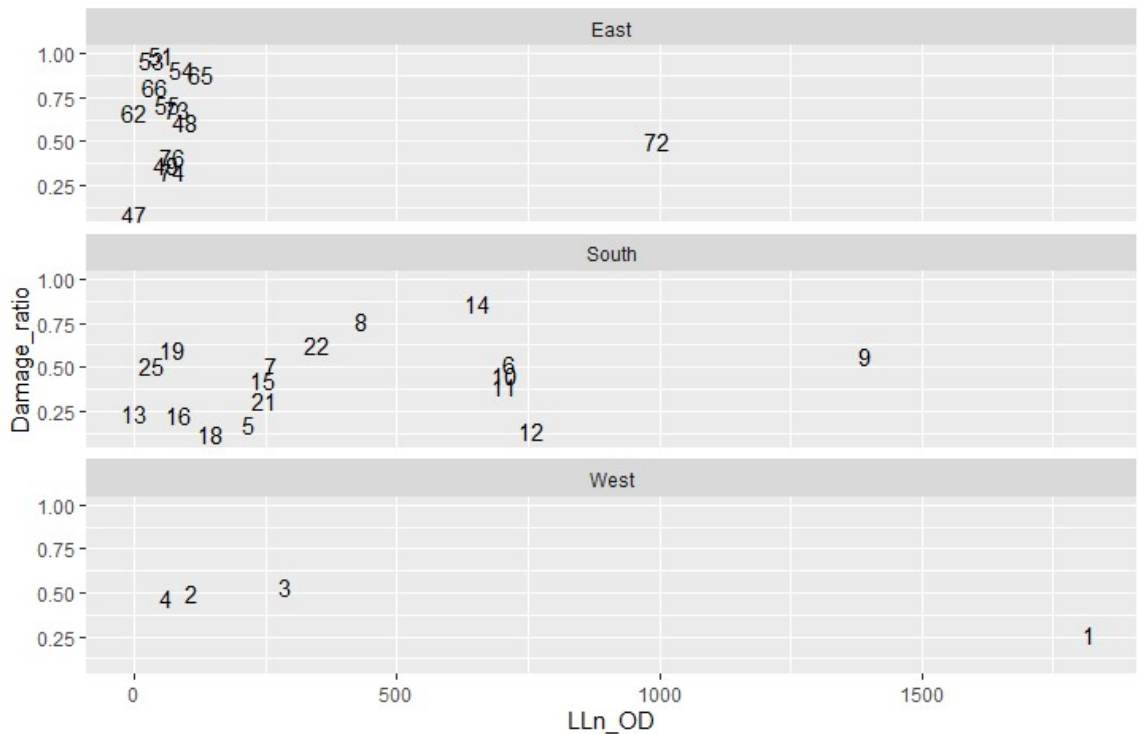
Figure 2-17 The effect of the barrier length in opening direction (LLn-OD) on the damage ratio for all lagoons in west, south and east. Numbers show the plots of lagoon

Few lagoons exposed damage at the upstream of the lagoon by failing the energy absorption entirely within the lagoon water body, as shown in Fig. 2-18. The safe limit of LLn-OD that did not transmit a powerful tsunami wave to cause damage at the upstream of a lagoon was found as 450 m. It can be identified that when LLn-OD < 450 m there is a possibility of causing damage at the upstream of a lagoon. It should be noted that there existed some lagoons regardless of LLn-OD < 450 m, the damage has not been observed at the upstream.
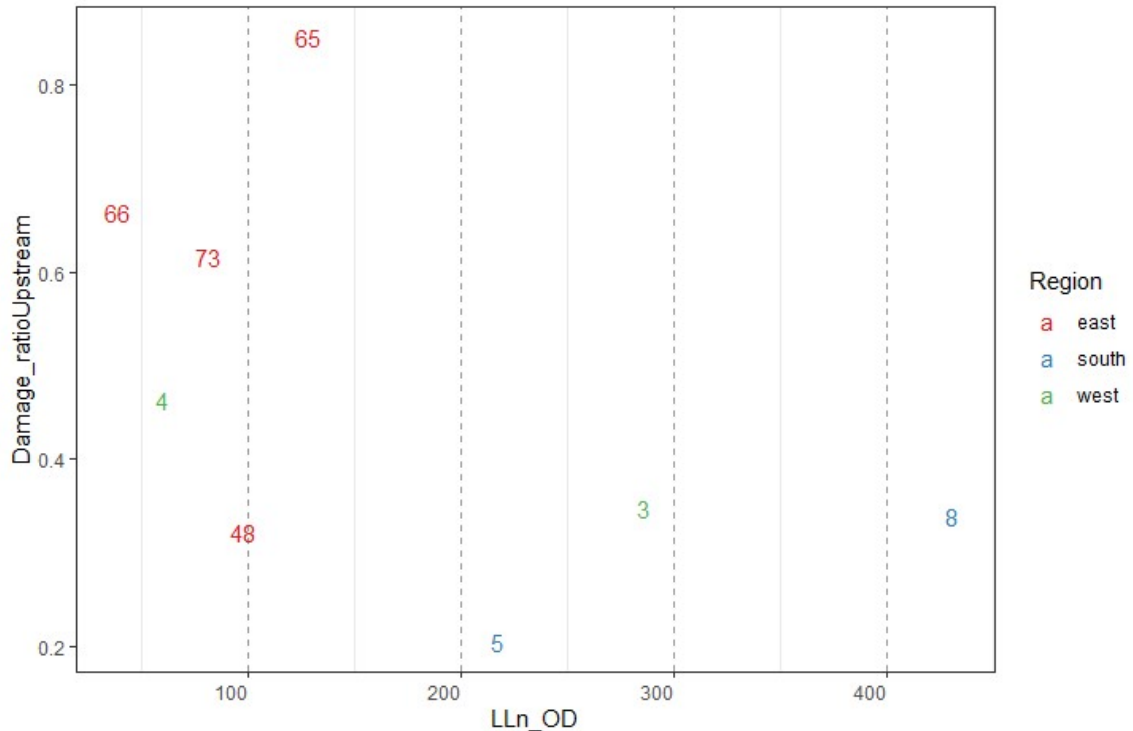
Figure 2-18 The effect of the barrier length in opening direction (LLn-OD) on the damage at the upstream for lagoons in west, south and east. Numbers show the plots of lagoon refer to Table 2-1. The colours categorized the region.

As observed by Wijetunge (2009b) that the inundation distance in the east of Sri Lanka was much higher than the south, caused higher damage ratio in the upstream of lagoons in the east.

2.3.5   Effect of lagoon length in the opening direction

Figure 2-19 demonstrates the effect of lagoon length in opening direction (LLg-OD) on the damage ratio. Except a few lagoons most of the damage occurred within the barrier length. Therefore, the effect of LLg-OD on the damage ratio can not be identified. Instead, for the lagoons that affected the upstream can be used to investigate the effect of LLg-OD as depicted in Fig. 2-20. The larger value of LLn-OD caused many damages (DTotalT = ComDam + ParDamUn + ParDamU). When the summation of LLn-OD and LLg-OD near to 750 m and beyond, the total number of damages appeared to be less. However, the larger value of LLg-OD caused a smaller number of total damages, implies that the distance to the coast is an important parameter in evaluating the total number of damages.
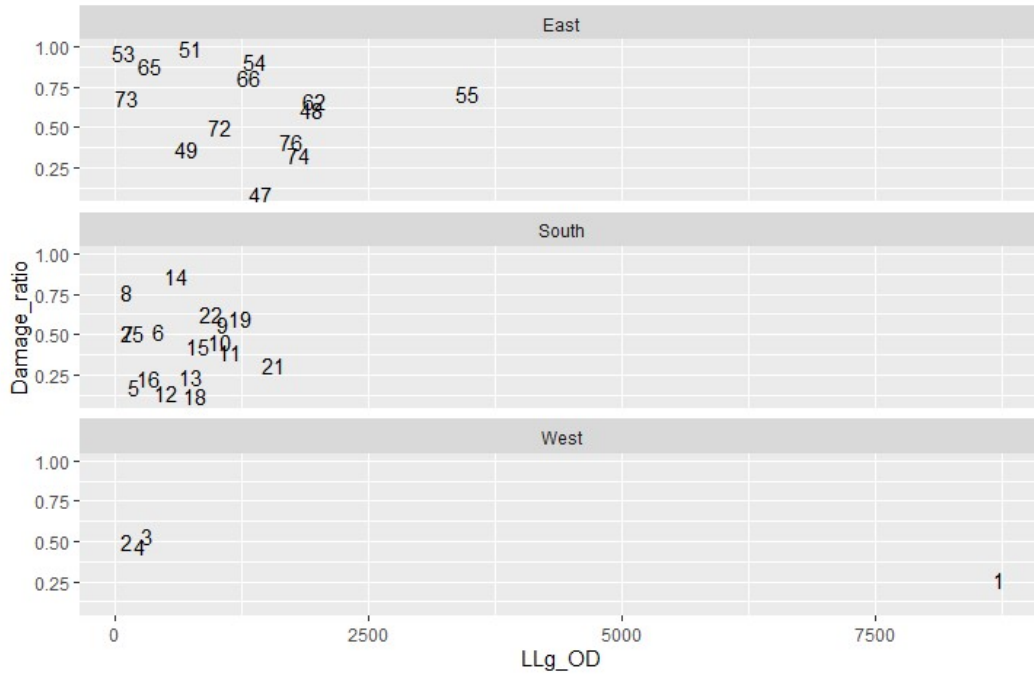
Figure 2-19 The effect of the lagoon length in opening direction (LLg-OD) on the damage ratio for all lagoons in west, south and east. Numbers show the plots of lagoon refer to Table 2-1.
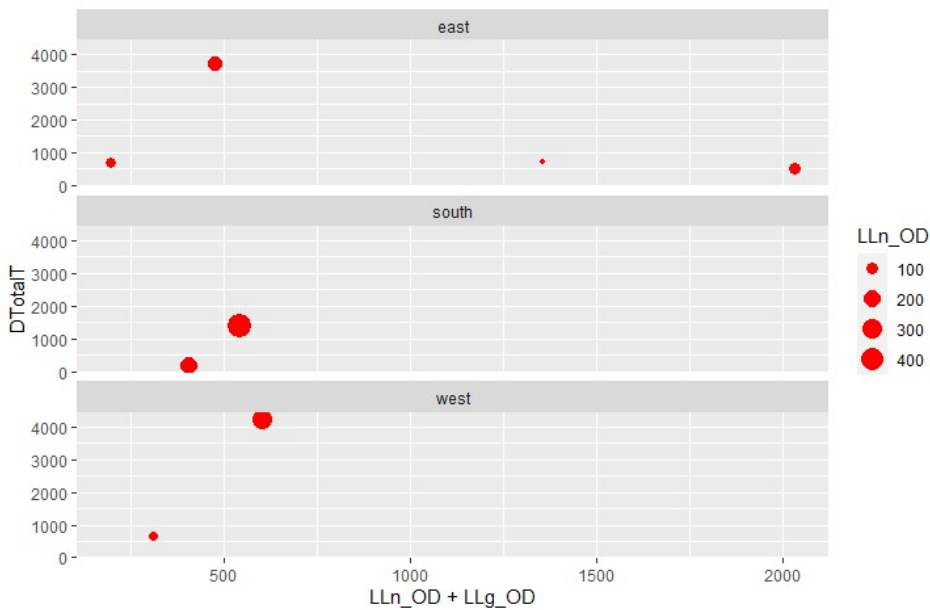
Figure 2-20 The effect of the summation of the barrier length (LLn-OD) and the lagoon length (LLg-OD) on the damage ratio in the opening direction for all lagoons in west, south and east. The size of the red colour plot indicates the largeness of the value of the barrier length in a lagoon.

2.3.6 Effect of lagoon width in the longshore direction/perpendicular to opening direction

The damage ratio was plotted against the width of the lagoon in longshore direction (or perpendicular to opening direction) for west, south and east part of Sri Lanka, as explained in Fig. 2-21. No trend could be observed concerning damage ratio and WLg-CD. Tsunami flows are high energetic surface gravity waves and cause less energy dissipation in the lateral direction. As seen in this study, the width of the lagoon was found as not an essential parameter in evaluating damages.
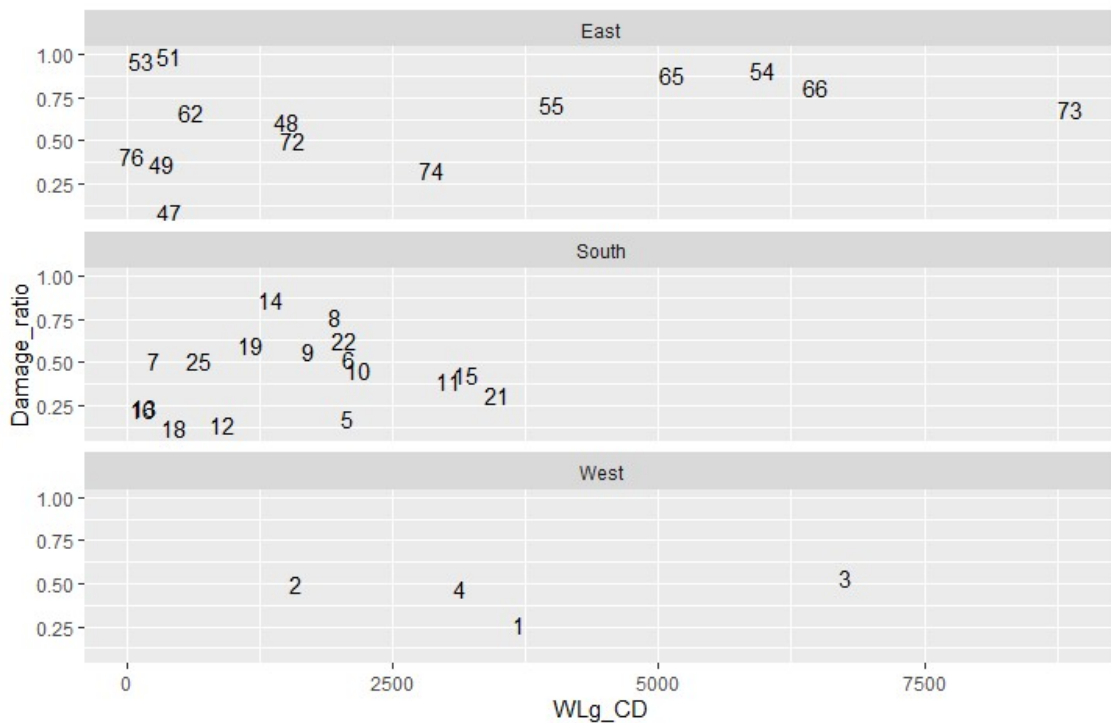
Figure 2-21 The effect of the width of a lagoon in longshore direction/perpendicular to opening direction (WLg-CD) for all lagoons in west, south and east. Numbers show the plots of lagoon refer to Table 2-1.

2.3.7 Effect of the area of the lagoon

The area of the lagoon was investigated, as shown in Fig. 2-22. The data appeared to more scattered, and no trend could be observed. Due to sudden and catastrophic nature of a tsunami, the wave may transmit through lagoon water body rather than gradually fill in the lagoon basin as seen in the case of river floods.
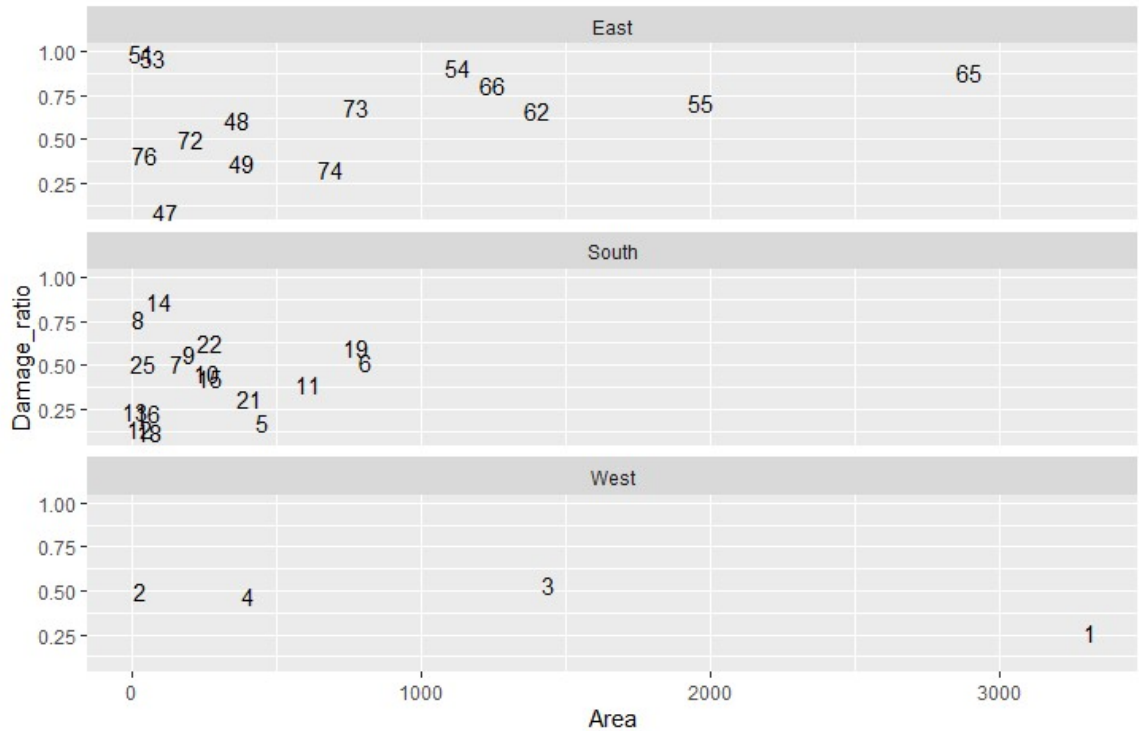
Figure 2-22 The effect of lagoon water body area for all lagoons in west, south and east. Numbers show the plots of lagoon refer to Table 2-1.

2.3.8 Effect of beach slope

The final beach slope can be considered as the main factor of estimating the long wave runup as theoretically derived by Kânoğlu and Synolakis (1998). This phenomenon was also verified by experimentally in this study, as explained in Chapter 4 by applying the empirical equation (Eq. 4-4) derived for the runup of solitary waves on a plane beach. The beach slope was estimated as the slope of the final segment above the mean sea water level. The GEBCO DEM data was used to obtain an approximate slope as SRTM DEM data was found to be spikier even though it has a higher resolution. Wijetunge (2009a) found that the measured direct inundation distance (only if tsunami travels along with dry land and in no contact with a water body) can be expressed in terms of average ground slope in the south part of Sri Lanka. Nevertheless, in this study, the damage ratio is analysed with the slope given by vertical height to horizontal height ratio showed no correlation, as seen in Fig. 2-23.
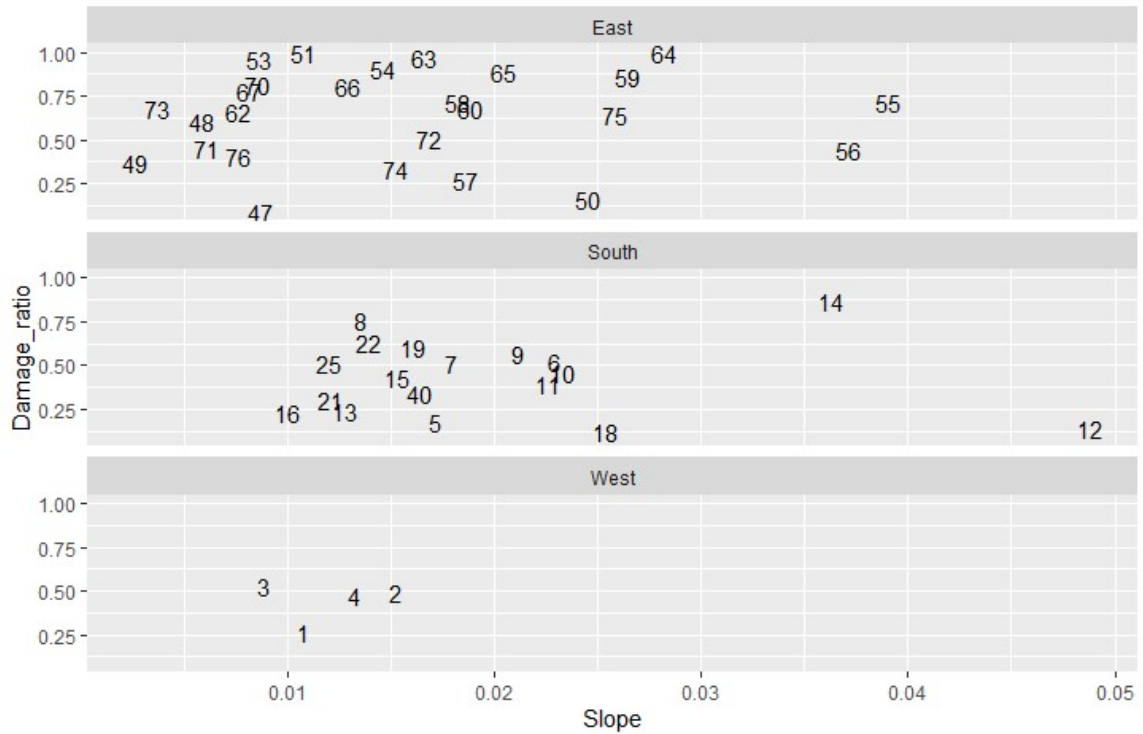
Figure 2-23 The effect of onshore slope for all lagoons in west, south and east. Numbers show the plots of lagoon refer to Table 2-1.

The large scattering may cause due to breaking condition based on the surf-similarity parameter (ξ, see Chapter 4 for more details) and the combined refraction, diffraction, and reflection as explained in Madsen et al. (2008). The presence of roughness may cause the change in energy dissipation of a tsunami (see Chapter 5, 6 and 7). The errors can be occurred due to the accuracy of GEBCO DEM data as the grid resolution was approximately 500 m. Better detail damage analysis by numerical simulation for offshore bathymetry and onshore topography with higher resolution may provide convincing results.

2.3.9   Effect of sand dune/barrier height

In some of the lagoons instead of a sand dune, the cliffs and revetments were found in front of a lagoon. The height of cliff or the crest level of the front barrier section was taken into consideration as the sand dune height as in this study, the reflection caused by obstruction height was investigated rather than focusing on the erosion. The sand dune height was investigated with regard to tsunami damage ratio instead of the runup as illustrated in Fig. 2-24. The data showed scattered, and no trend between the damage ratio and barrier height

could be seen. Possibly with the increment of sand dune height, energy may convey through less obstructed direction as seen by Liu et al. (2005) and cause severe damage in nearby areas. Also, the height of sand dune may accelerate tsunami inflow after passing over dune as discussed in Tanaka et al. (2007), causing extensive damage behind the sand dune. Since the sand dune heights were estimated by Google Earth image analysis, the error in grid resolution may cause an effect. However, it is worth to have a better-detailed damage analysis behind the sand dune with susceptible to erosion is recommended to obtain confident conclusions.

Figure 2-24 The effect of sand dune/barrier height for all lagoons in west, south and east. Numbers show the plots of lagoon refer to Table 2-1.

2.3.10 Effect of tsunami height

The damage ratio against the measured tsunami heights obtained from NOAA historical tsunami database was analysed, as shown in Fig. 2-25. In the west part of Sri Lanka, with the increment of tsunami wave heights, the damage rato has been increased. Nevertheless, all other regions, a trend could not be observed. Dias et al. (2009) have produced vulnerability curves based on tsunami heights and the completely damaged house data for Divisional Secretariat divisions. Since it was based on a larger administrative division, it

was found difficult to apply in the case of damage analysis in the lagoon scale. The estimation of tsunami heights during a field survey may cause errors in tracing and may not be reliable to treat as the most massive tsunami height along the direction of a tsunami inflow. The reliability of measurement values needs to be confirmed by the calculated values in numerical simulation. Moreover, the inundation depths along the direction of tsunami inflow may provide better results in comparison of tsunami mitigation by lagoons as compared by Inoue et al. (2007) for Palatupana lagoon and Tanaka et al. (2007) for the lagoon near Medilla. In order to acquire a better knowledge regarding the impact of the incident wave characteristics on the lagoons, the experimental study on solitary wave runup reduction by a sand dune coastal lagoon, a coral reef system and a forest was conducted as illustrated from Chapter 3 to Chapter 7.
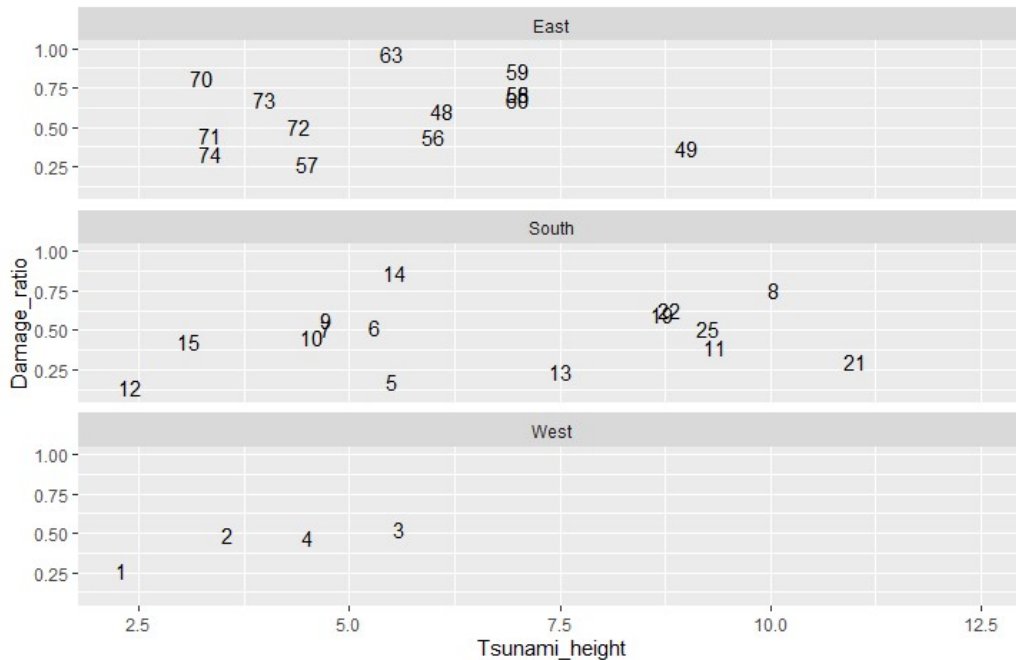
Figure 2-25 The effect of tsunami wave heights for all lagoons in west, south and east. Numbers show the plots of lagoon refer to Table 2-1.

2.4 Conclusion

The statistical and geospatial analyses were carried out for eighty-seven lagoons in Sri Lanka which were affected during 2004 IOT. Even though the lagoons show complex morphological variations, for simplicity in this study, a coastal lagoon was classified

concerning the opening of lagoon mouth, the position of forest patch, location settlements, link to the sea by channel and coastal structures nearby lagoon. The critical parameters that could affect tsunami damage such as land/barrier length in the opening direction, length of the lagoon in opening direction and width of the lagoon in the longshore direction/perpendicular to opening direction were investigated. Physical dimensions of a lagoon, that is, a beach slope, sand dune height, area of a coastal lagoon and the condition of the offshore bathymetry (i.e., Fringing reef or Reef lagoon) were investigated. The classification of mangrove forest based on previous research findings were investigated. Field surveying was conducted in lagoons around the tsunami-affected area to obtain the lagoon bathymetry data, the condition of lagoon opening and the existing hard structures near them and other relevant data which were supposed to be considered as essential to propose modifications for lagoon surrounding in the future. In addition, data on tsunami damaged houses of Sri Lanka, tsunami wave heights and land use GIS data, were used to analyse the vulnerability of Sri Lankan lagoons. The study focused on completely damaged, partial damaged which are usable and unusable in Sri Lanka to evaluate the damage ratio.

The results of the damage ratio showed complex trends with the parameters studied, and it was varied based on west, south and east part of Sri Lanka. In general, the building located close to the lagoon mouth and on barrier land were found to be extremely vulnerable to tsunami wave. The presence of a narrow channel connecting to a lagoon observed high tsunami damage ratio. The lagoons with the closed mouth also exhibited more severe damage in the east part of Sri Lanka. The location of the forest does not make much difference in tsunami damage, but the dense mangrove could reduce the damage, whereas patchy, scattered and swamps did not reduce the tsunami damage. Existence of coast protective structures and the drainage structures did not exhibit an effect on impact to tsunami damage. The offshore bathymetry (i.e., fringing reef or reef lagoon) did not influence on tsunami damage ratio. When the length of barrier length in opening direction was less than 650 m, cause extensive damage, and the effectiveness of lagoon could not be observed. When the summation of lagoon length and barrier length reached beyond 750 m the damage in the upstream of the lagoon was minimized which implies that the distance to the coast is a major governing factor in evaluating damage ratio. the beach slope, barrier height and the area of a lagoon were found to be no effective in estimating the damage ratio

for a particular area in the scale of GN division in Sri Lanka. Better detail concerning the damage analysis with inundation depths along a cross-shore direction is recommended to investigate the real mitigation impact of a tsunami with the parameters mentioned above.

The evidence by laboratory experiments that coastal lagoons can protect against tsunami impacts is more questionable because due to the disastrous nature of tsunami events and the experimental findings tend to be anecdotal. Therefore, a comprehensive study considering all the influential parameters will help in understanding the overall picture of the energy reduction capability of a tsunami. The forests, sand dune and coral reefs certainly reduce the tsunami energy by dissipation over their roughness. However, such coastal feature generally situated in mild sloping beaches which are vulnerable to the tsunami. Therefore, sufficiently large enough width of a forest or continuos large sand dune may help to mitigate the tsunami efficiently.

It is essential to understand the limitations of this study. As this study applied on the available statistics to estimate the damage ratio, some additional variables such as damage type with respect to distance from the coast might influence the housing damage ratio. The accuracy of damage estimations is recommended to be improved in future studies by accompanying such methods. It is worthy of mentioning that all this analysis was made on a single event of 2004 IOT. Different scale and the earthquake source of a tsunami could result in considerably various waveforms thereby might induce different impact. The construction materials and the adapted engineering practice in the construction could also deviate the damage ratio. However, the identification of the most critical parameters is highlighted in this study to design coastal landscapes based on Eco-DRR concept. In order to investigate the effect of offshore wave conditions with different roughness, the series of laboratory experiments were conducted with varying roughness to model trees and coral reefs.

Chapter 3

Runup on a plane beach

3.1 Introduction

The estimation of solitary wave runup on plane beaches has been studied in the study of tsunamis generated by rockfalls, landslides, snow and ice avalanches, caving of glaciers and earthquakes (Fuchs and Hager, 2015; Li and Raichlen, 2001; Synolakis, 1987). The runup is defined as the maximum elevation attained by seawater (on/along the beach) above the still water level, and as such defines the extent of wave action. Solitary wave runup solutions are useful for experimental investigations and calibration of runup modules in numerical models. Despite being widely used to represent tsunamis, Madsen et al. (2008) showed that both the length and time scales of an actual tsunami could not be tied with solitary waves. Larsen and Fuhrman (2019) demonstrated that undular bores with several shorter waves developed at the front of the tsunami did not influence the overall runup of the tsunamis. Therefore, they concluded that solitary wave runup solutions could not be used to evaluate the tsunami impact.

In the present study, an approximate solution for estimating solitary wave runup is presented covering slopes from 1/1 to 1/60 (noting that the bathymetry consists of a constant depth region and a planar beach). It is demonstrated that the newly defined empirical equation can estimate the runup heights regardless of whether the waves are breaking or non-breaking. At first, the existing solitary wave runup solutions and their limitations of applicability are discussed. Additional laboratory experiments for breaking and non-breaking solitary waves on 1/4, 1/7 and 1/10 slopes were performed to enrich the database of runup height data from previously published works. Then the relationship between the runup heights of solitary waves and corresponding surf similarity parameters is used to derive a unified empirical formula. The proposed empirical method is shown to

give similar expressions to existing empirical models in the literature. Finally, the conclusions obtained from this study are shown.

3.2   Literature review

The solitary waves are nonlinear shallow water waveforms which propagate without change of form on constant water depth. A solitary wave is characterised by a single crest of height, H, with an essentially undefined period T and wavelength L as both are infinite. The free surface displacement of a solitary wave, η for the horizontal coordinate, x and time, t is given by

$$\eta = H \operatorname{sech}^2[k(x - ct)] \tag{3-1}$$

The wavenumber, k and wave celerity, c can be expressed:

$$k = \sqrt{\frac{3H}{4h^3}} \text{ and } c = \sqrt{g(h + H)} \tag{3-2}$$

Here, h and g denote the water depth and gravity acceleration, respectively. The above expressions correspond to the first-order solitary wave solution (Boussinesq, 1872). The solitary wave solutions which relate to higher orders can be referred to in the literature (see, e.g., Fenton, 1972; Laitone, 1960). The effective wavelength and wave period of a solitary wave are:

$$L = \frac{2\pi}{k} \text{ and } T = \frac{2\pi}{kc} \tag{3-3}$$

In the literature, there are numerous relationships for solitary wave runup based on physical, analytical and numerical studies. Table 3-1 summarises the existing formulae to estimate solitary wave runups where s is the slope, β is the angle of the sloping beach in degrees, and g is the gravity acceleration. H, h, L, and T are the wave height, water depth, wavelength and wave period respectively at the toe of a sloping beach. R, is the maximum vertical runup, as shown in Fig. 3- 1. Previous studies have used either R/h (runup over water depth) or R/H (runup over wave height) as the non-dimensional parameter to develop solitary wave runup expressions.

Table 3-1 Overview of published formulas for prediction of solitary wave runup

Reference	Formulae	Applicability
Hall & Watts (1953)	$$\frac{R}{h} = 11s^{0.67}\left(\frac{H}{h}\right)^{1.9s^{0.35}}$$	$1/11.43 < s < 1/4.76$
	$$\frac{R}{h} = 3.05s^{-0.13}\left(\frac{H}{h}\right)^{1.15s^{0.02}}$$	$1/4.76 < s < 1/1$
Kaplan (1955)	$$\frac{R}{H} = 0.381\left(\frac{H}{L}\right)^{-0.316}$$	$s = 1/30$
	$$\frac{R}{H} = 0.206\left(\frac{H}{L}\right)^{-0.315}$$	$s = 1/60$
Saeki et al. (1971)[1]	$$\frac{R}{h} = K\left(\frac{H}{h}\right)^{\delta}$$	$s = 1/1$ to $1/150$
	$$\frac{R}{H} = \left(\frac{\sigma}{s}\right)^{1/3}$$	$1 \le \sigma/s \le 5$ Non-breaking
Kajiura (1984)	$$\frac{R}{H} = \left(\frac{\sigma}{s}\right)^{-0.85}$$	$10 \le \sigma/s \le 100$ Breaking
	$$\sigma = \left(\frac{2\pi}{T}\right)\sqrt{\frac{h}{g}}$$	
Synolakis (1987)	$$\frac{R}{h} = 2.831\cot\beta^{0.5}\left(\frac{H}{h}\right)^{1.25}$$	$\frac{H}{h} < 0.818s^{10/9}$ Non-breaking
	$$\frac{R}{h} = 1.109\left(\frac{H}{h}\right)^{0.582}$$	$s = 1/19.85$ Breaking
Kobayashi & Karjadi (1994)[1]	$$\frac{R}{H} = 2.955\xi_{KK}^{0.395}$$	$0.125 \le \xi_{KK} \le 1.757$ Breaking
Li & Raichlen (2001)	$$\frac{R}{h} = 2.831\cot\beta^{0.5}\left(\frac{H}{h}\right)^{1.25} + 0.293(\cot\beta)^{1.5}\left(\frac{H}{h}\right)^{2.25}$$	$1/2.08 < s < 1/19.85$
Hughes (2004)	$$\frac{R}{h} = 1.82\cot\beta^{0.2}\left(\frac{M_F}{\rho g h^2}\right)$$	Non-breaking
	$$\frac{R}{h} = (1.39 - 0.027\cot\beta)\left(\frac{M_F}{\rho g h^2}\right)^{0.5}$$	Breaking

	$$\left(\frac{M_F}{\rho g h^2}\right)_{max} = \frac{1}{2}\left[\left(\frac{H}{h}\right)^2 + 2\left(\frac{H}{h}\right)\right]$$ $$+ \frac{N_s^2}{2M_s}\left(\frac{H}{h}\right.$$ $$+ 1\left)\left\{\tan\left[\frac{M_s}{2}\left(\frac{H}{h}+1\right)\right]\right.$$ $$+ \frac{1}{3}\tan^3\left[\frac{M_s}{2}\left(\frac{H}{h}+1\right)\right]\right\}$$ $$M_s = 0.98\left\{\tanh\left[2.24\left(\frac{H}{h}\right)\right]\right\}^{0.44}$$ $$N_s = 0.69\tanh\left[2.38\left(\frac{H}{h}\right)\right]$$	
Hsiao et al. (2008)	$$\frac{R}{h} = 7.712(\cot\beta)^{-0.632}\left[\sin\left(\frac{H}{h}\right)\right]^{0.618}$$	$1/15 < s < 1/60$ Breaking
Fuhrman & Madsen (2008)	$$\frac{R}{H} = 3.9\xi^{0.42}$$ $$\frac{R}{H} = 2.831\xi^{-0.5}\left(\frac{H}{h}\right)^{-0.25}$$ $$\xi = \frac{s}{(H/h)}$$	Breaking Non-breaking
Madsen & Schaffer (2010)[1]	$$\frac{R_{up}}{H} = \chi_{elev}\pi^{0.25}\left(\frac{H}{h}\right)^{-0.25}\xi_{MS}^{-0.5}$$ $$\xi_{MS} = \sqrt{\pi}\left(\frac{H}{h}\right)^{-0.5}\left(\frac{\Omega^2 h}{g s^2}\right)^{-0.5}$$	$$\frac{R_{up}^{limit}}{H} = \frac{\chi_{elev}\cdot\chi_{break}}{\pi}\xi_{MS}^2$$ Non-breaking
Lo et al. (2013)[1]	$$\frac{R}{H} = 4.5\xi_{LO}^{0.5}$$	Breaking
Fuchs & Hager (2015)	$$\frac{R}{h} = 3(\tan\beta)^{-0.05}\left(\frac{H}{h}\right)$$	$1/1.5 < s < 1/5.0$
Wu et al. (2018)	$$\frac{R}{H} = \frac{4.5\xi_s^{1.52}}{0.04 + \xi_s^{1.19}}$$ $$\xi_s = \frac{s}{(H/h)^{0.9}}$$ $$\frac{R}{H} = \frac{4.04\xi^{1.49}}{0.05 + \xi^{1.20}}$$	Breaking

Note: 1. Please refer to original authors' work to clarify the definition of the mentioned parameters.
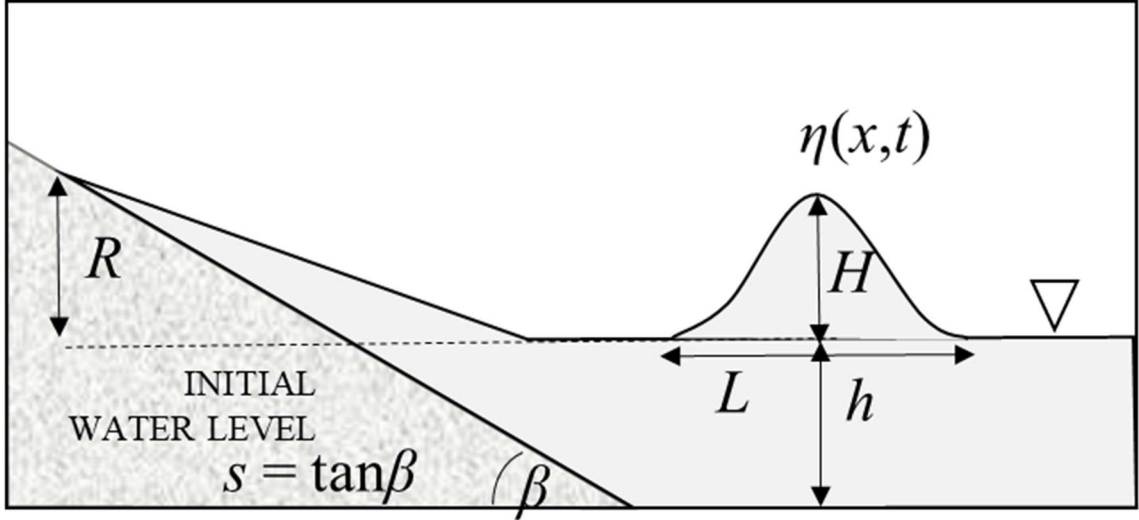
Figure 3-1   A definition sketch for a solitary wave climbing up a sloping beach

The empirical relationships for solitary wave runup as a function of wave height, wavelength, water depth and beach slope have been established in the series of laboratory investigations of Hall and Watts (1953), Kaplan (1955), Kishi and Saeki (1967), Saeki et al. (1971), Synolakis (1987), Hsiao et al. (2008), Lo et al. (2013), Fuchs and Hager (2015), Pujara et al. (2015) and Wu et al. (2018). In the study of Hall and Watts (1953), the runup on the sloping angles (β) of 5 °, 10 °, 15 °, 25 ° and 45 ° corresponding slope (s) to 1/11.43, 1/5.67, 1/3.73, 1/2.14 and 1/1 respectively was investigated. They found relationship for R/h concerning H/h in correlation with s as functions for two ranges for 5 to 12-degree slopes (1/11.43 $< s <$ 1/4.76) and 12 to 45-degree slopes (1/4.76 $< s <$ 1/1). Furthermore, they expressed relationships for R/h versus H/h by finding empirical coefficients, K and δ.

$$\frac{R}{h} = K \left(\frac{H}{h}\right)^{\delta} \tag{3-4}$$

The values of K are 2.15, 3.43, 3.75, 3.35 and 3.1, and the values of δ are 0.81, 1.04, 1.12, 1.12 and 1.15, for beach slopes of 1/11.43, 1/5.67, 1/3.73, 1/2.14 and 1/1 respectively. Kaplan (1955) used non-dimensionalised runup (R/H) and wave steepness (H/L) to develop the empirical relationships for plane slopes of 1/30 and 1/60. Kishi and Saeki (1967) and Saeki et al. (1971) expressed the non-dimensionalised runup R/h as a function of wave height to water depth ratio H/h for the slopes of 1/10, 1/15, 1/20, 1/30, 1/50, 1/100 and 1/150 including the work of Hall and Watts (1953) and Kaplan (1955). They plotted the

empirical coefficients, K and δ against the slope (s) in a graph as illustrated in the figures which can be found in Kishi and Saeki (1967) and Saeki et al. (1971). Kajiura (1984) correlated the solitary wave runups on the various slopes with a single parameter denoted by σ/s where s is the slope, and σ is a dimensionless number. He defined σ by non-dimensionalising with T, wave period, h, constant depth and g, gravity acceleration:

$$\sigma = \frac{2\pi}{T}\sqrt{\frac{h}{g}} \tag{3-5}$$

Hsiao et al. (2008) conducted large scale laboratory experiments for breaking solitary waves. They used their experimental data to re-examine existing formulae and proposed a different formula by regression analysis to predict the maximum non-dimensionalised runup (R/h) on a plane beach with slopes ranging from 1/15 to 1/60. They found that the discrepancies of the runup data correlated with similar wave height to depth ratio (H/h) are not significant based on their experimental work on the slope of 1/60. Fuchs and Hager (2015) conducted experiments for rather steep beach slopes. The proposed empirical formula shows the dependency of runup against the beach slope (s) is very low and higher correlation with the wave height to depth ratio (H/h).

The analytical work of non-breaking solitary wave runup has been extensively studied by Carrier and Greenspan (1958), Keller and Keller (1964), Shuto (1967), Synolakis (1987), Pelinovsky and Mazova (1992), Li and Raichlen (2001), Didenkulova et al. (2007) and Madsen and Schaffer (2010). The theoretical work by Synolakis (1987) represents a significant achievement by deriving an analytical runup solution for non-breaking solitary waves on a bathymetry consisting of a constant depth region and a plane beach.

$$\frac{R}{h} = 2.831 s^{-0.5} \left(\frac{H}{h}\right)^{1.25} \tag{3-6}$$

Various extensions for Synolakis (1987)'s expression can be found in the literature (see, e.g., Didenkulova et al., 2007; Fuentes et al., 2013; Madsen and Fuhrman, 2008; Madsen and Schäffer, 2010; Pujara et al., 2015; Sriram et al., 2016). Li and Raichlen (2001) improved the Synolakis (1987) runup law by adding a correction term based on nonlinear runup.

Hughes (2004) explored wave runup data for solitary waves on plane slopes and presented a different wave runup equation for both breaking and non-breaking types by introducing the maximum depth-integrated wave momentum flux parameter. He derived an expression for wave momentum flux parameter, M_F where ρ is the density of water, g is the gravity acceleration, and H is the wave height at a constant water depth, h.

$$\left(\frac{M_F}{\rho g h^2}\right)_{max} = \frac{1}{2}\left[\left(\frac{H}{h}\right)^2 + 2\left(\frac{H}{h}\right)\right] + \frac{N_s^2}{2M_s}\left(\frac{H}{h}+1\right)\left\{\tan\left[\frac{M_s}{2}\left(\frac{H}{h}+1\right)\right] + \frac{1}{3}\tan^3\left[\frac{M_s}{2}\left(\frac{H}{h}+1\right)\right]\right\}$$

(3-7)

The empirical coefficients, M_s and N_s, are given by

$$M_s = 0.98\left\{\tanh\left[2.24\left(\frac{H}{h}\right)\right]\right\}^{0.44}$$ (3-8)

$$N_s = 0.69\tanh\left[2.38\left(\frac{H}{h}\right)\right]$$ (3-9)

Hughes (2004), therefore illustrated the utility of the wave momentum flux parameter for nonperiodic waves such as solitary waves.

Pedersen et al. (2013) compared the theoretical and experimental results of maximum runup and concluded that the difference between the theoretical values and experimental values is because of the boundary-layer. Wu et al. (2018) compared the maximum runup results obtained by using different slope material (wood, Aluminum, plastic, Plexiglas, Perspex and concrete) and observed that there is no significant influence from the used slope material. Instead, they explained that the major difference between the experimental results of runup might occur due to the size of wave flume. In the small-scale experiments, the boundary-layer flows are likely to be laminar. In contrast, some of the boundary-layer flows in the large-scale experiments might be in the transition regime according to Sumer et al. (2010).

Significant improvements in the modelling of runup have appeared as a result of advancements in both computational techniques and theoretical understandings (see review by Kirby, 2017). Some of them are extended to capture the large roughness effect on runup by forests, mangroves, coral reefs and buildings. They have used either a constant roughness model, equivalent roughness model, drag and inertia forces using Morison-type

equations or macro-scale (wavelength) equations (see, e.g., Mei et al., 2014; Tanaka et al., 2018).

Synolakis (1987) and Borthwick et al. (2006) found non-dimensionalised maximum runup (R/h) follows two different regimes for breaking and non-breaking solitary waves. Synolakis (1987) proposed an empirical formula for estimating breaking wave runup by only using (H/h) for the slope of 1/19.85, which appears different from his analytical equation for non-breaking solitary waves.

$$\frac{R}{h} = 1.109 \left(\frac{H}{h}\right)^{0.582}$$
(3-10)

It is obvious that obtaining a relationship, as mentioned in Eq. (3-4) for the maximum runup by only considering (H/h) for a given beach slope may provide different values for K and δ as it depends on the data chosen for the estimation. For example, following Eq. (3-4) the results of Synolakis (1987) for non-breaking wave runup show empirical coefficients K and δ as 12.613 and 1.25; for breaking waves (i.e., relatively highly nonlinear waves) show empirical coefficients K and δ as 1.109 and 0.582 for the slope of 1/19.85. It is not feasible to find a theoretical solution for the runup of breaking solitary waves over a plane slope because of its complexity. The breaking criterion is useful for distinguishing breaking and non-breaking regimes as well as identifying the maximum runup limit (Grilli et al., 1997; Madsen and Fuhrman, 2008; Madsen and Schäffer, 2010; Synolakis, 1987). Synolakis (1987) derived an expression for the breaking criterion of solitary waves which is known as the theoretical breaking point.

$$\frac{H}{h} = 0.818s^{10/9}$$
(3-11)

Synolakis (1987) observed that waves which were expected to break according to the theoretical breaking criterion deduced by nonlinear shallow water equation theory, did not break during the runup of solitary waves in his laboratory experiments. This phenomenon was also observed and different wave breaking criteria were proposed, by Grilli et al. (1997) using fully nonlinear potential flow wave model, and by Pujara et al. (2015) analysing previous experimental works. Grilli et al. (1997) introduced the slope parameter (S_o).

$$S_o = 1.521s \left(\frac{H}{h} \right)^{-0.5} \tag{3-12}$$

Grilli et al. (1997)'s guidelines can be used to distinguish breaking types as Spilling breaking ($S_o < 0.025$), Plunging breaking ($0.025 < S_o < 0.3$), Surging breaking ($0.3 < S_o < 0.37$) and Non-breaking ($S_o < 0.37$). Pujara et al. (2015) suggested that the breaking criterion of Grilli et al. (1997), S_o should be 0.4 to 0.5 by observing higher runups in the vicinity of that range. The definitions for the wave breaking criterion used by the previous researchers in history can be found from the reviews by Peregrine (1983) and Robertson et al. (2013).

The surf similarity parameter (Battjes, 1974) or the Iribarren number (Iribarren and Nogales, 1949) ξ_{ir} is defined as the slope, s over the square root of wave height to wavelength ratio, H/L. ξ_{ir} have been extensively used to express the relationships of the runup heights for regular and random waves on a sloping beach.

$$\xi_{ir} = \frac{s}{\sqrt{H/L}} \tag{3-13}$$

Similarly, by introducing an effective wave period (T) or an effective wavelength (L) of a solitary wave into the Iribarren number (ξ_{ir}), Kobayashi and Karjadi (1994), Fuhrman and Madsen (2008), Lo et al. (2013) and Wu et al. (2018) proposed different surf similarity parameters and correlated with breaking solitary wave runups. Fuhrman and Madsen (2008) expressed a simplified expression for the surf similarity parameter of solitary waves.

$$\xi = \frac{s}{H/h} \tag{3-14}$$

Those mentioned above empirical and analytical formulae provide useful knowledge for practical applications. But they are mostly limited to either breaking or non-breaking waves or to a relatively small number of slopes.

The same surf similarity parameter, $\xi = s / (H/h)$ was chosen in both analytical solutions proposed by Fuhrman and Madsen (2008) for non-breaking waves and breaking waves. Hence the surf similarity parameter, ξ was utilised in this study to derive a unified formula for the estimation of solitary wave runup over a wide range of sloping beaches regardless of whether the waves were breaking or non-breaking.

3.3 Laboratory experiments

A series of experiments were conducted in a wave flume at Hydraulic Research Laboratory of Saitama University to investigate the solitary wave runup. The experiments were performed in the flume of length 25 m, width 0.3 m and depth 0.6 m equipped with a piston-type wavemaker installed at one end of the flume and testing the plane beach of slopes (s) of 1/4, 1/7 and 1/10 at the other end. The one sidewall of the flume was glass, and other sidewall and floor were made of smooth painted steel. The sloping beach was made of marine plywood painted with water-resistant paint. A schematic figure of the experimental setup is shown in Fig. 3-2.
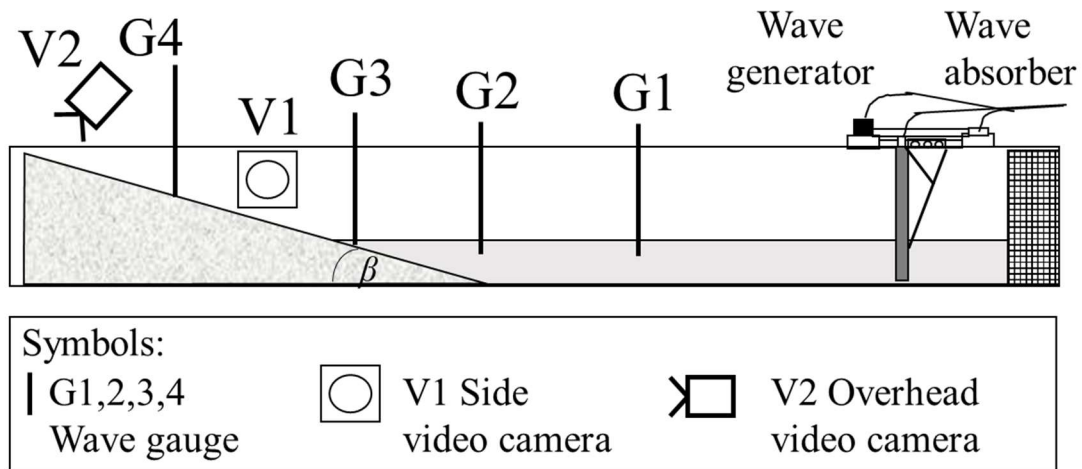
Figure 3-2 Experimental setup

The solitary waves were generated in the constant water depth region and were incident upon a plane beach of the uniform slope where it created a runup event. The target solitary waves were generated by a programmable wavemaker, and the algorithm of the generation was calculated using the Goring (1979) method. The water surface elevation was measured using capacitance-type wave gauges with a frequency of 100Hz. The calibration of wave gauges was done by the standard method of lowering systematically into the water and recording the output voltage accordingly. To establish the desired wave heights, H of the incident wave and to estimate the wave reflection, a preliminary run without any slope was conducted in the wave flume for all combinations of H and h values considered in this study. The reference wave gauge G1 was placed at 6 m from the piston. The horizontal

distance from the wave gauge G1 to the toe of the beach slope was kept more than 5 m. The results ensured that there was no significant peak reduction caused by the sloping beach. The input value to the wavemaker and the measured wave heights by reference wave gauge G1 were slightly different for all H values. Therefore, the measured wave heights by wave gauge G1 were used to define the offshore wave heights (H). Additional measurements of the water surface elevation were taken at the toe of the sloping beach and further onshore, as shown in Fig. 3-2. The water depths (h) were changed from 0.20 to 0.30 m, as shown in Table 3-2.

Table 3-2 Laboratory experimental wave conditions of solitary wave runups

s	h (m)	H (m)
1/4	0.20	0.028 – 0.078
	0.22	0.025 – 0.082
	0.30	0.028 – 0.082
1/7	0.20	0.028 – 0.080
	0.30	0.029 – 0.083
1/10	0.20	0.029 – 0.079
	0.23	0.028 – 0.081
	0.25	0.029 – 0.080
	0.26	0.028 – 0.079
	0.30	0.028 – 0.080

Seven different solitary wave heights, ranging from 0.03 m to 0.09 m for a water depth of h, was used as the input wave height values to the wavemaker program. The measured offshore wave heights (H) ranged between 0.025 m and 0.083 m. The wave height to depth ratio (H/h) was varied from 0.1 to 0.4. The surf similarity parameter (ξ) was altered in the range of 0.252 to 2.685. The Grilli et al. (1997)'s slope parameter (S_o) was varied between 0.241 and 1.246. The present experimental database includes 73 tests for the estimation of runup changing the settings of h, H and s. The maximum runup was tracked by an overhead

camera based on the marker lines on the runup board with an accuracy of 5 mm. The geometric form of the breaking type was observed using the side video camera recordings. Some tests were randomly repeated and found that the results of maximum runup showed consistency within 5 mm range for an input value of offshore wave height (H) to the wavemaker program. The measured data were employed to analyse the wave breaking and the runup height.

3.4   Model derivation

The relationship of non-dimensionalised runup of R/h against the surf similarity parameter, ξ for various slopes was investigated using the form of Eq. (3-15) for both present experimental results and the published works of Hall and Watts (1953), Synolakis (1987) and Hsiao et al. (2008). R/h was used as the non-dimensionalised runup parameter instead of R/H in this study to develop the empirical relationship. The disadvantage of using R/H, for small waves particularly, is that experimental error can be greatly increased as both runup height, R and wave height, H are measured values with greater ambiguity compared to the water depth, h.

$$\frac{R}{h} = a\xi^b \qquad \text{(3-15)}$$

Here the empirical coefficients a and b can be determined by the linear regression analysis for a given beach slope (s). The experimental dataset contains the slopes of 1/1, 1/2.14, 1/3.73, 1/4, 1/5.67, 1/7, 1/10, 1/11.43, 1/19.85 and 1/60 altogether. The database which was used to derive the empirical equation consists of 381 observations ($N = 381$). It included water depths (h) ranging from 0.0625 to 2.9 m and wave heights (H) ranging from 0.002 to 0.406 m, resulting in wave height to depth ratios (H/h) from 0.005 to 0.633 and surf similarity parameter (ξ) from 0.05 to 18.44. The relationship between the bathymetry slope (s) and the parameters a and b, was derived.

$$\frac{R}{h} = f_1(s)\xi^{f_2(s)} \qquad \text{(3-16)}$$

Here a and b can be viewed as the functions of a beach slope, s, as $f_1(s)$ and $f_2(s)$ respectively. The results of the analysis were used to derive a unified formula covering beach slopes from 1/1 to 1/60.

3.5   Results and discussion

The visual observations made by video camera recordings during the present laboratory experiments verified that the type of solitary wave breaking matched the prediction of Grilli et al. (1997)'s slope parameter, S_o, defined in Eq. (3-12). The plunging breaking type could be observed where $S_o < 0.3$. The surging breaking type could be seen where $0.3 < S_o < 0.37$. The breaking was not observed for $S_o > 0.37$. The spilling breaking type could not be seen for the wave conditions tested in this study.

For each slope, empirical coefficients for parameters a and b could be found in the form of Eq. (3-15) using regression analysis. The correlation coefficient, R^2, is over 0.9 for all the cases. The obtained results of a and b were plotted against the $\cot\beta = 1/s$, as shown in Fig. 3- 3.
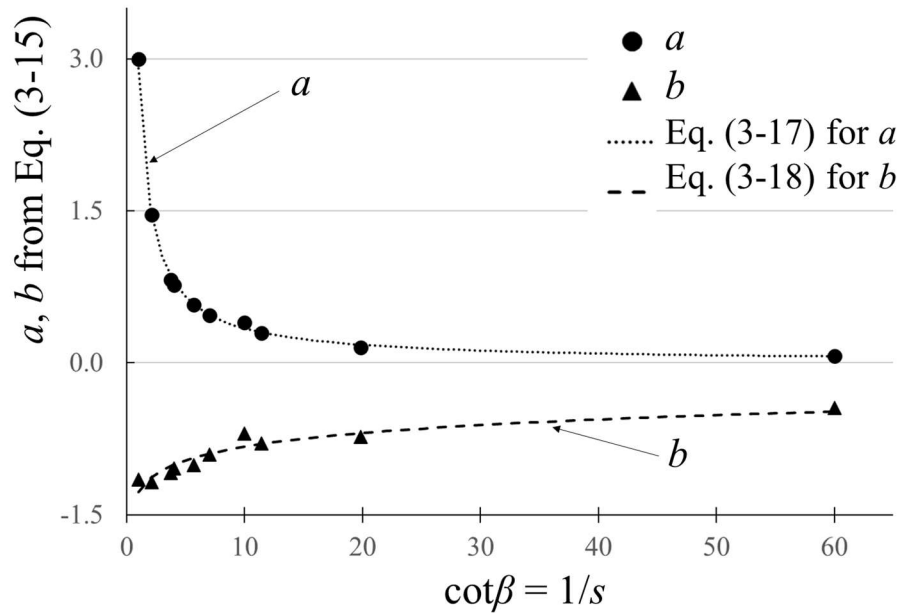
Figure 3-3 The relationship between the $\cot\beta = 1/s$ and the empirical coefficients a and b as calculated according to Eq. (3-15).

Hence the relationships for parameters a and b against s were derived by linear regression analysis as expressed in Eq. (3-17) for a which follows a power-function and Eq. (3-18) for b which follows the logarithmic function, giving correlation coefficient, R^2 as 0.994 and 0.904, respectively.

$$a = 2.9049s^{0.931} \tag{3-17}$$

$$b = -0.1931 \ln s - 1.2704 \tag{3-18}$$

By substituting expressions for empirical coefficients, a and b in Eq. (3-15), it gives;

$$\frac{R}{h} = 2.9049s^{0.931} \left[\frac{s}{(H/h)}\right]^{(-0.1931 \ln s - 1.2704)} \tag{3-19}$$

This method is quite similar to Hall and Watts (1953)'s method, but the main difference is that we have used $\xi = s / (H/h)$ instead of H/h. The technique used in the current study appears to provide a more reasonable basis for a broad range of slopes and wave height to depth ratios (H/h).

Runup values for different planar beaches from the published works of Chang et al. (2009), Pujara et al. (2015) and Smith et al. (2017) were also employed for validating the present formula as shown in Fig. 3-4a. The figure shows that all runup data for both breaking non-breaking solitary waves reproduced reasonably well and can be depicted by a single empirical equation, Eq. (3-19).

To compare with expressions for the literature, Fig. 3-4b shows the runup of solitary waves correspond to setting R/h = min(non-breaking expression, breaking expression) from Fuhrman and Madsen (2008) can be expressed by changing scaling from H to h.

$$\frac{R}{h} = \min\left\{\left[3.9\xi^{0.42}\left(\frac{H}{h}\right)\right], \left[2.831\xi^{-0.5}\left(\frac{H}{h}\right)^{0.75}\right]\right\} \tag{3-20}$$

It could be stated that Eq. (3-20) also covers the data reasonably. To assess the probable error using the Eq. (3-19), Fig. 3-5a shows the Goodness-of-fit in terms of runup heights between the measured values by experiments and calculated values from Eq. (3-19). In Figure 3-5a, the runup data are almost covered within 20% deviations from the perfect agreement. The proposed empirical equation predicts remarkably well apart from a few outlying points. There are discrepancies between Eq. (3-19) and experimental results for small runups (R/h < 0.08), very low wave nonlinearities (H/h < 0.02) and very high nonlinearities (H/h > 0.6) where Eq. (3-19) overpredicts, and also for the slope (s) of 1/1 where Eq. (3-19) underpredicts. The deviations might occur because of the use of the generalised least squares method in the regression analysis with equal weight distribution among data.
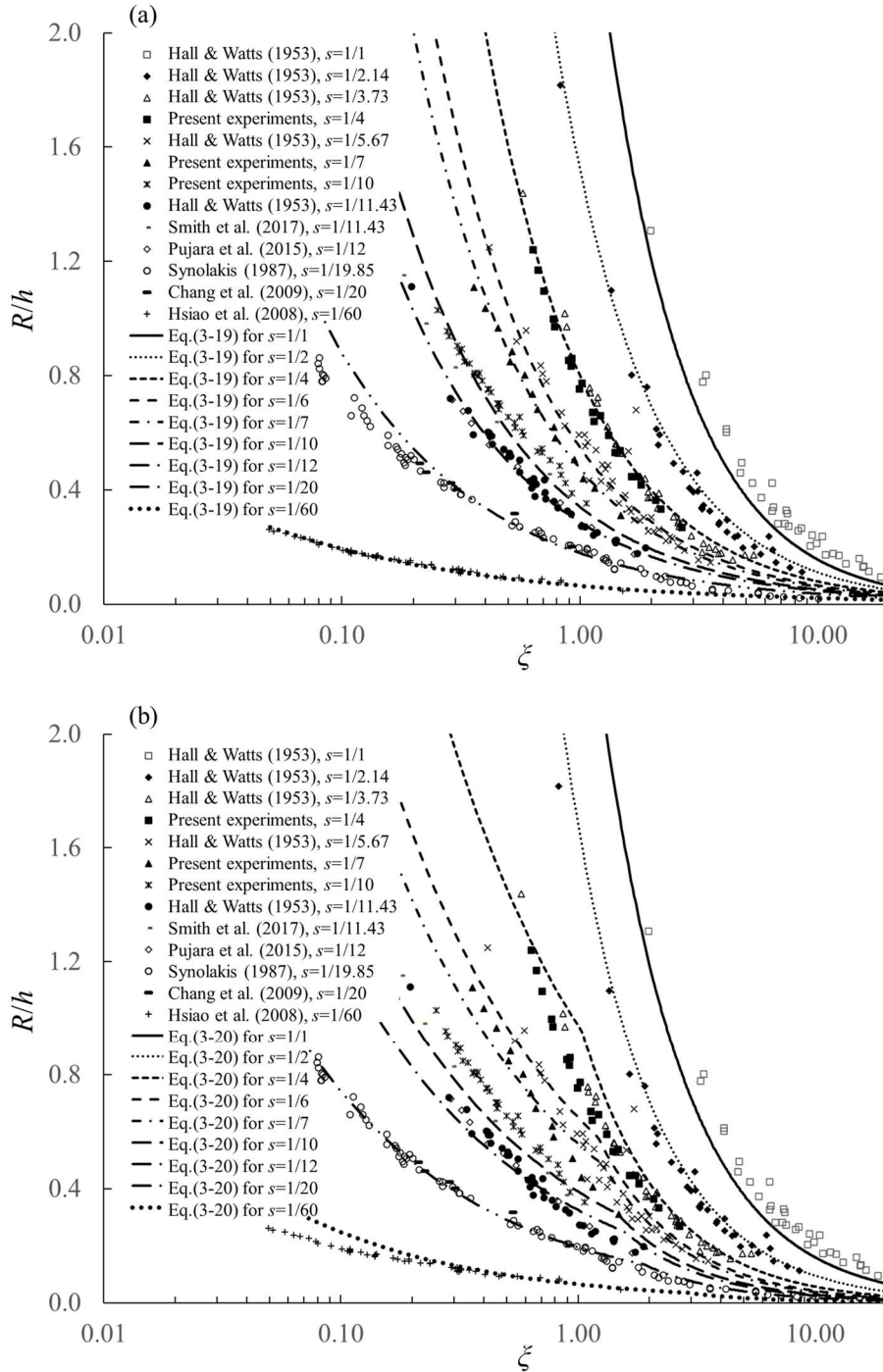
Figure 3-4 Comparison of non-dimensionalised runup R/h against surf similarity parameter ξ for a slope (s) in the experimental work carried out by Hall and Watts (1953), Synolakis (1987), Hsiao et al. (2008), Chang et al. (2009), Pujara et al. (2015), Smith et al. (2017) and present authors: (a) with the present empirical equation Eq. (3-19), (b) with the combined expression of Furhman and Madsen (2008) denoted by Eq. (3-20).
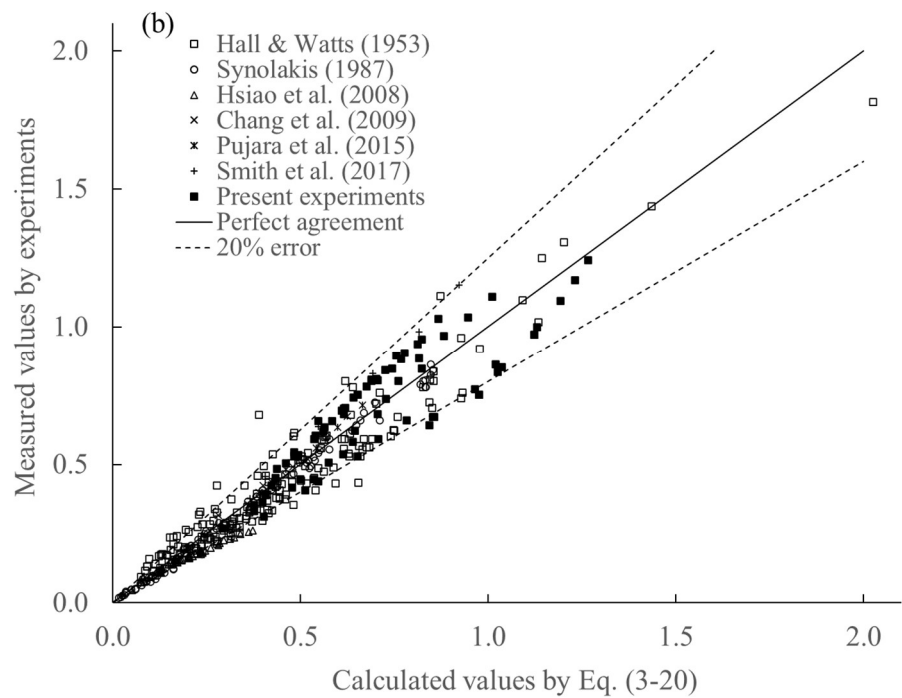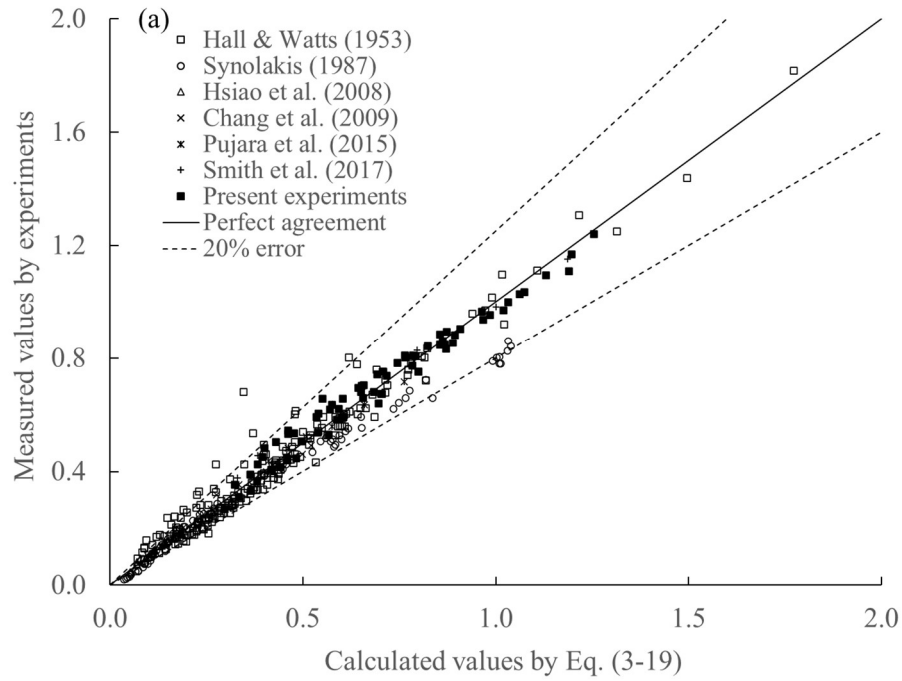
Figure 3-5 Direct comparison of the experimental results of Hall and Watts (1953), Synolakis (1987), Hsiao et al. (2008), Chang et al. (2009), Pujara et al. (2015), Smith et al. (2017) and present experiments: (a) with the present empirical equation Eq. (3-19), (b) with the combined expression of Furhman and Madsen (2008) denoted by Eq. (3-20).

Moreover, the statistical measures of the mean absolute error, MAE $=\sum_{i=1}^{N}|C_i - M_i|/$

N, the root-mean-square, RMSE $= \sqrt{\frac{1}{N}\sum_{i=1}^{N}(C_i - M_i)^2}$, the scatter index, SCI = RMSE/$\bar{M}$

and correlation coefficient, $R^2 = \frac{\left[\sum_{i=1}^{N}(C_i-\bar{C})(M_i-\bar{M})\right]^2}{\sum_{i=1}^{N}(C_i-\bar{C})^2 \sum_{i=1}^{N}(M_i-\bar{M})^2}$ were calculated. C_i and M_i denote

the calculated and the measured data, respectively and N, is the total number of evaluated

data points. The results for the present proposed method show that MAE = 0.037, RMSE

= 0.003, SCI = 0.007 and R^2 = 0.966. Also, an agreement index C_R (Willmott, 1981) was

used to evaluate the accuracy of the empirical equation, which is defined as in Eq. (3-21).

$$C_R = 1 - \frac{\sum_{i=1}^{N}(C_i-M_i)^2}{\sum_{i=1}^{N}[|C_i-\bar{M}|+|M_i-\bar{M}|]^2} \tag{3-21}$$

The value of C_R gives as 0.991, implying the proposed empirical solution satisfy well

with the collected data points. The combined expression of Fuhrman and Madsen (2008)

given by Eq. (3-20) was compared with the present runup data, as shown in Fig. 3- 5b. The

statistical measures of MAE, RMSE, SCI, R^2 and C_R for the comparison between the

experimental results and Eq. (3-20), give 0.055, 0.006, 0.013, 0.937 and 0.983, respectively.

Based on these measures, it could be mentioned that Eq. (3-20) performs well, but Eq. (3-

19) is superior. Eq. (3-20) shows some discrepancy with the experimental values for the

slope, s = 1/1 where it underpredicts. Eq. (3-20) overpredicts by more than 20% for the

experimental values of s = 1/60 and S_o < 0.07.

Eq. (3-19) can be rearranged and expressed as in Eq. (3-22).

$$\frac{R}{h} = 2.9049 s^{(-0.1931\ln s-0.3394)}\left(\frac{H}{h}\right)^{(0.1931\ln s+1.2704)} \tag{3-22}$$

The present empirical equation, Eq. (3-19) is also similar to some extent of Synolakis

(1987) runup law for non-breaking waves except the empirical coefficients. The new runup

relationship was compared with the existing empirical models proposed by Hall and Watts

(1953), Pedersen and Gjevik (1983) for Langsholt (1981)'s experiments, Baldock et al.

(2012), Yao et al. (2015) and Fuchs and Hager (2015). The result of the comparison for

their empirical coefficients K and δ by following Eq. (3-4) with Eq. (3-19) is presented in

Table 3-3.

Table 3-3 Comparison of Eq. (3-19) with deduced empirical coefficients by following Eq. (3-4) as obtained by previous authors

Author(s)	slope (s)	Deduced as per Eq. (4)		Calculated by Eq. (19)		Difference in estimation (%)	
		K	δ	K	δ	K	δ
Hall & Watts (1953)	1/1	3.10	1.15	2.90	1.27	6	-10
	1/2.14	3.35	1.12	3.36	1.12	0	0
	1/3.73	3.75	1.12	3.25	1.02	13	9
	1/5.67	3.43	1.04	2.93	0.94	15	10
	1/11.43	2.15	0.81	2.11	0.80	2	1
Pedersen & Gjevik (1983)	1/2.75	3.48	1.13	3.36	1.08	3	5
Baldock et al. (2012)	1/9.35	2.04	0.68	2.36	0.84	-16	-23
Fuchs & Hager (2015)	1/1.5	3.06	1.00	3.23	1.19	-5	-19
	1/1.25	3.14	1.00	3.37	1.09	-7	-9
	1/5	3.25	1.00	3.04	0.96	6	4
Yao et al. (2015)	1/8	2.28	0.77	2.55	0.87	-12	-13

It can be seen that most of the data support the trend of Eq. (3-19). Therefore, the present unified formula shows reasonable applicability in predicting maximum runup in a broad range of wave conditions and beach slopes irrespective of breaking criterion. The current empirical equation was deduced from laboratory data for a solitary wave in one-horizontal dimension (1-HD), where the energy dissipation might not scale well due to boundary layer dissipation and wave breaking, and the refraction, diffraction and resonance are ignored. Hence, the applications of this equation in the field conditions should be implemented cautiously.

3.6 Summary and conclusions

A total of 73 laboratory experiments were conducted, covering three types of breaking as non-breaking, surging breaking and plunging breaking on three sloping beds. A total number of 403 data points were compared in the analysis, including the other researchers'

laboratory solitary wave runup results. A simple unified formula for prediction of solitary wave runup is proposed. The formula uses the surf similarity parameter, as well as additional (slope-dependent) coefficients, whose exact functional forms have been derived from the aforementioned experimental data. The formula works reasonably well for both breaking and non-breaking waves. A reasonable agreement was found, except for minor discrepancies concerning small runups ($R/h < 0.08$), low wave nonlinearities ($H/h < 0.02$), and high nonlinearities ($H/h > 0.6$), where present empirical model overpredicts. It was also observed that the present model predicts lower than experimental values where slope (s) is 1/1. The tests of the reliability of the proposed equation included the agreement index (C_R), the correlation coefficient (R^2), the mean absolute error (MAE), the root-mean-square error (RMSE), and the scattering index (SCI) gave results of 0.991, 0.966, 0.037, 0.003 and 0.007 respectively. Based on comparison with other empirical models found in the literature, it has been demonstrated that the newly proposed solitary wave runup formula is applicable for plane beach slopes ranging from 1/1 to 1/60. The empirical equation can also be applied for different breaking types, such as plunging, surging and non-breaking waves. The equation is deduced from laboratory data where the energy dissipation might not scale well due to boundary layer dissipation and wave breaking. The refraction, diffraction and resonance effects are ignored in the present experimental conditions. It is worthy of mentioning that the longwave runup in the coastal region experiences the effect of larger roughness by forests, mangroves, coral reefs and building structures and can deviate from the presented empirical model results.

Chapter 4
Runup on compound slopes

4.1 Introduction

In the literature, there are numerous relationships for solitary wave runup based on physical, analytical and numerical studies. Comprehensive review about solitary wave runup on plane beaches is given in Vinodh and Tanaka (2020). The existing formulae consist of parameters to estimate solitary wave runups where s is the slope, β is the angle of the sloping beach in degrees, and g is the gravity acceleration. H_o, h_o, L_o, and T are the wave height, water depth, wavelength and wave period respectively at the toe of a sloping beach. R is the maximum vertical runup. Previous studies have used either R/h_o (runup over water depth) or R/H_o (runup over wave height) as the non-dimensional parameter to develop solitary wave runup expressions.

Vinodh and Tanaka (2020) derived an empirical expression which is valid for slopes ranging from 1/1 to 1/60 for both breaking and nonbreaking waves as expressed in Eq. (3-19) in Chapter 3.

A reasonable agreement has been found in the above equation, except for minor discrepancies concerning small runups ($R/h_o < 0.08$), low wave nonlinearities ($H_o/h_o < 0.02$), and high nonlinearities ($H_o/h_o > 0.6$), where present empirical model overpredicts. It has also been observed that the current model predicts lower than experimental values where slope (s) is 1/1.

A typical tsunami generally consists of a wave train where wave period between successive waves can be varied up to several hours and subsequent waves may become more prominent than the first incident wave. It is acceptable to assume that the maximum runup of a wave train will be primarily affected by the runup of the leading wave that emerges from the wave train (Kajiura, 1965; Synolakis, 1988). In the case of the runup of consecutive two solitary waves where the wave is followed by one with larger amplitude, Chan and Liu (2012) found that the maximum runup is smaller than that of a single solitary wave. The runup associated with the second wave is weakened by the drawdown of the first wave in case of nonbreaking waves. The behaviour was found to be more problematic

if a wave breaks on the sloping beach. They further concluded that for a single wave, the accelerating phase of the incident wave commands the maximum runup height. Lo et al. (2013) found that in runups caused by the first wave are not affected by the second solitary wave, regardless of the separation time and are the same as single solitary wave runups.
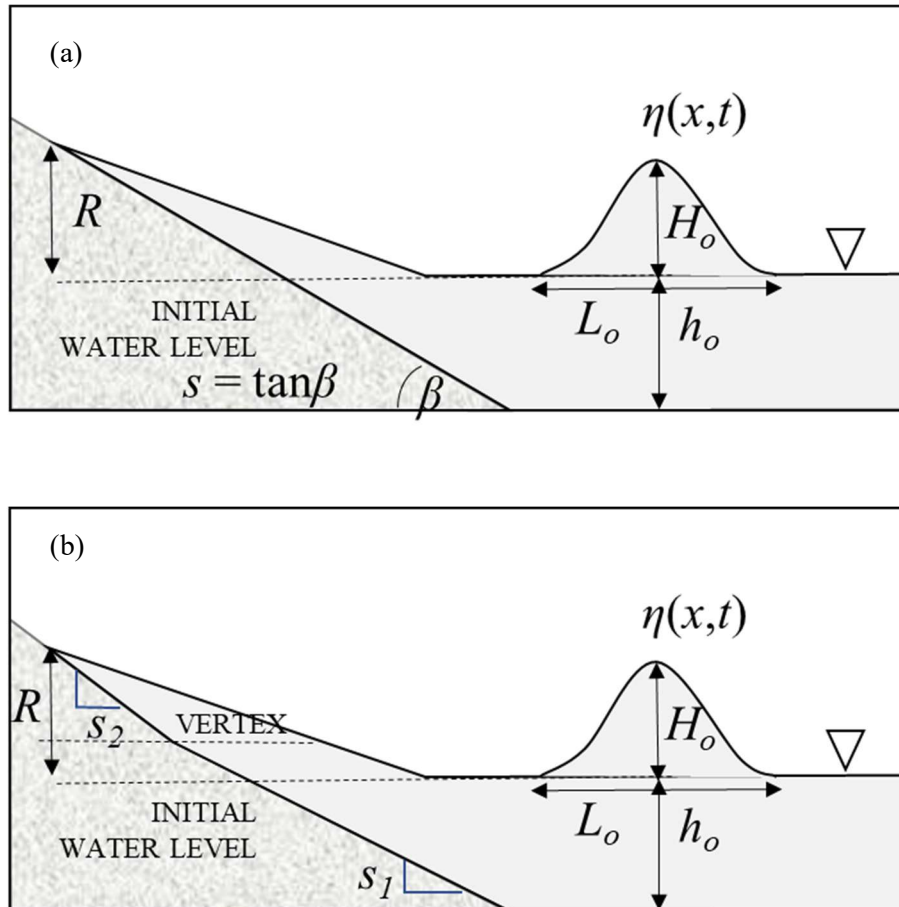
Figure 4-1 Definition of parameters for solitary wave runup on (a) plane beach, (b) compound slope.

Saville (1957)'s method for regular waves uses successive approximations which involved the substitution of the actual composite slope with a single imaginary slope obtained from the breaking depth (d_b) or breaking height (H_b) as given by the solitary wave equations of Munk (1949) and an estimated wave runup (R) value. Saville found the wave runup (R) predicted by his method to be generally within ten per cent of experimental values except for the longer berms tested. After a horizontal berm had reached a certain width, further widening had no significant effect in runup reduction. Saville found when

the berm widths greater than one-fourth of the incident wavelength (L_o), the reduction in berm effectiveness to be caused by the phenomenon of 'wave setup' on the berm. This 'setup' of water (increase in water depth on the berm) was caused by the forward transport of water by waves. Saville found that the wave runup (R) affected by reformed waves or surges on the berm. Mayer and Kriebel (1994) extended Saville's method by incorporating Hunt (1959) formula for estimating regular wave runup. Park et al. (2015) also introduced an empirical approach to analysing the runup on composite slopes. Park et al. (2015) observed a weak positive correlation between runup height and onshore slope when analysing runup heights on compound slopes (i.e., offshore slope and onshore slope) by using Boussinesq simulation. Still, it was observed a large scattering between the numerically analysed data and their proposed empirical results. However, all the proposed methods above are either for regular waves and random waves or showed extensive scattering data compare with the proposed solution.

Kânoğlu and Synolakis (1998) have shown analytically that the runup height depends only on the slope of the section closest to the shoreline for a broad range of transitions depths and can be estimated by Synolakis (1987) runup law which is valid only for nonbreaking waves.

In this chapter, it is focused on the solitary wave runup on compound slopes and the applicability of solitary wave runup on a plane beach to the case of compound slopes. For the comparison, the previous research works in addition to the current experimental database, were also tested for validation.

4.2   Materials & Methods

A series of experiments were conducted in a wave flume at Hydraulic Research Laboratory of Saitama University to investigate the solitary wave runup. The experiments were performed in the flume of length 25 m, width 0.3 m and depth 0.6 m equipped with a piston-type wavemaker installed at one end of the flume and testing the compound beach slopes (i.e., offshore slope and onshore slope). The solitary waves were generated in the constant water depth region and were incident upon a plane beach of the uniform slope where it created a runup event. The solitary waves were generated by a programmable wavemaker. The algorithm of the generation was calculated using the Goring (1979) method. The

generation trajectories of the solitary waves by the wavemaker can be graphed concerning time as in Fig. 4-2. ξ is the position of the paddle concerning time t. S is the total stroke length, and T is the entire time of the movement of the paddle, which can be considered as the wave period. Curve progression is independent of the still water depth, h_o in which the wave is generated. The paddle trajectory is point-symmetric to its centre (i.e., starting position of the paddle before moving for generation) and of tangent-hyperbolical-like shape with the steeper inclination for more considerable wave height to water depth ratio (H_o/h_o). As shown in Fig 4-2, the paddle accelerates in the first half of the stroke, whereas it decelerates during the second half.
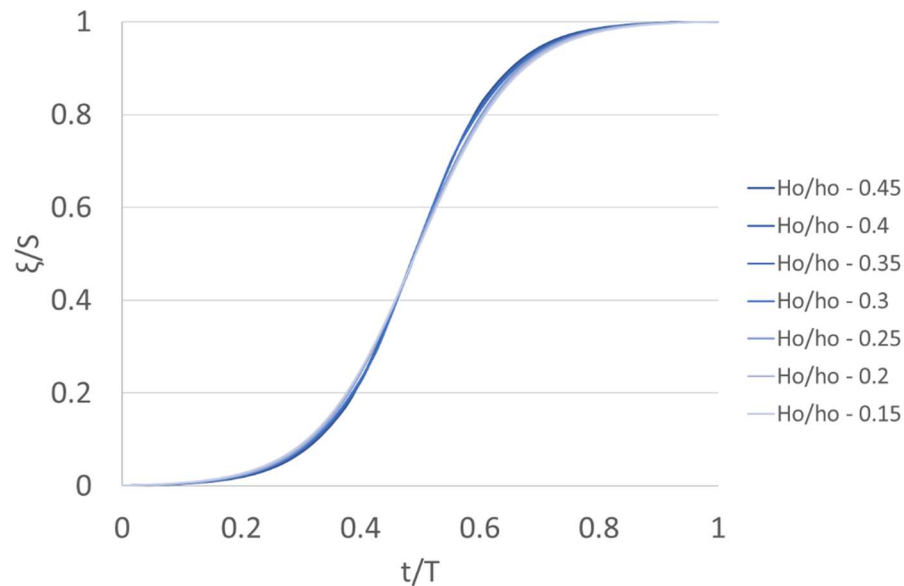
Figure 4-2 Solitary wave generation mechanism. ξ is the position of the paddle with respect to time t. S is the total stroke length, and T is the entire time of the movement of the paddle. H_o – wave height, h_o – still water depth.

The one sidewall of the flume was glass, and other sidewall and floor were made of smooth painted steel. The compound sloping beach was made of marine plywood painted with water-resistant paint. A schematic figure of the experimental setup is shown in Fig. 4-3. The maximum runup on the compound slopes was observed to investigate the effect of offshore slope (s_1) and onshore/final slope (s_2). The foreshore slope (s_1) was changed as

1/7 and 1/10, whereas the onshore slope (s_2) was fixed as 1/4. The vertex of the compound slope was set at 23cm from the bottom of the flume. The water depths (h_o) of 20, 23, 26 and 30cm are used as given in Table 4-1. Seven different solitary wave heights, ranging from 3 to 9 cm for a water depth of h_o, was used as the input wave height values to the wavemaker program. The measured offshore wave heights (H_o) ranged from 2.4 to 8.3 cm. The wave height to depth ratio (H_o/h_o) was varied from 0.1 to 0.4. The current experimental database includes 84 tests for the estimation of runup changing the settings of h_o, H_o and s.

Table 4-1 Experimental condition for compound slope case. s_1 – foreshore slope, s_2 – onshore slope.

Case	$1/s_1$	$1/s_2$	H_o	h_o
Present-7-4	7	4	2.4-8.3	20,23,26,30
Present-7-10	7	10	2.4-8.3	20,23,36,30
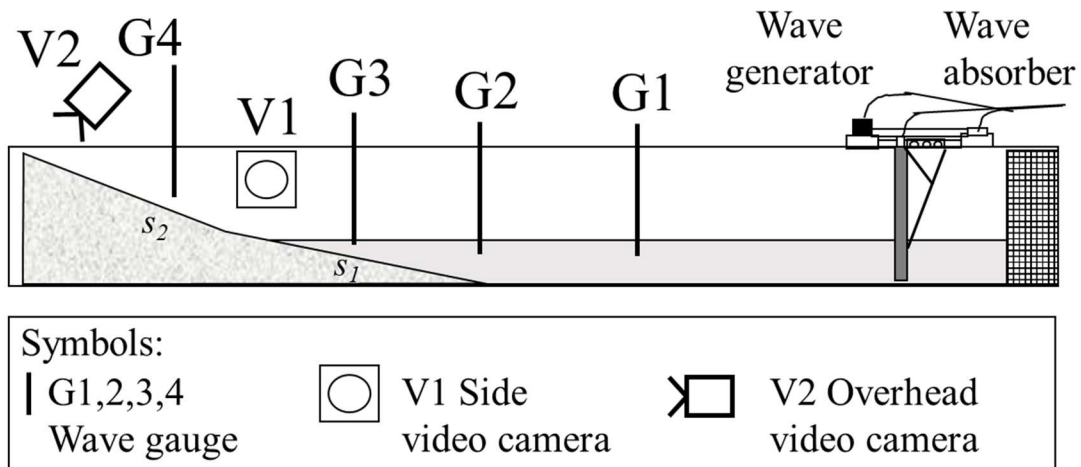
Figure 4-3 Experimental setup for compound slope.

The change of water surface elevation was measured using capacitance-type wave gauges with a frequency of 100Hz. The calibration of wave gauges was done by the standard method of lowering systematically into the water and recording the output voltage accordingly. To establish the desired wave heights, H_o of the incident wave and to estimate

the wave reflection, a preliminary run without any slope was conducted in the wave flume for all combinations of H_o and h_o values considered in this study. The reference wave gauge G1 was placed at 6 m from the piston. The horizontal distance from the wave gauge G1 to the toe of the beach slope was kept more than 5 m. The results ensured that there was no significant peak reduction caused by the sloping beach. The input value to the wavemaker and the measured wave heights by reference wave gauge G1 were slightly different for all H_o values. Therefore, the measured wave heights by wave gauge G1 were used to define the offshore wave heights (H_o). Additional measurements of the water surface elevation were taken at the toe of the sloping beach and further onshore, as shown in Fig. 4-3.

The maximum runup was tracked by an overhead camera based on the marker lines on the runup board with an accuracy of 5 mm. Some tests were randomly repeated and found that the results of maximum runup showed consistency within 5 mm range for an input value of offshore wave height (H_o) to the wavemaker program. The measured data were employed to analyse the wave breaking and the runup height. The applicability of Eq. (3-19) was tested for compound slope cases conducted in the present experiments and with Camfield and Street (1969), Baldock et al. (2009), and Saelevik et al. (2013).

4.3 Results and Discussion

The actual result of wave transformation was minorly deviated from the input H_o value into the program for a particular still water depth, h_o. The results of wave generated profiles with the Boussinesq first-order wave solution given by Eq (3-1) was compared. It was found that for higher wave height to depth ratios ($H_o/h_o > 0.2$) the generated solitary wave profile deviated from the theory as shown in Fig. 4-4, where the undulating tail was observed for higher-order waves as also identified by Goring (1979).
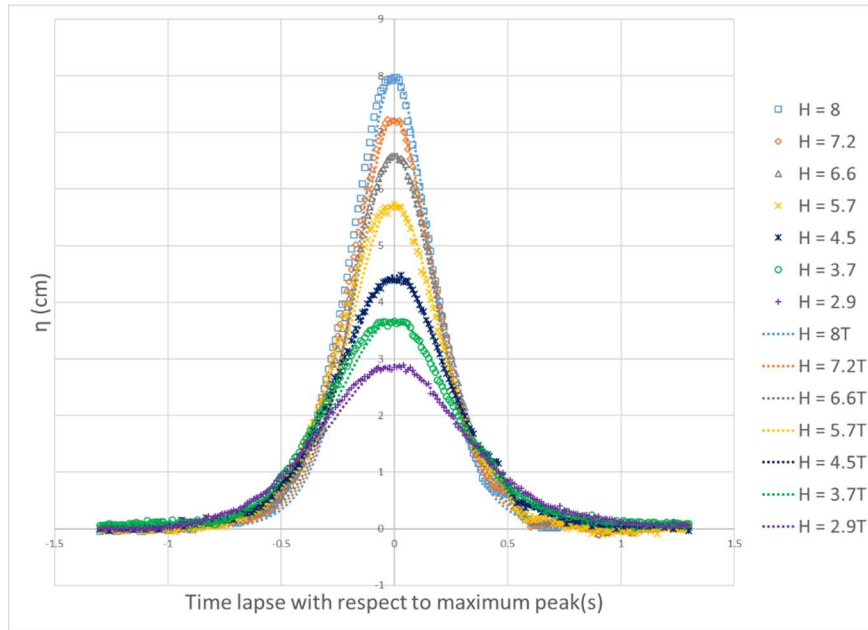
Figure 4-4 The comparison of generated wave profile (H_o) with the respective wave theoretical profile given by Eq. (3-1). Open plots denote the measured values and dotted lines denote the theroretical results.

Many researchers used non-dimensionalised runup as runup over wave height (R/H_o) to use their expressions (Vinodh and Tanaka, 2020). They have shown for a given H_o/h_o, the non-dimensionalised runup (R/H_o) tends to increase as the slope decreases up to the point where the waves begin to break. Then the non-dimensionalised runup of breaking waves declines as the slope continues to decrease. At near breaking, the maximum runup could be observed for a particular (H_o/h_o). The non-dimensionalised runup (R/H_o) of nonbreaking waves also increases as the wave height to depth ratio (H_o/h_o) increases as a result of nonlinear effects. The non-dimensionalised runup of breaking waves decreases as the wave height to depth ratio increases as a result of turbulent dissipation. The disadvantage of using R/H_o, especially for small waves, is that experimental error can be significantly amplified since both R and H_o are measured values with more significant uncertainty compared to the still-water depth h_o. Hence the use of the form of R/h_o is better for the derivation of empirical models.

Table 4-2 shows the experimental conditions of previous researchers' work which have been used in this study. The experimental results were plotted in Fig. 4-5. Camfield and Street's work (CS(1969)), Baldock and others' work (B(2009)), and Sælevik and others' work (S(2013)) were also included in Fig. 4-5.

Table 4-2 Experimental conditions for compound slope case of other researchers work (B(2009) – Baldock et al. (2009), CS(1968) – Camfield & Street (1969), S(2013) – Sælevik et al. (2013).. s_1 – foreshore slope, s_2 – onshore slope).

Case	$1/s_1$	$1/s_2$
S(2013) 5.7-14.3	5.7	14.3
CS(1968) 100-7.1	100	7.1
CS(1968) 50-7.1	50	7.1
CS(1968) 100-14.3	100	14.3
CS(1968) 50-14.3	50	14.3
B(2009)	15	30
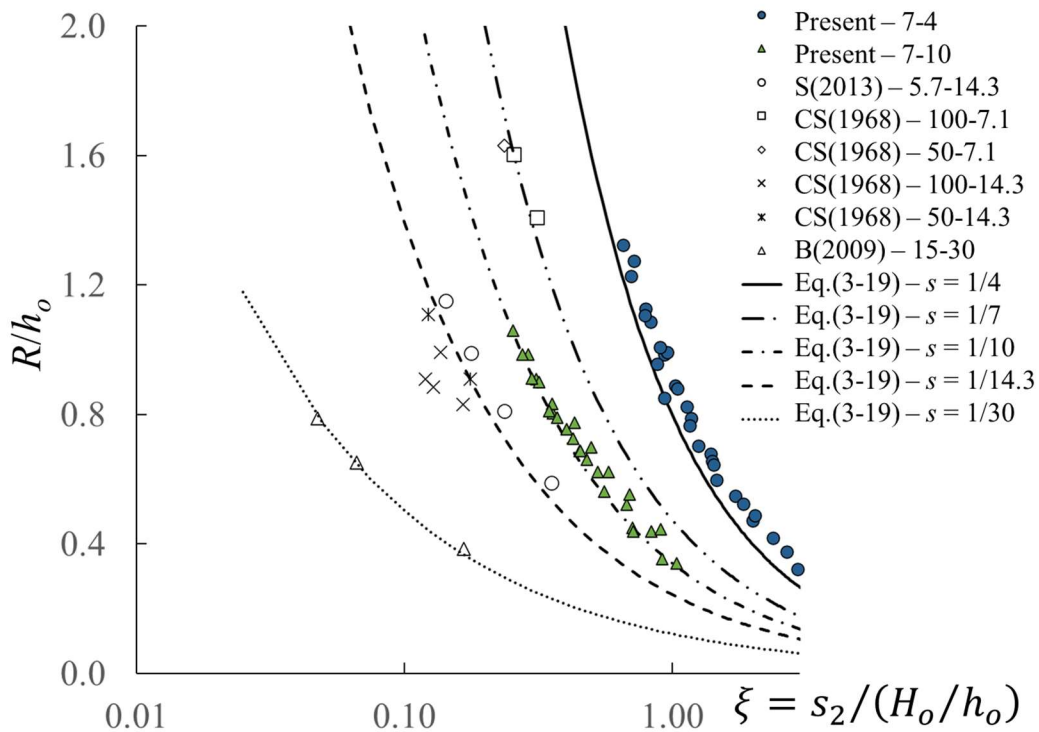
Figure 4-5 Experimental results for compound slopes of present work and other researchers work (B(2009) – Baldock et al. (2009), CS(1968) – Camfield & Street (1969), S(2013) – Sælevik et al. (2013)).

It could be observed that the non-dimensionalised runup (R/h_o) for a compound slope is well explained by Eq. (3-19) by substituting s as onshore slope/final slope, s_2. The results also comply with the analytical derivation of Kanoglu and Synolakis (1998). These results inspired us to derive an equation for the estimation of solitary wave runup on dune coastal lagoon using the slope, s_2 by following the form of the Eq. (3-19) as discussed in Chapter 6.

The scattering was observed for highly nonlinear wave ($H_o/h_o > 0.6$) where empirical equation overpredicts. The condition of underprediction for highly nonlinear waves was also noticed in the results of runup on a plane beach (Vinodh and Tanaka, 2020).

4.4   Conclusion

Solitary wave runup on compound slopes consisting of 1/10 and 1/4 as onshore slopes and 1/7 as fixed foreshore slopes, has been tested. The present experimental results and the previous research works carried out by Camsfield and Street (1969), Baldock et al. (2009) and Sælevik et al. (2013) were also compared by using Vinodh and Tanaka (2020)'s empirical equation for solitary wave runup on a plane beach. It was found that the runup on compound slopes can be estimated by substituting the final beach slope value into the Vinodh and Tanaka (2020)'s equation. Therefore, it can be concluded that the final beach slope is the most influential parameter in the estimation of runup on compound slopes, where the still water level is not so below the vertex. The result also complies with the analytical proof by Kânoğlu and Synolakis (1998).

Chapter 5

Runup with Forest

5.1 Introduction

The coastal forests and mangroves were observed to help protect beaches from both long waves like tsunami waves (Tanaka et al., 2007) as well as short waves like wind waves (Massel et al., 1999) have been proved by field studies. By observing the importance of coastal trees in tsunami mitigating, there are numerous field studies, numerical, analytical and experimental findings to understand the hydrodynamics and the physical process related to the coastal trees. A forest is useful as it stops water-borne driftwoods and debris, reduces both flow velocity and inundation height provides lifesaving means by catching persons carried off by the tsunamis. In addition, forest collects windblown sand and raises sand dunes, which act as a barrier against tsunamis (Tanaka et al., 2009, 2007). Based on data analyses by Tanaka et al. (2009) and Samarakoon et al. (2013), a forest with two layers in the vertical direction of dense *Casuarina equisetifolia* and *Pandanus odoratissimus* grown in beach sand were found to be useful in tsunami mitigation due to their complex aerial root structure and density. A pilot project in the Matara City of Sri Lanka has already initiated (Tanaka, 2009) and become successful in planting with the participation and support from local authorities and communities. An adverse opinion is that a forest may be ineffective against a huge tsunami, as trees themselves could become destructive forces to houses if they uprooted by the tsunami (Tanaka et al., 2013). Depend on the tree species, and their vegetation characteristics, the reduction effect of tsunami inundation depth varies and is mostly lost in case of tsunami inundation depth reached beyond 5 to 6m (Shuto, 1987; Tanaka et al., 2007; Yanagisawa et al., 2009). Chatenoux and Peduzzi (2007) statistically analysed the seagrass areas. They found that lower impacts in the area behind seagrass beds implying that either seagrass bed acting as a damping filter that helps to

reduce the energy of the wave or because the seagrass beds are located in areas where the configuration of bathymetry is not favourable for wave amplification.

Laboratory experiments have been widely used to study wave-current-vegetation interactions and relevant physics (Nepf, 2012). In most of the experimental studies, an array of rigid cylinders is usually used to represent coastal trees and mangroves to derive analytical expressions. Flexible tubes or even natural vegetation are used to model wetlands or marshes. Huang et al. (2011) and Yao et al. (2015) conducted laboratory experiments on solitary waves with an array of emergent rigid cylinders in different sizes and both staggered and tandem arrangements. Yao et al. (2015) found that the runup reduction difference between tandem and staggered configurations of the trees could reach up to 20%. Irtem et al. (2009) investigated the runup with coastal forest by modelling as artificial trees and cylindrical timber sticks on a sandy slope. Irtem et al. (2009) in their experimental cases, found that with the artificial trees, runup heights were reduced by 15% and 22% for tandem and staggered layouts respectively. Ismail et al. (2012) found that the densities of the mangrove forest do not influence the runup reduction as significantly as the forest widths, and mangrove roots are more effective in reducing the runup compared to the trunks and canopies. Iimura and Tanaka (2012) investigated the tsunami mitigation capability of vegetation by changing the density distribution. They found that dense vegetation increased the reflection, and hence the resistance by vegetation was also increased because of the water surface slope in the vegetated region was increased. Strusinska-Correia et al. (2013) have done extensive studies with the parameterised tree models, which simplify the chaotic root structure of mangroves of *Rhizophora* species.

The forest patches are more generally observed in the coastal region. Thuy et al. (2009) experimentally and numerically studied the effect of an open gap in a coastal forest on wave runup. They found that the open gaps within coastal forests significantly enhanced the damage to those areas behind gaps. Irish et al., (2014) investigated on patchy macro-roughness, like that created by coastal forest and have shown that lead to increased protection in some areas and decreased protection in other areas. Yang et al. (2017) show that patchy vegetation with an appropriate configuration can be useful as a continuous forest belt in tsunami mitigation.

Significant improvements in the modelling of runup have appeared as a result of advancements in both computational techniques and theoretical understandings (see review by Kirby (2017) and Shuto (2019)). Some of them are extended to capture the large roughness effect on runup by forests. They have used either a constant roughness model or equivalent roughness model with numerical simulations based on nonlinear long-wave equations, Reynolds-averaged Navier-Stokes (RANS) and/or large eddy simulation (LES), drag and inertia forces using Morison-type equations, macro-scale (wavelength) equations or multi-scale perturbation technique (homogenisation theory) (see, e.g., Chang and Liu, 2019; Dalrymple and Hwang, 1984; Mei et al., 2014; Stoesser et al., 2010; Tanaka et al., 2018).

Massel et al. (1999) showed that when a wave transmits through vegetation, wave energy is dissipated by turbulence, which is correlated to work done by the drag forces. The localised presence of arrays of emergent cylinders causes high energy dissipation at the bottom of or throughout the water depth causes an incident waves to diffract and attenuate (Dalrymple and Hwang, 1984; Zhu and Chen, 2017). The applications of these theoretical models need proper calibrations of the drag coefficient (C_D) performed by best fitting the experimental or modelled wave heights (Chen and Zhao, 2012). Parameterisations of C_D using wave and vegetation-related quantities, such as the Reynolds number (Re) and Keulegan-Carpenter number (KC), can be found in the literature (Mendez and Losada, 2004; Tanino and Nepf, 2008). Dean and Bender (2006) described the problem of runup with a forest by using wave setup phenomena. When the waves propagate through vegetation, the energy loss by asymmetries of the near-bottom water particle velocities will cause a transfer of momentum and an associated wave setup or wave setdown. Nepf (2012) showed that vegetation creates spatial variation to flow. Within a plant canopy, the critical length scales change from the flow depth (associated with unobstructed flows) or flow depth and channel width (for bathymetrically constrained flows) to scales defined by the stem diameter (D), stem length (l), stem spacing (ΔS) and frontal area density (A). This change of scales modifies the velocity profiles and results in damping of larger-scale motions but introduces turbulence (through vortex shedding and wake generation) at smaller stem scales. The behaviour of flows is also governed by the level of submergence defined as the ratio of plant height to water depth (l/h).

Although those above numerical, analytical and empirical models describe the phenomena of wave-current-vegetation interaction well, the runup effect of forest on a sloping beach is poorly understood. Empirical runup expressions for tsunami-like solitary waves are convenient for obtaining a first assessment of tsunami impact on the beach. Both analytical and empirical solutions which describe solitary wave runup on the plane slopes (i.e., a constant depth region followed by a plane slope) exist and well explained. Besides, such models either have been ignored the effect of vegetation for simplification or can only be applicable for limited wave conditions and slopes. Hence in this chapter, the derivation of an empirical model which includes the effect of bathymetry slope and forest density and the comparison with existing previous research work is presented.

5.2   Materials and Methods

The flume arrangement and the experimental procedure were similar to the cases of the plane beach and compound slopes, as explained in Section 4.2. The coastal trees were modelled by vertical, rigid and surface piercing cylinders, where the effects of branches and roots are neglected. The scale of 1:100 was used for the experimental study for measuring the runup against the forest model. The spacing (ΔS) and diameter (D) were chosen as 23mm and 5mm respectively which give the proportion of volume occupied by the solid canopy (ϕ) as 0.037 ($\phi = (\pi/4)(D/\Delta S)^2$) and the frontal area density (A) as 0.009 ($A = D/\Delta S^2$). The present arrangement of the tree model also implies that it may often be valid to neglect the interactions between stems as ϕ <0.08 (Mullarney and Henderson, 2018; Raupach, 1992). The forest model width (W) was changed as 20cm and 40cm in cross-shore direction, and it was arranged in a staggered system and modelled as the rigid trunk of trees which was enough to keep the top of trees under the emergent condition for all wave conditions. The forest model was placed on the slopes (s_1) of 1/4 and 1/7, as shown in Fig.5-1. It corresponds to the case where a tree trunk is above water. Yao et al. (2015) have studied the cases correspond to a high tide condition where a significant portion of the mangrove tree trunk underwater. The water surface elevations were measured at four locations using four capacitance-type wave gauges. The maximum runup was measured by V1 overhead camera, as shown in Fig. 5-1. Incident solitary wave conditions and the forest model configurations for the present is given in Table 5-1.
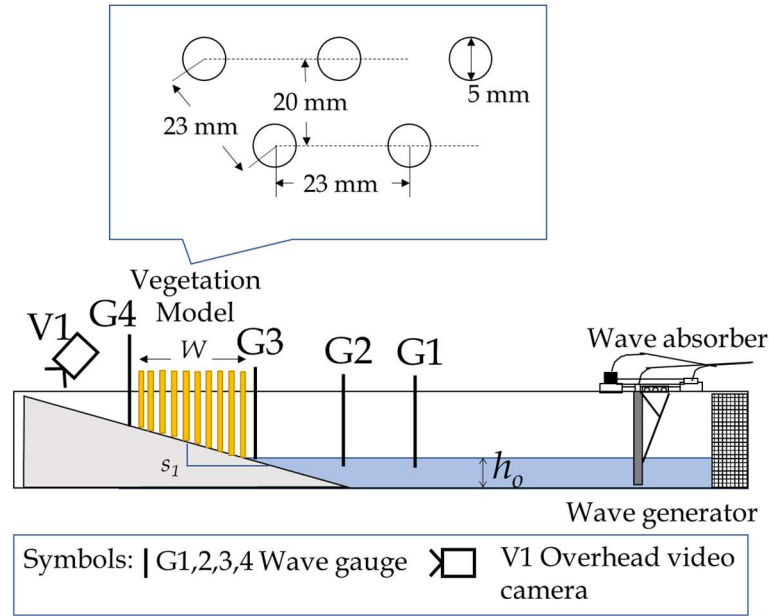
Figure 5-1 Experimental setup for forest model on a sloping beach.

Table 5-1 Experimental condition for present work. W, Φ, s, H_o and h_o are indicated as the width of forest model, solid volume ratio, slope, initial wave height and still water depth, respectively.

Case	W(cm)	Φ	Arrangement	$1/s$	H_o (cm)	h_o (cm)
S4				4	2.4-8.3	20,22,30
S4W20St0.037	20	0.037	Staggered	4	2.4-8.3	20,22,30
S4W40St0.037	40	0.037	Staggered	4	2.4-8.3	20,30
S7				7	2.4-8.3	20,30
S7W20St0.037	20	0.037	Staggered	7	2.4-8.3	20,30

The current experimental database includes 55 observations with a forest model by changing the slope of the beach and the width of the forest. At first, the runup results of a sloping beach with and without forest model was compared with the empirical solution given by Eq. (3-19) and effect of solid volume ratio (Φ) and width of forest (W) in the form of expression given below.

$$\left(\frac{R}{h}\right)_{forest\ on\ slope} = f\left[\left(\frac{R}{h}\right)_{slope}, \phi, W\right] \tag{5-1}$$

68

Also, the results of Yao et al. (2015) who tested the runup on a different slope (i.e., $s=1/8$) and changing the tree model arrangement by staggered and tandem, were also compared with Eq. (3-19). Finally, the present experimental results with Yao et al. (2015) experimental results were used to derive an empirical model which include the parameters of slope (s) and solid volume ratio (Φ) by using linear regression analysis.

5.3   Results and Discussion

The solitary wave evolution and the runup results have already been explained in detail in Vinodh and Tanaka (2019). The derivation of the empirical equation is shown in this chapter. The experimental conditions for Yao et al. (2015), which was used in this study are given in Table 5-2. Photo snapshots taken for the runup with and without a forest model on the sloping beach are shown in Fig. 5-2.

From the Fig. 5-3, by comparing the values of the runup on a plane beach and the forest on a sloping beach, it is evident that the runup has been reduced significantly for all slopes of 1/4, 1/7 and 1/8. By increasing the width of the forest (W) by twice (i.e., S4W20St0.037 and S4W40St0.037), the runup was further reduced. In the experimental work of Yao et al. (2015), by increasing the solid volume ratio, and from tandem to a staggered arrangement, the runup has been further reduced. Based on 80 observations including present work and Yao et al. (2015) and using multiple linear regression analysis, for maximum runup (R) can be derived in the form of Eq. (5-1) and can be expressed

$$\frac{R}{h_o} = (2.9049 s^{0.931} - C_1 \phi s) \left[\frac{s}{(H_o/h_o)} \right]^{(-0.1931 \ln s - 1.2704 + \, _2 \phi s)} \tag{5-2}$$

where s is the slope, Φ is solid volume ratio, H_o is wave height, and h_o is still water depth. The coefficients C_1 is 17.30 and C_2 is 15.98. Hence the forest width analysed in this study were varied as 20, 30 and 40cm, both C_1 and C_2 can be dependent on forest width.

Figure 5-2 Photo snapshots of solitary wave runup on beach slope (*s*) of 1/4, wave height (*H_o*) of 8.3cm and water depth (*h_o*) of 22 cm.

Table 5-2 Experimental conditions for Yao et al. (2015). W, Φ, s, H_o and h_o are indicated as the width of forest model, solid volume ratio, slope, initial wave height and still water depth, respectively.

Case	W(cm)	Φ	Arrangement	$1/s$	H_o (cm)	h_o (cm)
Y8	30			8	2-10	30
Y8W30Ta0.022	30	0.022	Tandem	8	2-10	30
Y8W30St0.022	30	0.022	Staggered	8	2-10	30
Y8W30St0.044	30	0.044	Staggered	8	2-10	30
Y8W30Ta0.087	30	0.087	Tandem	8	2-10	30
Y8W30St0.087	30	0.087	Staggered	8	2-10	30
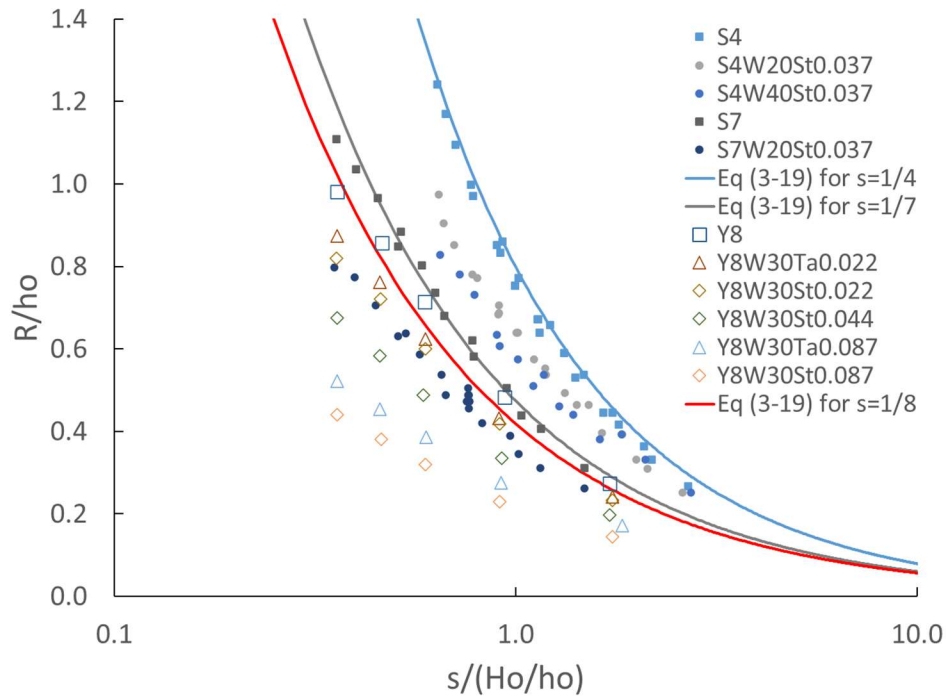
Figure 5-3 Experimental results for the forest on a sloping beach of present work and Yao et al. (2015). Filled symbols and open symbols represent the data for current work, and Yao et al. (2015), respectively. For the abbreviations, refer to Table 5-1 and Table 5-2.
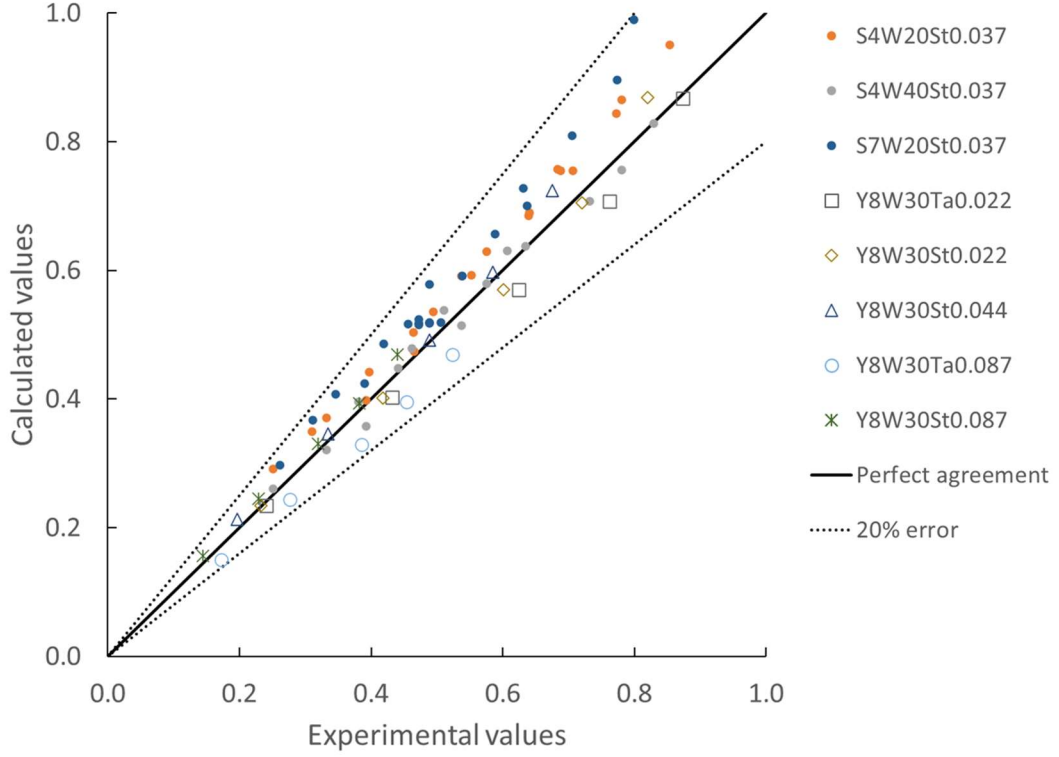
Figure 5-4 Comparison of experimental values and calculated values by Eq. (5-2) for present work and Yao et al. (2015). Filled symbols and open symbols represent the data for current work, and Yao et al. (2015), respectively. For the abbreviations, refer to Table 5-1 and Table 5-2.

Moreover, the statistical measures of the mean absolute error, MAE $=\sum_{i=1}^{N}|C_i - M_i|/N$, the root-mean-square, RMSE $=\sqrt{\frac{1}{N}\sum_{i=1}^{N}(C_i - M_i)^2}$, the scatter index, SCI = RMSE/$\bar{M}$ and correlation coefficient, $R^2 = \frac{[\sum_{i=1}^{N}(C_i - \bar{C})(M_i - \bar{M})]^2}{\sum_{i=1}^{N}(C_i - \bar{C})^2 \sum_{i=1}^{N}(M_i - \bar{M})^2}$ were calculated. C_i and M_i denote the calculated and the measured data, respectively and N, is the total number of evaluated data points. The results for the present proposed method show that MAE = 0.041, RMSE = 0.003, SCI = 0.005 and R^2 = 0.959. Also, an agreement index C_R (Willmott, 1981) was used to evaluate the accuracy of the empirical equation.

$$C_R = 1 - \frac{\sum_{i=1}^{N}(C_i - M_i)^2}{\sum_{i=1}^{N}[|C_i - \bar{M}| + |M_i - \bar{M}|]^2} \qquad (5\text{-}3)$$

The value of C_R gives as 0.983, implying the proposed empirical solution satisfy well with the collected data points. The statistical measures show that the correlation between the experiments and the calculated by the proposed equation is very high. Note that the

72

proposed Eq. (5-2) does not contain the parameter, W, the width of the forest as in this experimental database the forest width was varied between 20cm to 40cm giving lesser impact in the deviation to the results. However, the proposed empirical solution is shown goodness of fit with experimental data as all the data lies within the 20% error range as in Fig. 5-4. Hence the proposed empirical equation can be used to apply for estimating solitary wave runup on sloping beach with the forest.

The forest effectively reduces solitary wave runup around 4% to 28% and higher runup reduction was occurred on mild slopes with highly nonlinear waves. By increasing the forest width by twice its previous value, the runup reduction can be further increased from 6% to 27%.

5.4   Conclusion

Laboratory experiments were conducted using solitary waves to understand the wave runup on a sloping beach with forest. The forest effectively reduces solitary wave runup from 4% to 28%. The higher runup reduction occurred on mild slopes with highly nonlinear waves. By increasing the forest width by twice, the runup reduction can be further increased from 6% to 27%. By using 80 observations from the present experiments, including 25 observations from other researchers' work, an empirical equation was derived using multiple linear regression analysis. It was found that the proposed empirical equation predicts the runup reasonably well that all data found to be satisfactorily posed in 20% error range. Statistical measures mean absolute error (MAE), root-mean-square error (RMSE), scatter index (SCI), correlation coefficient (R^2) and agreement index (C_R) were calculated and found as 0.041, 0.003, 0.005, 0.959 and 0.983, respectively. Therefore, the proposed empirical equation can be used to predict solitary wave runup on a sloping beach with a forest model of finite width.

Chapter 6

Runup with Sand Dune Coastal Lagoon

6.1   Introduction

It could be observed that nearby the lagoon the tsunami impact was low during the post-tsunami field surveys of the 2004 IOT (Dahdouh-Guebas et al., 2005b; Inoue et al., 2007). In Palatupana of Sri Lanka, the inundation depth at the back of the lagoon is around 60% less than the inundation depth at the front of the lagoon, indicating that the tsunami would be reduced by the lagoon as illustrated by Inoue et al. (2007). Wijetunge (2009a) has shown that the relatively massive extents of the salterns have also acted as sinks to absorb and spread water whilst the sand dunes, where present with sufficient elevation, prevent the buildings in their shadow being damaged from the direct impact of the tsunami. Wijetunge (2006) reported that around Batticaloa and Kalkudah, the lagoons and other water bodies have helped convey the tsunami surge large distances inland. Wijetunge (2006) also observed that the deepest tsunami wave penetration in the south coast was at Hambantota, up to three kilometres near the saltpans, and near Bundala with the aid of the bay. Hungama-Tangalle beach to the west of Hambantota has recorded a significant inundation, mainly where tsunami surges had been transmitted inland through lagoons and lakes from the opening to the sea. Wijetunge (2009b) found that the surging tsunami had propagated over the barrier spits and then into the lagoons in Batticaloa, which in some instances,

unable to absorb all of the overland flow. Hence, the tsunami had spilt over and flooded inland areas that would otherwise not have received direct inundation. In Hambantota, hundreds of buses, many allegedly carrying passengers, were reportedly swept into the Karagan Lewaya behind Hambantota town, necessitating a massive clearance effort (Synolakis et al., 2005). Another negative aspect of tsunami damage was the decrease in flood control capacity of the lagoon due to the deposition of the enormous amount of sediments brought in by the seawater. However, the trapping debris inside a lagoon and forming a pool of water higher than the mean sea level would reduce the further damage by the following tsunami waves in a wave train towards the inland after hit by first few tsunami waves.

In real tsunami overflowing conditions, the runup experiences a truncated beach if it exceeds the dune crest, and then inundated and runup. The transformation of waves across the lagoon is a complex problem, including the processes of shoaling, focusing and defocusing, breaking and energy dissipation by bottom friction. An integrated study concerning solitary wave interact against the vegetation and lagoon is relatively limited and in need of evaluating the capability of the coastal lagoon in tsunami mitigation. The runup reduction and the wave evolution characteristics have been explained in the authors' previous work (see Vinodh and Tanaka, 2018a, 2018b, 2018c). An approximate and accurate prediction of wave runup with the interaction with the coastal landscape is crucial for the applications in coastal engineering. Hence, this study aims to derive a runup formula for solitary waves on a sand dune coastal lagoon in one horizontal dimension based on the experimental laboratory conditions.

6.2 Materials and Methods

The problem of runup and overtopping along a lagoon has not been agreeable to complete theoretical treatment due to the complexity in analytically explaining as many factors involved. Dimensional analysis is utilized to define the essential non-dimensionalised parameters to describe the problem.

Fig. 6-1 shows the experimental setup and essential parameters in this study. Referring to Fig. 6-1(a) and Fig. 6-1(c), if a functional relationship exists between the runup and the description of the incident wave characteristics and the physical parameters of the lagoon,

for solitary waves impinging on a coastal lagoon at normal incidence in 1HD, this relationship can be expressed;

$$f(R, H_o, L_o, h_o, L_b, h_D, s_1, D, l, \Delta S, W, \tan \alpha, s_2, h_L, L_L) = 0 \qquad (6\text{-}1)$$

Figure 6-1 (a) Definition of parameters for solitary wave runup with vegetated-sand dune-coastal lagoon, (b) Experimental setup, (c) Arrangement of forest model.

The maximum runup (R) at the landward end of the lagoon can be identified depending on the incident wave characteristics, the upstream wave height (H_o), wavelength (L_o) and

water depth in the constant depth region (h_o), and lagoon physical characteristics, beach length (L_b), sand dune height (h_D), beach slope (s_1), the diameter of trees (D), tree height (l), vegetation spacing (ΔS), forest width in cross-shore direction (W), the back slope of the sand dune ($\tan\alpha$), slope of landside in the lagoon (s_2), initial lagoon water depth (h_L) and the lagoon length in cross-shore direction (L_L). The water surface elevation change, $\eta\,(x, t)$ concerning time t was measured. Space x was chosen near the toe of the beach slope ($x=X_o$) for incident wave height (H_o) and at the toe of rearmost slope ($x=X_T$) for wave transmission height (H_T) to analyse the wave evolution nearby the lagoon. Fig. 6-1(c) explains the definition of vegetation arrangement. The transmission coefficient (H_T/H_o) and the non-dimensionalised runup denoted by R/h_o (maximum runup over water depth) and R/H_o (maximum runup over wave height) were used in analysing the effect against the single slope, the lagoon model and the forest model.

The experiments were performed in a flume with 20m, 0.3m and 0.6m in length, width, and height, respectively, at Hydraulic Laboratory in Saitama University. The measurement of water level was done by using wave gauges with a sampling frequency of 100Hz and an accuracy of 0.1mm. The scale of 1:100 was used for the experimental study for measuring runup against the lagoon model with and without forest model. The front beach slopes (s_1) of 1/1, 1/2, 1/4, 1/7 and 1/10 was tested to obtain plunging breaking, surging breaking and nonbreaking solitary waves. The connecting sand dune ridge between the beach slope and the lagoon bottom was established as a trapezoidal section with a lagoon inside slope ($\tan\alpha$) as 1/7. The experiments with a convex slope section made by a smooth plastic sheet were conducted instead of the trapezoidal section to observe the effect of back slope ($\tan\alpha$) of a sand dune. The model continued a horizontal bed followed by a slope (s_2) of 1/4, and they were made of wooden planks painted with water-resistant paint. A simplified approach to physical modelling of the sand dune has been presented here assuming the slope of both beach and sand dune are same and nonerodable. Better details regarding erosion process and different slopes are required when dealing against the real sand dune with vegetation as dune protection. The horizontal distance from the wavemaker to the still water shoreline was kept more than 7 m always, which is approximately equal to the wavelength of the lengthiest wave generated. More than 10 minutes of waiting time were allowed in between two successive experimental runs, to make sure that the water surface returned to the

quiescent state. The side video camera, V1 was used to visualise the wave phenomena occurred inside of the forest model and the breaking characteristics at the beach slope. The breaking features inside the lagoon was observed by a side video camera, V2. The maximum runup was examined by overhead camera V3 and measured by image analysis to the accuracy of 5mm based on the marker lines on the runup board. The wave gauge G1 and G4 were placed to measure the incident wave height (H_o) and the transmitted wave height (H_T), respectively. The parameters were changed according to Table 6-1.

Table 6-1 Experimental cases for sand dune coastal lagoon (TR – trapezoidal shape, CO – convex slope). The parameters referring to s_1, s_2, h_o and h_L are beach slope, final slope/landside slope, sand dune height and lagoon inside water depth, respectively.

Case No	$1/s_1$	$1/s_2$	h_o(cm)	h_D(cm)	h_L(cm)	TR/CO
1	1	4	20	3	4	TR
2	2	4	20	3	4	TR
3	4	4	20	3	4	TR
4	7	4	20	3	4	TR
5	10	4	20	3	4	TR
6	7	4	22	1	6	TR
7	7	4	20	3	4	CO
8	7	4	21	2	5	CO
9	7	4	22	1	6	CO
10	7	4	20	3	12	CO
11	7	4	20	5	10	CO
12	7	4	22	3	12	CO
13	7	4	20	5	12	CO
14	7	4	21	4	13	CO
15	7	4	22	3	14	CO

In all experimental cases with the lagoon model, the water level in both seaside and lagoon inside were kept as same by changing the initial lagoon depth (h_L) and changing upstream water depth (h_o). Note that during the flood tide and ebb tide the water level fluctuates and the water level is not the same. In this study, those fluctuations were not considered and hence ignored the effect of current produced by tidal change and concentrated on the wave component only. The sand dune height (h_D) was also adjusted by raising in the case of the convex slope as the back slope (s_2) and beach slope (s_1) as 1/7. The lagoon length (L_L) was fixed as 50cm for all the cases. The effect of crest width and lagoon length in cross-shore direction was not taken into modelling physically, and the horizontal length scale of a tsunami was found to be challenging to match with real conditions due to the limited length scale of the flume. More attention was given in to find out energy dissipation by turbulence and wave reflection rather than the bed friction losses due to wave travelling over the crest width and along the cross-shore.

The forest model was placed on the front slope of a sand dune (LFV), on the middle of the sand dune (LMV), on the back slope of a sand dune (LBV) and the front, middle and back of a sand dune (LAV), as shown in Fig. 6-2 and Table 6-2. The forest model was used to represent the forest grown on a sand dune and the rigid trunk of trees which was enough to keep the top of trees under the emergent condition for all wave conditions.

Table 6-2 Experimental conditions for sand dune coastal lagoon with the forest

Case	Front Slope ($1/s_1$)	Water depth (h_o, cm)	Vegetation width (W, cm)	Model arrangement
LFV	7	20	20	Lagoon model with forest on front slope of sand dune
LMV	7	20	20	Lagoon model with forest on horizontal surface of sand dune
LBV	7	20	20	Lagoon model with forest on back slope of sand dune
LAV	7	20	60	Lagoon model with forest on front, middle and back of sand dune
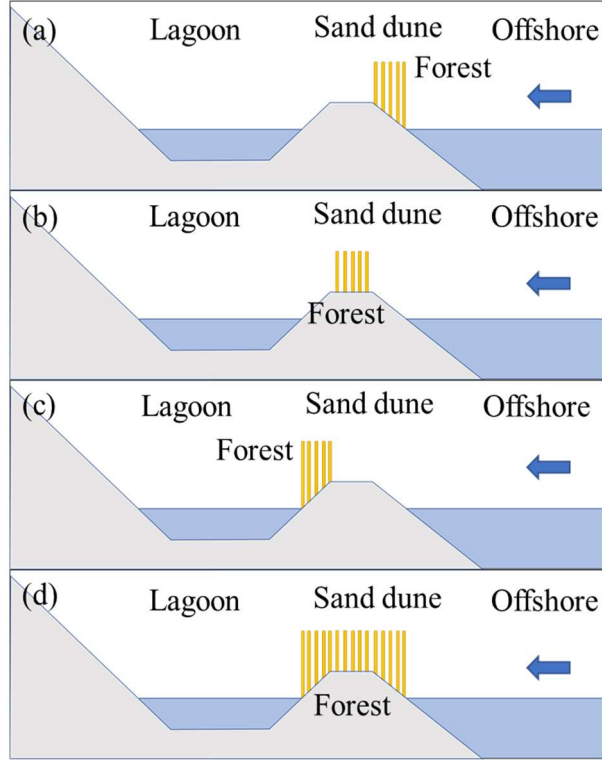
Figure 6-2 The placement of forest model for $s_1=1/7$, $s_2=1/4$, $h_o=20$cm, $h_D=3$cm and $h_L=4$cm (a) front slope (LFV), (b) horizontal bed (LMV), (c) back slope (LBV) and (d) combination of all (LAV).

The forest model width (W) was changed as 20cm in LFV, LMV and LBV, and 60cm in LAV along the cross-shore direction. The water depth (h_0) was kept constant as 20cm for experiments with lagoon model and forest model to obtain a runup relationship.

The maximum orbital velocity in open water, U_o occurs under the wave crest, is given by (Pujara et al., 2015).

$$U_o = \frac{H_o}{h_o}\sqrt{gh_o} \tag{6-2}$$

According to Sumer et al. (2010), who studied the transition from the laminar bottom boundary layer to turbulence in a solitary wave, relevant Reynolds number, Re_o was defined as

$$Re_o = \frac{a_o U_o}{\nu} \tag{6-3}$$

Here v is the kinematic viscosity of water and a_o is the length scale which is the half-excursion-length for a water particle, given by

$$a_o = \frac{U_o}{kc} \qquad (6\text{-}4)$$

where k and c are wavenumber and wave celerity, respectively. In all cases, the range of Reynolds number in the constant depth region (Re_o) is from 1.5 x 10^4 to 7.2 x 10^4 which falls under the regime of transition to turbulence at Re_{cr} 5 x 10^5 (Sumer et al., 2010). In these test conditions, the water temperature was 20˚C and kinematic viscosity was taken as 1.0×10^{-6} m^2 s^{-1}. The tree spacing (ΔS) is 23mm which give the proportion of volume occupied by the solid canopy (ϕ) as 0.04 ($\phi = (\pi/4)(D/\Delta S)^2$) and the frontal area density, A as 0.009 ($A = D/\Delta S^2$). This also implies that it is valid to neglect the interactions among the stems as $\phi < 0.08$ (Mullarney and Henderson, 2018; Raupach, 1992).

A stem Reynolds number Re_t, is defined by

$$Re_t = \frac{DU_o}{v} \qquad (6\text{-}5)$$

In the present experiments, 9.26 x $10^2 < Re_t < 2.8$ x 10^3.

6.3 Results and Discussion

6.3.1 Wave transformation and runup on a sand dune coastal lagoon without a forest

The results for the maximum runup with a sand dune coastal lagoon model (R/h_o) for the cases illustrated in Table 6-1, were plotted against the surf-similarity parameter, ξ given by $s_2/(H_o/h_o)$. The maximum runup on a single slope is reduced by introducing the sand dune coastal lagoon model with final slope (s_2) as 1/4 for all the cases. However, the Case 9 where higher wave height to water depth ratios (H_o/h_o) with still water depth (h_o), lagoon inside water depth (h_L) and sand dune height (h_D) equals to 22, 6 and 1 cm respectively, has shown relatively less runup reduction compare with the other cases given in Table 6-1. The reason for the amplification of runup can be explained by the resonance phenomena where the horizontal distance from the seaside end of sand dune ridge to the toe of the final slope was approximately equal to the one-fourth of incident wavelength (L_o). In Chapter 7, the resonance phenomena are further discussed.
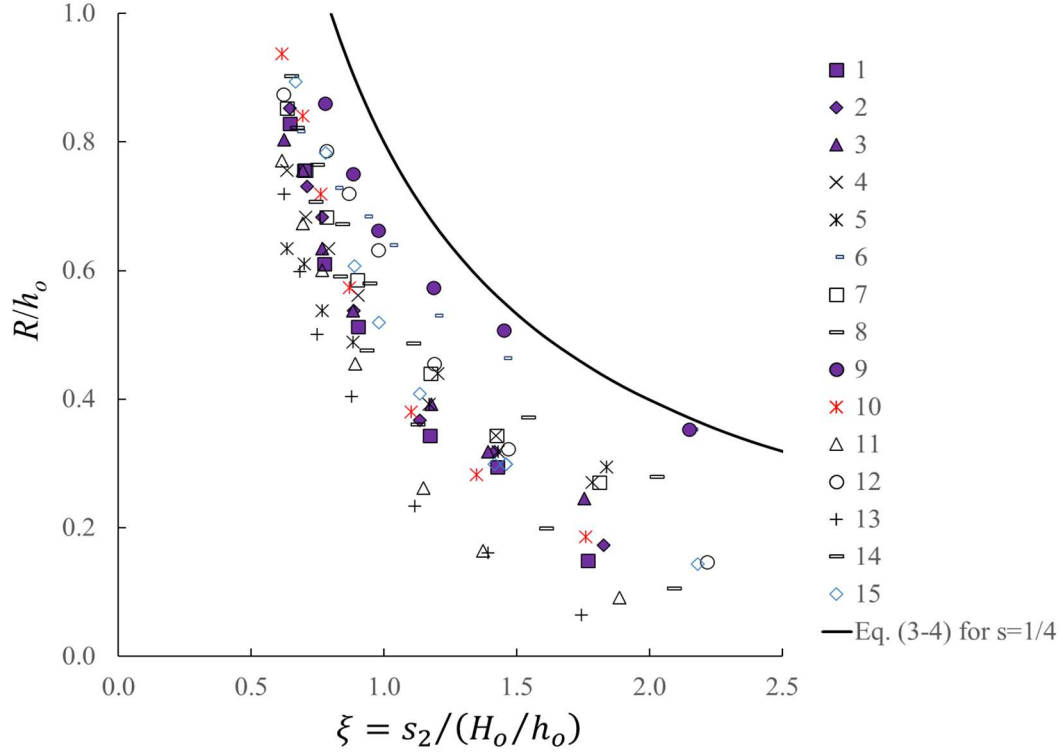
Figure 6-3 The non-dimensionalised runup (R/h_o) against the surf-similarity parameter, ξ is given by $s_2/(H_o/h_o)$ where s_2, H_o and h_o are final slope, wave height and water depth in constant depth region, respectively. Cases no. 1 to 15 are concerning Table 6-1.

Based on the 114 observations as included in Table 6-1, an empirical equation for estimating the solitary wave runup (R/h_o) on sand dune coastal lagoon which consists of the parameters, sand dune height (h_D), final slope (s_2), wave height (H_o), still water depth (h_o) and surf-similarity parameter ($\xi = s_2/(H_o/h_o)$) can be expressed as

$$\frac{R}{h_o} = \left(C_3 - C_4 \frac{h_D}{H_o}\right) s_2^{C_5} \xi^{(-C_6 \ln s_2 - C_7)} \tag{6-6}$$

The empirical coefficients of C_3, C_4, C_5, C_6, and C_7 gives 2.7911, 1.3809, 0.9828, 0.2002 and 1.0479, respectively. The statistical measures of mean absolute error (MAE), the root-mean-square (RMSE), scatter index (SCI), correlation coefficient (R^2) and agreement index (C_R) were found as 0.04, 0.003, 0.005, 0.944 and 0.985 respectively. The statistical measures show that the correlation between the experiments and the calculated by the proposed Eq. (6-6) is very high. It is observed that even the proposed empirical

equation does not include the parameters of the lagoon inside water depth (h_L), foreshore slope (s_l) and back slope of the lagoon, the equation predicts reasonably well for the experimental laboratory results. The proposed empirical solution is shown goodness of fit with experimental data as almost all of the data lies within a 20% error range as in Fig. 6-4.
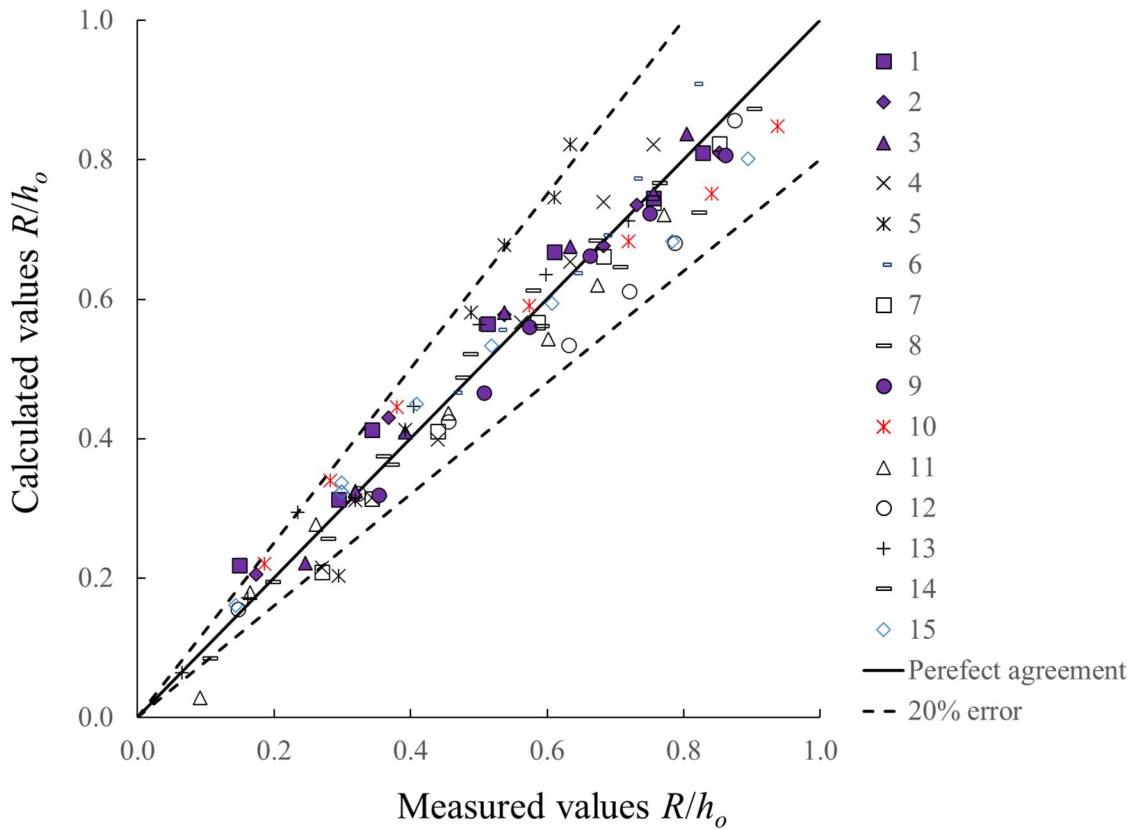
Figure 6-4 Comparison of the measured values and the calculated values by Eq. (6-6) for experimental results for runup with a sand dune coastal lagoon. Cases are regarding Table 6-1.

Hence the proposed empirical equation can be used to apply for estimating solitary wave runup on a sand dune coastal lagoon without the forest condition. The sand dune height restricts the overtopping volume passing over it and retards the wave energy by wave reflection which causes the lesser runup in the downstream (See Vinodh and Tanaka, 2018a, 2018b, 2018c). This reduction was slightly changed depending on the breaking condition at beach slope when other different slopes were introduced as beach slope (s_l). The runup reduction can be explained by plotting results of non-dimensionalised runup

using R/H_o (i.e., maximum runup over wave height) versus S_o (slope parameter) introduced by Grilli et al. (1997) as shown in Fig. 6-5.

$$S_o = 1.521s \left(\frac{H}{h}\right)^{-0.5}$$ (6-6)
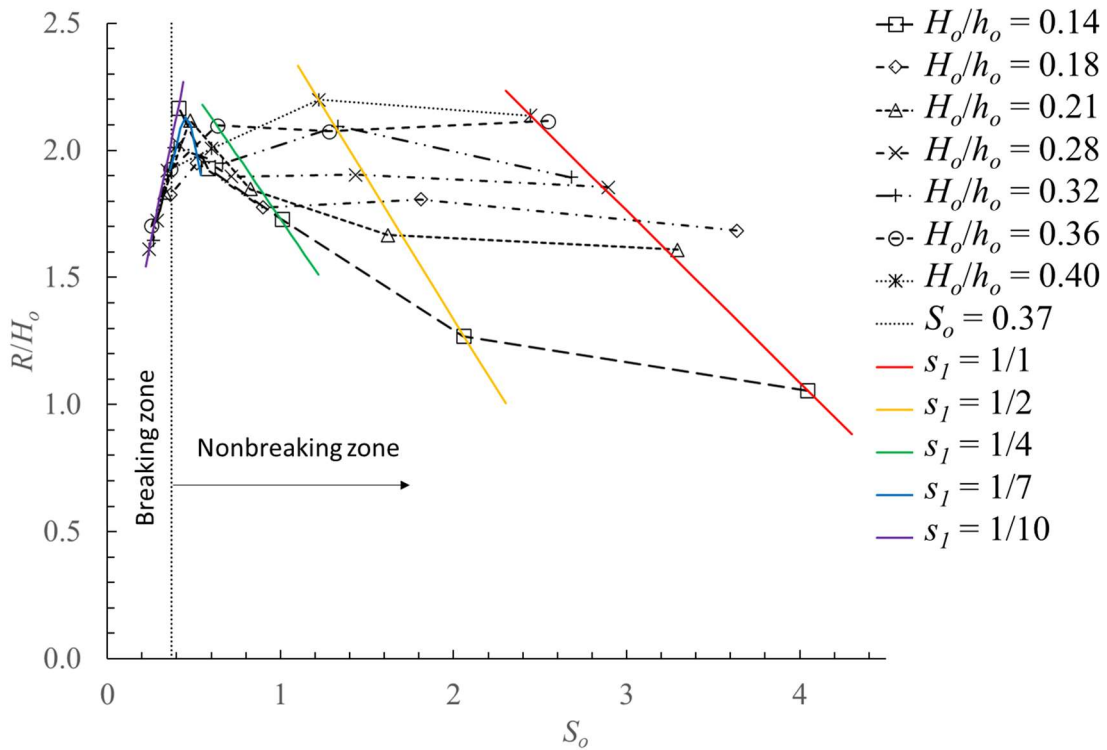
Figure 6-5 The non-dimensionalised runup (R/H_o) against the slope parameter (S_o) where s_1, H_o and h_o denotes beach slope, wave height and still water depth, respectively.

Grilli et al. (1997)'s guidelines can be used to distinguish breaking types as Spilling breaking ($S_o < 0.025$), Plunging breaking ($0.025 < S_o < 0.3$), Surging breaking ($0.3 < S_o < 0.37$) and Non-breaking ($S_o < 0.37$). The visual observations made by video camera recordings during the present laboratory experiments verified that the type of solitary wave breaking matched the prediction of Grilli et al. (1997). The plunging breaking type could be observed where $S_o < 0.3$. The surging breaking type could be seen where $0.3 < S_o < 0.37$. The breaking was not observed for $S_o > 0.37$. The spilling breaking type could not be seen at the beach slope for the wave conditions tested in this study.

The wave runup after overtopping for nonbreaking waves of highly nonlinear (i.e., solitary bores, $H_o/h_o > 0.18$) does not exhibit a dependence on either the slope (s) or the

slope parameter (S_o) in case of steep beach slopes (s_1) of 1/1 and 1/2. The maximum runup for breaking waves follows a linear relationship with slope parameter when the slope parameter, S_o <0.37. At near breaking, the solitary waves show a rapidly increasing trend where S_o is reaching 0.37. The runup increases with slope when it gets milder for nonbreaking weakly nonlinear waves (i.e., solitary waves, H_o/h_o = 0.14) and it shows the lower bound of non-dimensionalized runup height for nonbreaking waves. The wave runup after overtopping for breaking waves shows lesser runup than the nonbreaking waves of same wave height over water depth (H_o/h_o). The differences in breaking characteristics the lagoon inside caused minor variations in the runup.

The transmission coefficient (H_T/H_o) was calculated for the cases 1 to 5 by changing beach slope, and the results were plotted against the surf-similarity parameter, ξ given by $s_1/(H_o/h_o)$ as shown in Fig. 6-6. As the wave passes from deep water to shallow water onto the lagoon, the waves become highly nonlinear. The waves become oscillatory inside of the lagoon with significantly reduced periods as compared with the initial wave. The turbulent bores were observed inside the lagoon for all the cases. The breaking type in Fig. 6-6 is categorized as per the geometric form of breaking identified at the beach slope. Near breaking condition like the results of maximum runup, the transmission coefficient (H_T/H_o) is rapidly increasing and reduces after breaking occurred. Nonbreaking incident waves on the slope (s_1) of 1/10 caused the highest transmission coefficient (H_T/H_o) out of all other cases where energy dissipation was minimum.

Figure 6-6 Transmission coefficient (H_T/H_o) versus surf-similarity parameter, ξ given by $s_1/(H_o/h_o)$. Case numbers are concerning Table 6-1. BT – breaking type at beach slope, NB – nonbreaking, PL – plunging breaking and SU – surging breaking.

6.3.2   Wave transformation and runup on a sand dune coastal lagoon with a forest

Time series of a typical set of results (h_o =20cm, H_o=8cm, s_1=1/7, s_2=1/4) for the free-surface elevation with and without forest model are plotted in Fig.5-7. It can be seen that wave height reduction in the cases of LFV, LMV and LBV (i.e., 20 cm width of the forest) and the wave height is further reduced in the cases of LAV (i.e., 60 cm width of the forest). The presence of forest caused the water level in front of a forest to increase due to backwater effects and/or multiple wave reflection from the flow obstruction caused by the forest model (See Fig. 6-2) and the delay in wave arrival in downstream. Undulations in the reflected wave recorded by G2 (i.e., x/h_o = 14.8, at the toe of beach slope) and G3 (i.e., x/h_o = 7.8, at the shoreline), as in Fig. 6-7, suggested the presence of incident and reflected waves and may cause due to the presence of partial standing waves as shown by Mei et al. (2014) in addition to the reflection by a slope. The multiple reflected waves formed inside the forest are radiated into the offshore, as observed in Fig. 6-7, which was also identified by Chang and Liu (2019).

86

Figure 6-7 Wave evolution with and without forest model. Cases are regarding Table 6-1 and Table 6-2. The definitions of the parameters are shown in Figure 6-1. Ho, HG2, HG3 and HT are referring to the water surface elevation measurements at the locations of wave gauges.

In Fig. 6-7, where forest model was placed on the back slope of the sand dune (LBV) such undulations were not observed as recorded by G2 and G3. Since the forest model was placed on the back slope of a sand dune, the reflection by the forest is weak compare to the incoming flow. The slope parameter (S_o) described the runup similarity well with breaking phenomena. Hence, it was used to interpret the maximum runup results with the forest and without forest, as shown in Fig. 6-8.
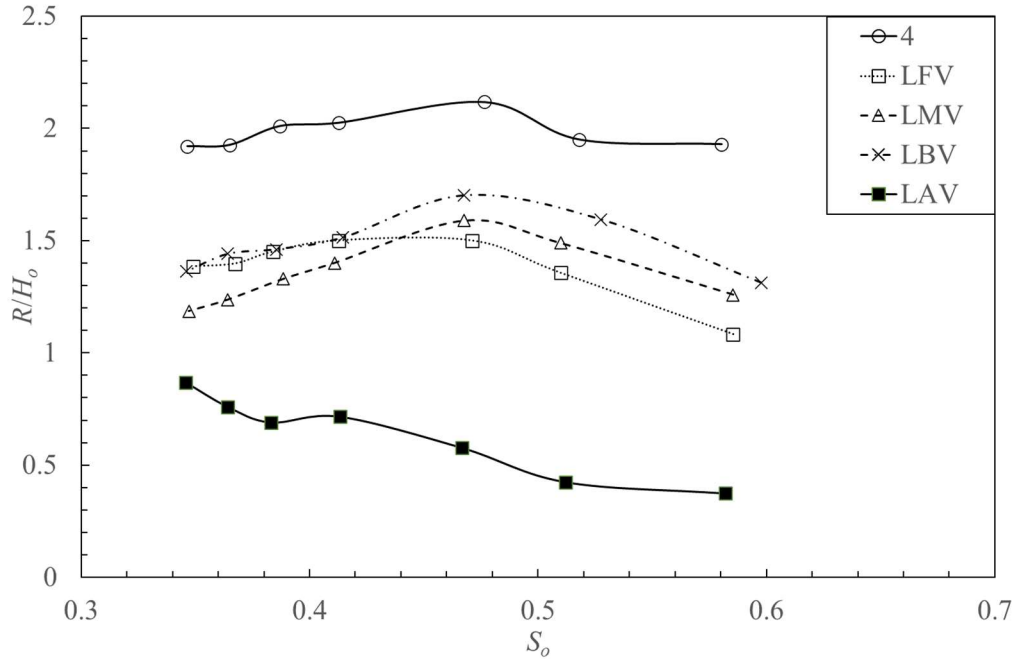
Figure 6-8 The maximum runup (R/H_o) versus the slope parameter (S_o) for sand dune coastal lagoon with and without forest model. Cases are with reference to Table 6-2.

These results suggest that the reduction of solitary wave runup with the forest is responsive to the change of incident wave height. The attenuation of maximum wave runup is neither increased nor decreased monotonically with the wave height. At near breaking where S_o varies 0.46 to 0.48, the maximum runup could be observed in both cases with lagoon model and lagoon model with a forest width (W) is 20 cm. The runup reduction was 17% to 18% at near breaking. For weakly nonlinear waves (low H_o/h_o) with forest width of $W = 20$ cm, the runup reduction is much higher, and it was recorded as 21% to 45%. The maximum runup reduction occurred at when forest model is at front beach slope (LFV) and then on the horizontal bed (LMV) for weakly nonlinear waves. This is because the closer the barrier is to the shoreline, the more intense the flow interacting with the barrier are, which is when the momentum can be expected as high. These high intense interactions provide a loss of energy as the flow impacts with itself and against the forest barrier. The least runup reduction occurred at forest model at the back slope (LBV) in case of modelling with forest width of W is 20 cm which causes minimum wave reflection back to offshore. For highly nonlinear waves (high H_o/h_o) the runup reduction was varied in a range of 26%

to 36% where maximum runup reduction was observed at forest model on the horizontal bed (LMV). When the forest model is on the horizontal bed, the water column for the interaction with vegetation is happened to be higher than the forest model on slopes. When the forest width (W) is increased as three times as before (i.e., W from 20 cm to 60 cm) the runup reduction was observed as 55% to 81%. For near breaking point (S_o is 0.46 to 0.48) the runup reduction was recorded as 72%. Highly nonlinear waves showed lesser runup reduction in comparison with the weakly nonlinear waves.

The transmission coefficients (H_T/H_o) against the slope parameter (S_o) for the cases with forest model are shown in Fig. 6-9. It could be seen that the transmission coefficient increases with the slope parameter (S_o) until the near breaking stage for W equals 20 cm and then reduces after the breaking occurred. Nevertheless, overall, the effect of wave attenuation and the runup reduction by changing the location of the forest in a sand dune found less significant. When the forest width was increased three times of previous width (i.e., W is 60 cm), the transmission coefficient (H_T/H_o) decreases with increasing slope parameter (S_o) monotonically. Overall, amplitude attenuation by the forest is evident from Fig. 6-9.

Similarly, as observed in Fig. 6-8 for maximum runup with the forest model, wave attenuation for highly nonlinear waves are less compare to weakly nonlinear waves. Therefore, a larger forest width was found to be more efficient in wave energy dissipation even when energy reduction at the beach slope is not sufficient enough but found to be relatively less effective for highly nonlinear waves. The effectiveness of wave runup reduction is also found to be dependent on surf-similarity of the beach.
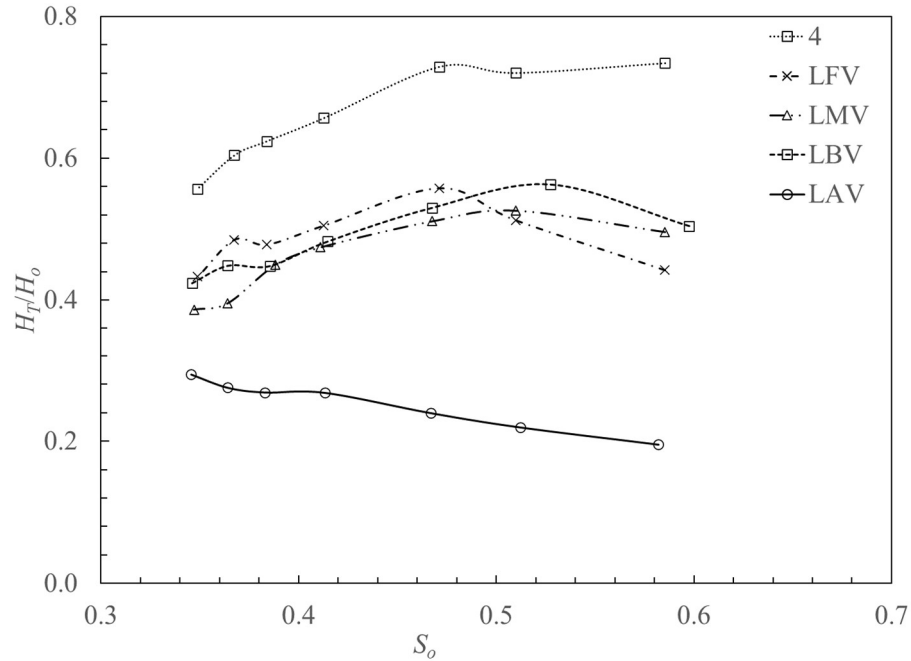
Figure 6-9 The transmission coefficient (H_T/H_o) versus the slope parameter (S_o) for sand dune coastal lagoon with and without forest model. Cases are regarding Table 6-2.

The wave transformation across the lagoon is a complicated problem, and it is true that numerical models, particularly concerning modelling energy losses, provide accurate results than both analytic and empirical expressions (Kirby, 2017). One common feature of numerical simulations referred to is that it is difficult to get quantitative data from the computational models without reiterating the solution process, except for those values of the parameters for which the governing equations were incorporated into each study. Local focusing, refraction, diffraction and reflection effects may play an essential role in tsunami runup. Still, it is elementary to explain the observations employing either analytical or empirical solution for runup using was the local beach slope and wave height to depth ratio.

As the sand dune is vulnerable to disturbance by tsunami inundation of prolonged period, the strengthening of sand dune by vegetation is required. In case the first wave in tsunami destroys the sand dune, the energy reduction for preceding waves (Eco-DRR function) becomes less. More study is needed in future on this point. It is noteworthy to acknowledge that other than limitations in physical space, constraints such as the producing tsunami-like solitary wave in laboratory scale, the forest width, the diameter of the coastal

trees and setting the beach slope encountered some technical troubles. Due to that fact, it is recommended for further studies, including numerical modelling, are required to investigate the influence of properties in a coastal zone against the tsunami runup in a precise form. Past field survey and historical data information are also crucial in calibrating the numerical model. Nonetheless, the results of the present model may prove beneficial for the initial estimate and understand the phenomena in tree planting projects for development projects nearby coastal lagoons.

6.4   Conclusion

The maximum runup on the landward slope of a sand dune coastal lagoon with and without forest was measured by changing the incident wave characteristics, beach slope, sand dune height and lagoon inside water depth. The resultant wave due to overtopping of plunging breaking, surging breaking and nonbreaking waves were observed with the Lagoon model. In order to observe the maximum runup effect with a lagoon, the beach slope of 1/1, 1/2, 1/4, 1/7 and 1/10 was used. The solitary waves of wave height to depth ratio from 0.1 to 0.4 were used in the experiments. Hence using 114 observations of maximum runup with a sand dune coastal lagoon model without forest, an empirical equation was derived by multiple linear regression analysis. The equation shows good correlation with data by giving mean absolute error (MAE), the root-mean-square (RMSE), scatter index (SCI), correlation coefficient (R^2) and agreement index (C_R) as 0.04, 0.003, 0.005, 0.944 and 0.985 respectively. The present empirical model does not include the parameters of the lagoon inside water depth and the front beach slope. Besides, almost all the tested laboratory-measured values are within the 20% error range. Hence it can be used as an initial estimate and verify numerical models in solitary wave runup.

Mild beach slopes have the advantage of inducing the breaking of the incident wave, which can reduce the runup height. Still, such beach slopes are vulnerable for nonbreaking relatively weakly nonlinear incident waves (low wave height to water depth ratio) as such waves on milder slopes cause higher wave transmission and runup. The runup on a sand dune coastal lagoon with a forest of finite width is reduced effectively by 17% to 45% depending on the slope parameter of front beach slope which is associated with the breaking phenomenon. At near-breaking condition, the effectiveness of coastal trees is

found to be comparatively less. However, by introducing a larger forest width, the runup can be further reduced by 55% to 81%. It is also noticed that the wave attenuation and the runup reduction by forest are relatively lesser for highly nonlinear waves (i.e., higher wave height to water depth ratio). The placement of forest on a sand dune is discussed and found that when the forest is situated at the front of a sand dune, it causes slightly higher runup reduction for weakly nonlinear waves (low wave height to water depth ratio). When a forest is located on the horizontal surface of the sand dune, the higher runup reduction is occurred for highly nonlinear waves / high wave height to water depth ratio. However, overall, the effect of wave attenuation and the runup reduction by changing the location of the forest in a sand dune found less significant compare to the impact of forest width.

Other than constraints in physical space, producing tsunami-like solitary wave in laboratory scale, modelling the coastal trees and setting the beach slope encountered some technical troubles. It is recommended for further studies, including numerical modelling, are required to investigate the influence of properties in a coastal zone against the tsunami runup in a precise form. Past field survey and historical data information are also crucial in calibrating the numerical model. Nonetheless, the results of the present study may prove beneficial for the initial estimate and understand the fundamental phenomena in Eco-DRR projects for coastal lagoons.

Chapter 7

Runup with coral reef

7.1 Introduction

Coral reefs are natural structures which are highly precious in many ways as they represent immense ecological value. Coral reefs also play a role in safeguarding the beaches behind them and offer many potentials for recreation and tourism in a country.

The protective role of reefs in tsunami mitigation aroused the attentions of the researchers as a result of the post-disaster surveys on tsunami hazards. Many anecdotal reports proposed that intact and healthy coral reefs reduced tsunami damage to communities on the coast effectively. Kunkul et al. (2006) showed by using numerical simulation that the effectiveness of coral reef system depends on the wave height and wavelength of the tsunami, the geometry and health of the reef, and the reef flat width. Fernando et al. (2005) observed that illegal coral mining along unsupervised beaches as in Peraliya, Sri Lanka had created low-resistance paths which allowed funnel the energy of tsunami into the land and cause intensive damages. Wijetunge (2014) suggested that, in general, the influence of onshore topography to have been more influential in enhancing the tsunami impact in the stretch of Akurala relative to the neighbouring areas to the north and the south. Pomonis et al. (2006) reported that the damage in the southern part of town between Thiranagama and Dodanduwa did not seem so severe, probably due to the natural breakwater protection by the coral reef. They also observed that hotels along the coast underwent minor structural damage and were open to tourists at the time of their field mission. Gelfenbaum et al. (2011) showed that embayment that narrow landward that have an incised deep channel can cause a considerable rise in tsunami wave heights, velocities and inundation distances whereas wide embayment, induce some tsunami amplification, but not as much as per the case of narrow embayment. Ford et al. (2014) explained that the tsunami wave transmission across the reef flats is shown to be tidally dependent. Wave heights are increasing towards the shoreline at high tide and decreasing at low tide. Nakaza et al. (1991) observed bore-like surf beat resonantly excited incoming wave groups in reef coasts. In reef-type bathymetry profiles, a very short wave-breaking zone over the steep reef face facilitates the freeing of infragravity (low-frequency) period fluctuations (surf

93

beat) with little energy loss (Cheriton et al., 2016). Gawehn et al. (2016) observed resonant very low-frequency waves had nonlinear, bore-like wave shapes, which have a larger influence on the shoreline than sinusoidal waveforms. Further, they classified the very low-frequency motions into four different classes as resonant, standing (non-resonant), progressive-growing, and progressive dissipative waves. Roeber et al. (2010) showed that it is essential to know about the local resonance to mitigate hazard than the origin and direction of the tsunami.

Baird et al. (2005) illustrated that healthy reefs could not mitigate the damages on land, and the inundation distance was mainly determined by the incident wave height and the onshore topography. Chatenoux and Peduzzi (2007) in a statistical analysis covering several tsunami-affected countries by IOT including Sri Lanka, found no considerable influence of the existence of coral reefs in reducing the tsunami damage. Damages to the coral reefs have also been reported. Rajasuriya et al. (2006) found that coral reefs were severely damaged by the debris and smothered by sand transported during the incoming and withdrawal of the tsunami in Sri Lanka.

Waves that propagate over the reef result in a bimodal wave spectrum that consists of a combination of sea-swell (high-frequency) waves and infragravity (low-frequency) waves (Pomeroy et al., 2012). That is why many laboratory investigations on the interaction between waves and coral reef platforms focused mainly on the transformation of regular waves (e.g., Gourlay and Colleter, 2005) or irregular waves (e.g. Takayama et al., 1977; Nwogu and Demirbilek, 2010; Yasuda et al., 2020). Solitary waves have been utilized in many studies to model the leading wave of a tsunami wave train as they represent many essential properties of a tsunami than both regular and irregular waves. According to the author's knowledge, the laboratory studies on the tsunami-like solitary wave transformation on coral reefs are studied only by Quiroga and Cheung (2013) and Yao et al. (2018). Besides both researchers have not studied the resonance phenomena excited by a coral reef platform which can be considered as the worst-case scenario in a tsunami.

The common challenge for knowing the hydrodynamics in all canopies is appropriately accounting for the highly fluctuating spatial flow structure that occurs within even the simplest morphologies (Nunes and Pawlak, 2008). In the literature, there have

been attempts to directly observe or numerically simulate the three-dimensional turbulent flow structure through individual branching coral colonies (Chindapol et al., 2013). However, for tsunami simulation, such methods are costly computationally, requiring flows to be resolved down to scales on the order of millimetres. Thus, it remains unfeasible to resolve the roughness geometries of coral reefs at the scale of entire reef communities or systems. Therefore, in the numerical simulation of wave and circulation, variability in reef geometry occurs at a scale finer than the resolution of a computational grid. Hence, drag due to the small-scale coral reefs must be parameterized. On reefs, bottom friction is a critical term in the momentum balance and the dissipation loss. The correct parameterisation of the bottom drag can be done by either calibrating with field data analysis or laboratory modelling (Jaramillo and Pawlak, 2011; Monismith, 2007).

Surface wave-driven flows can be considered as a general feature of many coral reefs. As a result, it is appeared to follow predictions of theories based on the concept of radiation stress gradients. Most of the models of surface wave-driven flow over reefs (e.g., (Gourlay and Colleter, 2005)) are based on the suggestion of Longuet-Higgins& Stewart (1962). Even wave energy is dissipated by turbulence, in principle, the conservation of momentum requires that there should be a force exerted on the obstacle, equal to the rate of change of a wave momentum. This force is a manifestation of the radiation stress as hypothesised by Longuet-Higgins and Stewart (1964). No theory existed, and only empirical suggestions could be found for estimating the wave setup induced by breaking waves (Bowen et al., 1968; Dean and Walton, 2017; Longuet-Higgins and Stewart, 1964; Stockdon et al., 2006). Hearn (1999) pointed out that a change in reef water depth alters the across-reef current because of two principal physical effects. When the reef water depth is shallow, will be dampened due to the strong friction, whereas when the reef water depth is higher, will be weakened because of the limited breaking and hence cause small radiation stress gradients (Gourlay, 1996a, 1996b; Gourlay and Colleter, 2005). Thus, there will be a reef water depth at which the surface wave-driven flow at its maximum.

Moreover, tidal fluctuations will variate mean flows over the reef. Most of the reef-based studies mentioned above are conducted without modelling the roughness of corals. The researchers those who have modelled the coral reef roughness, have chosen either array of cylinders (Lowe, 2005; Yao et al., 2018) or array of concrete cubes (Buckley et

al., 2016) or timber beams at regular intervals (Quiroga and Cheung, 2013). Yao et al. (2018) found that the ratio of the reef water depth to the incident wave height is the dominant parameter to estimate the wave run-ups and suggested empirical runup expressions. Quiroga and Cheung (2013) investigated on pitch ratio and concluded that the solitary wave propagation and the dissipation is based on roughness height and water depth and not on the pitch ratio.

Laboratory experimental conditions make available for detail measurements to be performed such that the hydrodynamics over the reef can be studied in precise form. The flume experiments are also suitable to model the measurements in the surf zone where the waves are breaking, which can be challenging to conduct field experiments because of the energetic conditions at that surveying point. The study aims to use the laboratory experiments based on solitary wave runup on a coral reef system to understand better and describe tsunami wave transformation over a coral reef system.

7.2 Materials and Methods

A series of experiments for a coral reef system was conducted at Hydraulic Engineering Laboratory in Saitama University. Flume dimensions are 20m, 0.3m and 0.6m in length, width, and height, respectively. Fig. 7-1 defines all the bedform configurations of the current experimental setup and the parameters involved in the study following the work of Gourlay (1996b) and Yao et al. (2018).

The maximum runup (R) at the landward end of the reef flat or lagoon can be identified depending on the incident wave characteristics, the upstream wave height (H_o), wavelength (L_o) and water depth in the constant depth region (h_o), and physical characteristics of a coral reef system, fore reef slope (s_1), the back slope of the seaward reef crest (tanα), the landward slope of reef platform (s_2), initial lagoon water depth (h_L) in case of the lagoon and reef water depth in case of reef flat, width from reef edge to the toe of final slope (L_r), and the lagoon length in cross-shore direction (L_L). Fig. 7-2 shows the schematic layout of the experimental setup. A piston-type wavemaker was installed at wave generation end.
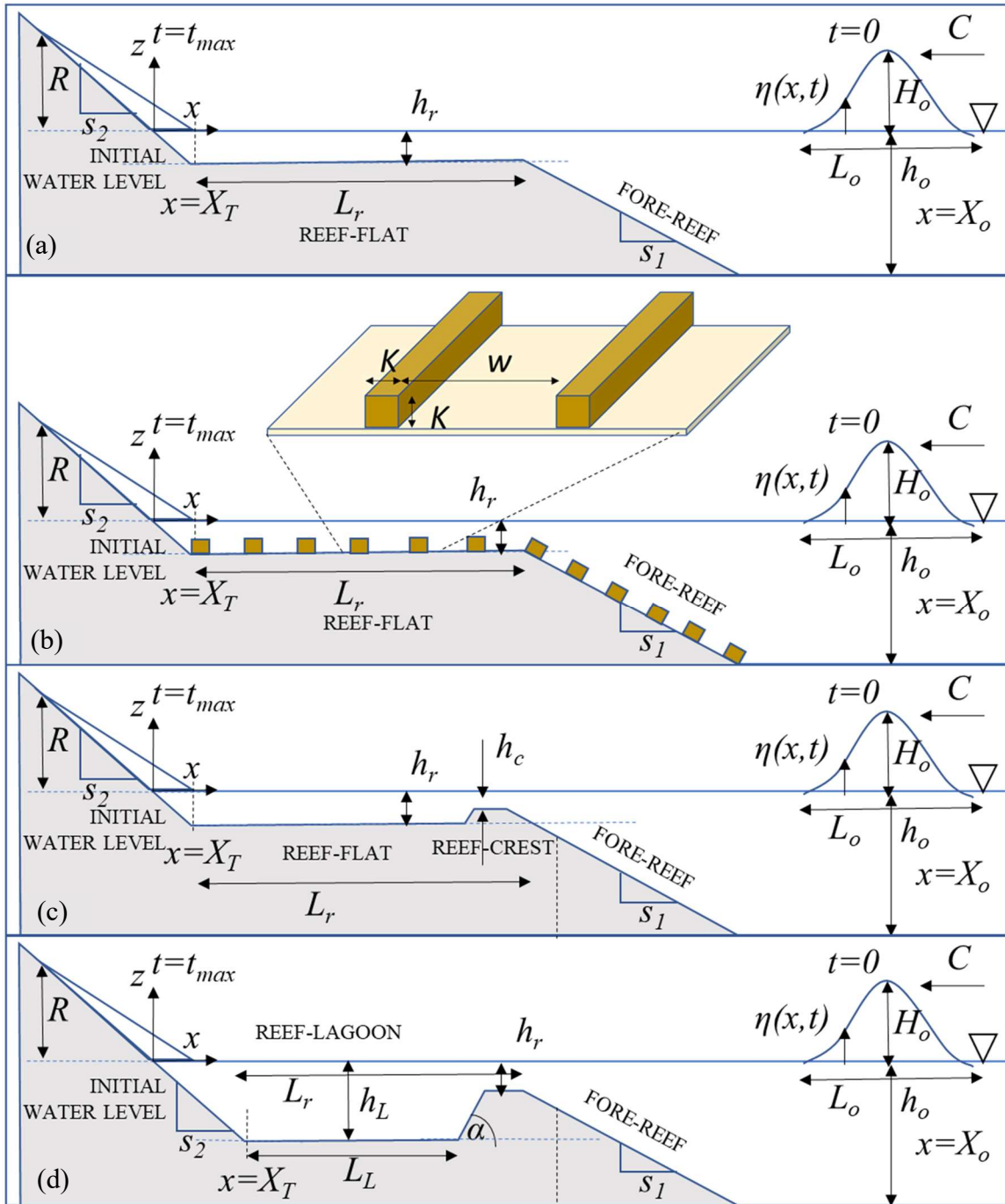
Figure 7-1 Definition of parameters for the idealized coral reefs; (a) Reef-flat, (b) Reef-flat with roughness elements, (c) Reef-crest, (d) Reef-lagoon
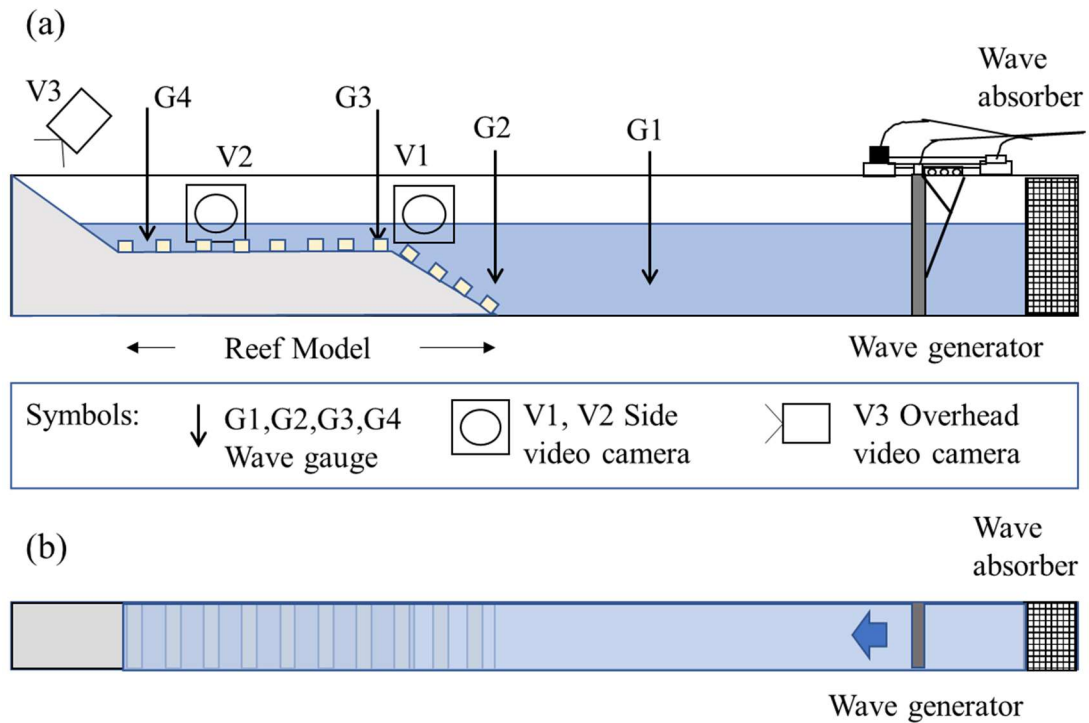
Figure 7-2 Schematic view of experimental setup for coral reef system; (a) Section view, (b) Plan view.

The reef platform and the fore-reef slope were constructed of marine plywood painted with water-resistant paint. The model scale was chosen as 1:100. The height of the reef-flat was 23 cm from the top surface to the bottom of the flume bed. Following Quiroga and Cheung (2013), the roughness was created by glueing rectangular strips having cross-sectional dimensions ($K \times K$) of 1cm x 1cm on both the fore-reef slope of 1/7 and the reef-flat with a space between roughness elements, w of 1.3, 4, 6, 7 and 9 cm. The resultant pitch ratio defined by w/K (ratio between the space and height of roughness elements) according to Fig. 7-2 varied from 1.3 to 9 which describes the wave interactions and energy dissipation mechanism (Leonardi et al., 2007, 2003; Perry et al., 1969). Here w/K of 1.3 can be identified as 'd' type roughness, and w/K of 4, 6, 7 and 9 can be considered as 'k' type roughness. The reef-flat width (L_r) was fixed at 147 cm. The reef-crest was 2 cm in height and 20 cm in top width with front slope and back slope of 1/7. Hence, the set of coral reef roughness used in this study can define general one-dimensional flow variation in a coral reef system. Identical test runs were performed with both smooth surface and bed with different roughness on the reef flat and forereef.

The water surface elevation was measured using four capacitance-type wave gauges with a frequency of 100Hz, as shown in Fig. 7-2. The calibration of wave gauges was done by the standard method of lowering systematically into the water and recording the output voltage accordingly. The reference wave gauge G1 was placed at 6 m from the piston. The horizontal distance from the wave gauge G1 to the toe of the beach slope was kept at 5.35 m where wave gauge G2 was placed. The wave gauge G3 was placed at the near edge of reef ridge which was 7 m away from G1. In order to measure transmitted height, H_T, the wave gauge G4 was placed near the toe of the final slope, which is 8.05 m away from the wave gauge G1. The wave measurement locations of G1, G2, G3 and G4 were fixed for all the bedform configurations and wave conditions. The maximum values of the surface elevation recorded by G1, G2, G3 and G4 were defined as incident wave height (H_o), wave height at the toe of the beach slope (H_{bst}), wave height at the reef-edge (H_{cr}) and the transmitted wave height (H_T), respectively in the study. The results ensured that there was no significant peak reduction caused by the fore-reef slope in the readings of the wave gauge G1. The water depths (h_o) were changed from 20 cm to 30 cm, as shown in Table 7-1. The corresponding h_r was varied from 0 cm to 7 cm (i.e., $h_r = h_o - 23$ for $h_o > 23$ and $h_r = 0$ for $h_o \leq 23$). In the case of reef-lagoon, the corresponding h_L was changed from 4 cm to 14 cm (i.e., $h_L = h_o - 16$). In all experimental cases with the lagoon model, the water level in both offshore and reef-side was kept as same by changing the initial reef water depth (h_r) in case of reef-flat or initial reef-lagoon water depth (h_L) in case of reef-lagoon depth and changing upstream water depth (h_o). Note that during the flood tide and ebb tide the water level fluctuates and the water level is not the same. In this study, those fluctuations were not considered and hence ignored the effect of current produced by tidal change and concentrated on the wave-driven component only.

Table 7-1 Experimental conditions for a coral reef system. K, w, H_o and h_o are height of roughness element, spacing between roughness elements, incident wave height and still water depth, respectively.

Case No	Case	w/K	H_o (cm)	h_o (cm)
RF	Reef-flat	N/A	2.4-8.3	23,25,26,30
RC	Reef-crest	N/A	2.4-8.3	23,25,26,30
RFR1.3	Reef-flat with roughness	1.3	2.4-8.3	23,25,26,30
RFR4	Reef-flat with roughness	4	2.4-8.3	23,25,26,30
RFR6	Reef-flat with roughness	6	2.4-8.3	23,25,26,30
RFR7	Reef-flat with roughness	7	2.4-8.3	23,25,26,30
RFR9	Reef-flat with roughness	9	2.4-8.3	23,25,26,30
RL	Reef-lagoon	N/A	2.4-8.3	20,21,22,23,24,25,26,27,28,30

Seven different solitary wave heights, ranging from 2.4 cm to 8.3 cm for a water depth of h_o, was used. The wave height to depth ratio (H_o/h_o) was varied from 0.1 to 0.4. The current experimental database includes 308 tests for the estimation of runup changing the settings of three types of bed transformations (i.e., reef-flat, reef-crest and reef-lagoon) including the change of still water depth (h_o), wave height (H_o), and pitch ratio (w/K). The maximum runup, which is defined as vertical extent of wave action above still water level, was tracked by an overhead camera based on the marker lines on the runup board with an accuracy of 5 mm. The geometric form of the breaking type was observed using the side video camera recordings. Some tests were randomly repeated and found that the results of maximum runup showed consistency within 5 mm range for an input value of offshore wave height (H_o) to the wavemaker program. This experimental study showed measurements of solitary wave transformation over a reef with and without roughness elements and the effect of spacing of roughness elements varied under a broad range of solitary wave conditions. The controlled laboratory environment allows a view of the bed-

form changes on wave shoaling, breaking, transmission and runup. The present experimental results are also compared with Yao et al. (2018).

In the case of the resonance phenomenon, the reef flat can be schematised as an open basin with one closed-end and one open-end (Nwogu and Demirbilek, 2010). The lowest order of oscillation (i.e., fundamental mode) that can exist in a typical reef flat is a wave with a node on the open-end (i.e., at the reef crest), and an antinode on the closed-end, at the beach. The period of this oscillation can be roughly estimated by using the cross-shore distance between the node and antinode is one-fourth of the incident wavelength or by using the wave period. The natural oscillation, T_n of the open basin can be estimated by

$$T_n = \frac{4L_r}{(2n+1)\sqrt{gh_r}} \tag{7-1}$$

Here L_r is the cross-shore distance of reef-flat, h_r is water depth over the reef-flat region, n is mode number and g is the gravitational acceleration. The fundamental mode of $n = 0$ mode has the maximum period. In contrast, the other modes (the overtones of the main fundamental) have periods equal to one-half, one-third, one-fourth and so on, of the fundamental period. However, the actual resonance period deviates from Eq. (7-1) as the wave celerity reduction by bottom friction, the correction to the cross-shore distance of reef-flat (L_r) and reef water depth (h_r) to account the presence of the beach slope and the wave setup.

7.3 Results and Discussion

7.3.1 Wave transformation along the Reef-crest, Reef-flat with and without roughness

The measured water surface elevation corresponding to initial wave height (H_o) and transmitted wave height at the toe of beach slope (H_{bst}), reef-edge (H_{cr}) and at the toe of final slope (H_T), respectively, indicated the wave evolution along with the reef bedform configurations and incident wave characteristics. Fig. 7-3 shows the non-dimensionalised transmitted wave height (H_{bst}/h_o) concerning wave height to depth ratio (H_o/h_o) for the case of reef-crest (RC), reef-flat (RF) and reef-flat with roughness with pitch ratio (w/K) of 1.3 (RFR1.3), 4 (RFR4), 6 (RFR6), 7 (RFR7) and 9 (RFR9) as the cases explained in Table 7-1.
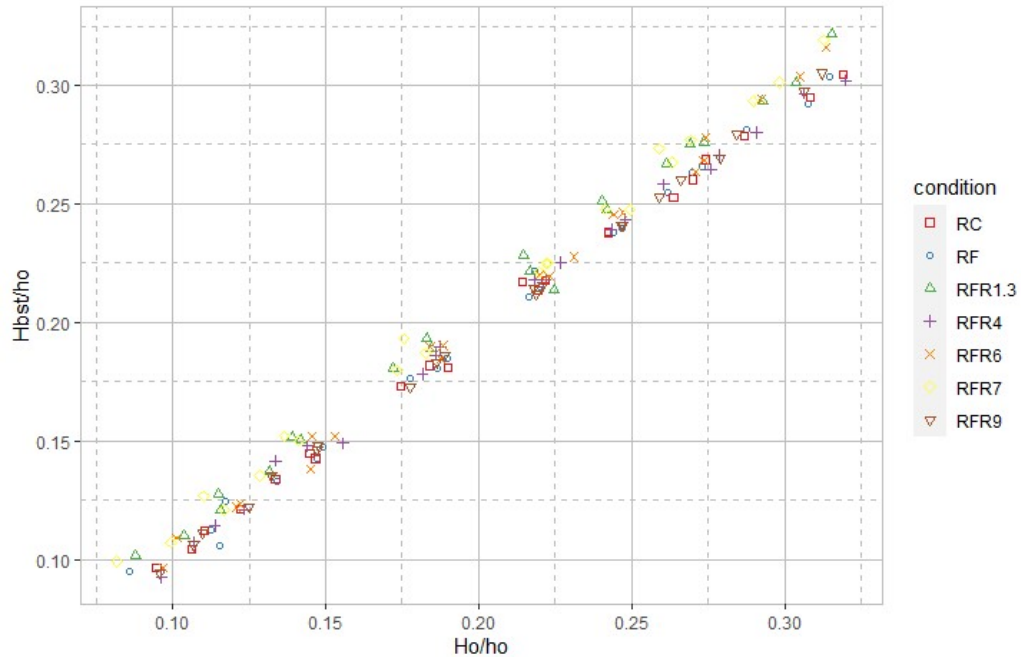
Figure 7-3 Transmitted wave height at beach slope over water depth (H_{bst}/h_o) against the initial wave height to water depth ratio (H_o/h_o) for $h_r > 0$, RC – reef-crest, RF – reef-flat without roughness, RFR1.3 – reef-flat with w/K of 1.3, RFR4 – reef-flat with w/K of 4, RFR6 – reef-flat with w/K of 6, RFR7 – reef-flat with w/K of 7 and RFR9 – reef-flat with w/K of 9.

The shoaling of the transmitted wave at beach slope (H_{bst}) concerning the incident wave height (H_o) was within 25% range. As the length of the fore-reef slope is smaller than the incident wavelength (L_o), the amplitude of the solitary wave increases, and the wave shape becomes pitched-forward. However, the shoaling process is not fully evolved in the region of fore reef. Therefore, the leading front of the wave reaches the shoreline while some part of the waveform remains offshore from the fore reef. As a result, part of wave energy is transmitted to the reef flat. The waves which break at the reef-flat induce wave setup to cause a rise in the water level above the reef-flat, as shown in Fig. 7-4.
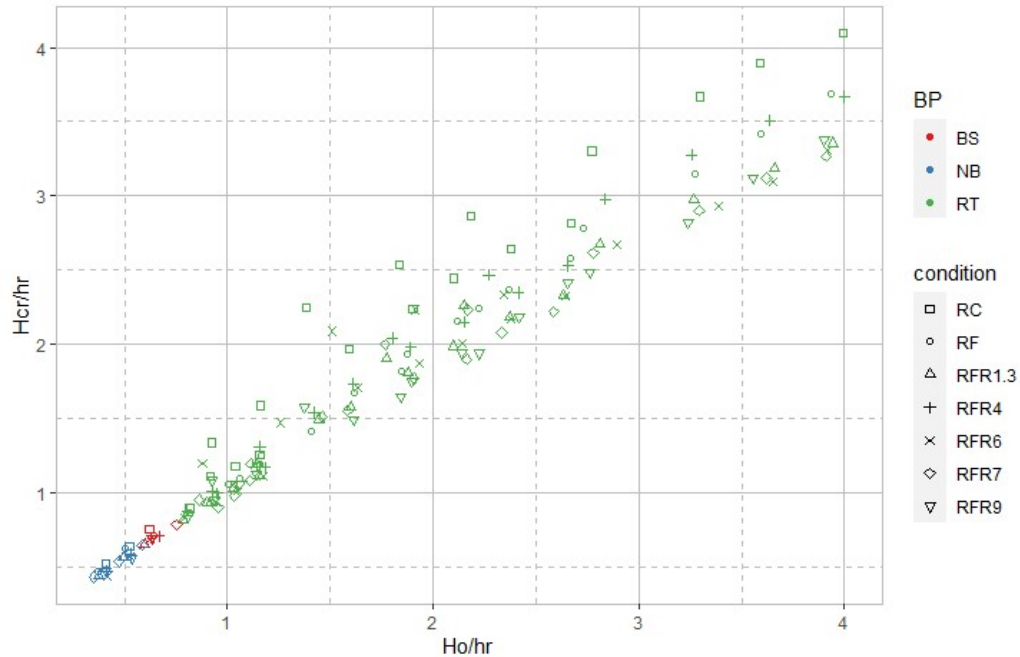
Figure 7-4 Transmitted wave height at reef ridge over reef water depth (H_{cr}/h_r) against the incident wave height to reef water depth ratio (H_o/h_r) for $h_r > 0$, BP- breaking point, BS – breaking at final slope, NB – nonbreaking, RT – breaking at reef top, RC – reef-crest, RF – reef-flat without roughness, RFR1.3 – reef-flat with w/K of 1.3, RFR4 – reef-flat with w/K of 4, RFR6 – reef-flat with w/K of 6, RFR7 – reef-flat with w/K of 7 and RFR9 – reef-flat with w/K of 9.

In the case of reef-crest (RC), the measurements in water surface elevation taken at position G2 was situated on the fore-reef slope near the reef-crest, which also a part of the fore-reef slope. Therefore, the values of H_{cr} were appeared to be higher than the reef-flat cases where it was under shoaling stage due to fore-reef slope and the energy leakage over the reef-flat part during the wave passing at G2 position was barely minimum. For highly nonlinear waves (higher H_o/h_o) which break at reef-flat (i.e., denoted by RT in Fig. 7-4), due to the wave energy dissipation by depth limited breaking and bed friction, the transmitted wave heights (H_{cr}) were further reduced. The nonbreaking waves and waves that break at final slope denoted by NB and BS respectively propagated passing the reef ridge with comparatively minimum energy dissipation. The wave transformation results given by wave gauge G4 near the toe of final beach slope are shown in Fig. 7-5.
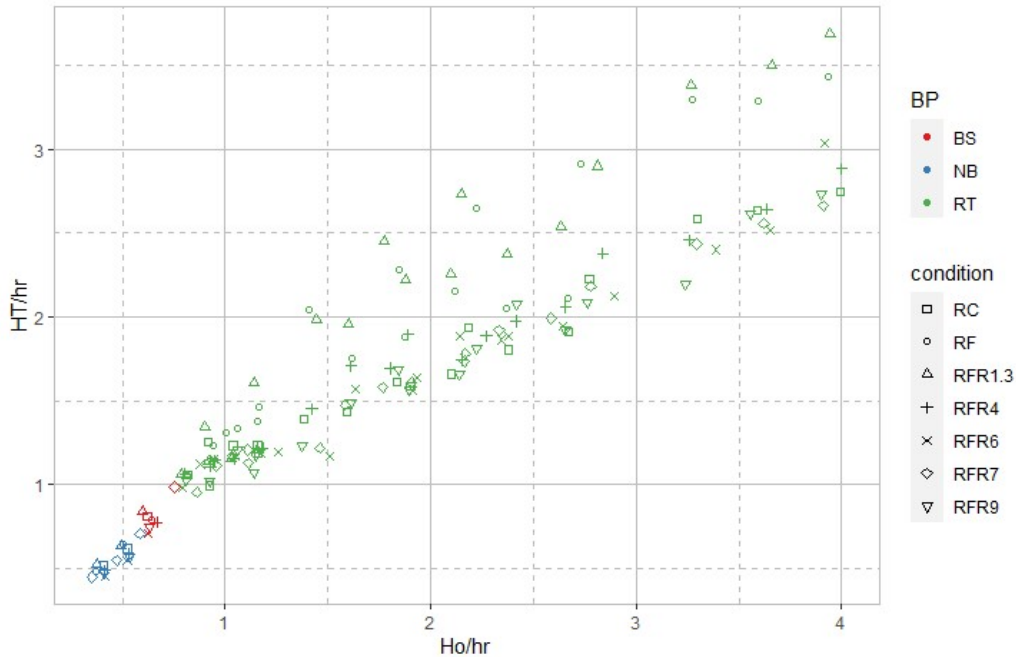
Figure 7-5 Transmitted wave height at final beach slope end over reef water depth (H_T/h_r) against the incident wave height to reef water depth ratio (H_o/h_r) for $h_r > 0$, BP- breaking point, BS – breaking at final slope, NB – nonbreaking, RT – breaking at reef top, RC – reef-crest, RF – reef-flat without roughness, RFR1.3 – reef-flat with w/K of 1.3, RFR4 – reef-flat with w/K of 4, RFR6 – reef-flat with w/K of 6, RFR7 – reef-flat with w/K of 7 and RFR9 – reef-flat with w/K of 9.

The waves that break at reef-flat (denoted by RT in Fig. 7-5) shows further reduction in wave heights due to energy dissipation by bottom roughness and the turbulence. The waves that break at final slope were observed as surge breaking (bore type) and the waves that break at reef-flat was observed as spilling breaking. However, in the case of RFR3 (i.e., reef-flat with pitch ratio, w/K is 3) where 'd' type roughness can be observed, the transmitted wave heights were relatively higher implying that dense roughness cause less energy dissipation. The energy dissipation by intermediate roughness elements (i.e., 'k' type roughness in RFR4, RFR6, RFR7 and RFR9) where pitch ratio (w/K) equals to 4, 6, 7 and 9 was much higher than both the reef-flat without roughness (RF) and reef-flat with dense roughness (RFR1.3), cause wave height reduction. The wave height reduction by changing pitch ratio (w/K) in 'k' type roughness cases did not show a significant difference. Quiroga and Cheung (2013) also found that the height of the roughness element (K) and reef water depth (h_r) define the bore propagation and energy dissipation rate on the reef-

flat instead of the pitch ratio (w/K) in 'k' type roughness cases. The wave height reduction by the reef-crest (denoted by RC) also showed similar capabilities as the 'k' type roughness cases did. The nonbreaking waves (NB) and the waves that break at the final slope (BS) showed shoaling effect due to the reflection by the final slope. The transmitted wave height was higher than the incident waves for low offshore incident wave heights (H_o) in high water depths (h_r) indicating an amplification regardless of the energy dissipation by bottom roughness. The depth limited breaking criterion for present experimental conditions was found as 0.6. When the incident wave height to reef water depth ratio (H_o/h_r) was above 0.6, waves either break at the final slope of 1/4 or reef flat. For $H_o/h_r < 0.6$, the waves propagate throughout the coral reef system without any breaking. The present results of depth limited breaking value deviated with the theoretical breaking criterion, which was introduced by McCowan (1894) by following the maximum possible wave height of the solitary wave in a horizontal bed. Grilli et al. (1997) showed that a maximum wave height to depth ratio of 0.78, will only break for a plane slope, s < 1 / 4.7 ($\beta < 12^0$). Tait (1972) showed that the wave breaking ratio is dependent on the fore-reef slope. The wave breaking ratio decreases into the surf zone with continuing energy dissipation (Hearn, 1999). Since the incident wave height (H_o) also deformed at the place of breaking and the wave gauge could not capture the exact point of breaking, it is reasonable to deviate the actual result of wave breaking ratio from the theoretical breaking criterion. Besides, it can be expected that breaking criterion may depend on the fore-reef slope and the bottom roughness.

7.3.2 Wave runup with the Reef-crest, Reef-flat with and without roughness

The results of maximum runup (R/H_o) with reef-crest (RC), reef-flat (RF) and reef-flat with the roughness of w/K equals to 1.3 (RFR1.3), 4 (RFR4), 6 (RFR6), 7 (RFR7) and 9 (RFR9) versus wave height to reef water depth ratio (H_o/h_r) were plotted as shown in Fig. 7-6. The breaking point (BP) was categorized as breaking at reef-flat (RT), breaking at the final slope (BS) and nonbreaking (NB). When the wave height to reef water depth ratio (H_o/h_r) is below the value of 0.6, the waves propagate through the reef without breaking (denoted by NB) as shown in Fig. 7-6. Beyond the value of H_o/h_r of 0.6, the breaking occurred at the final slope (BS), and for higher H_o/h_r the breaking occurred in the reef-flat (RT). The runup (R/H_o) was increased with H_o/h_r for nonbreaking waves. The highest runup could be observed from the waves which broke at beach slope (BS). The runup (R/H_o) was decreased

with increasing for H_o/h_r for breaking waves which showed the opposite trend of the nonbreaking wave runup.
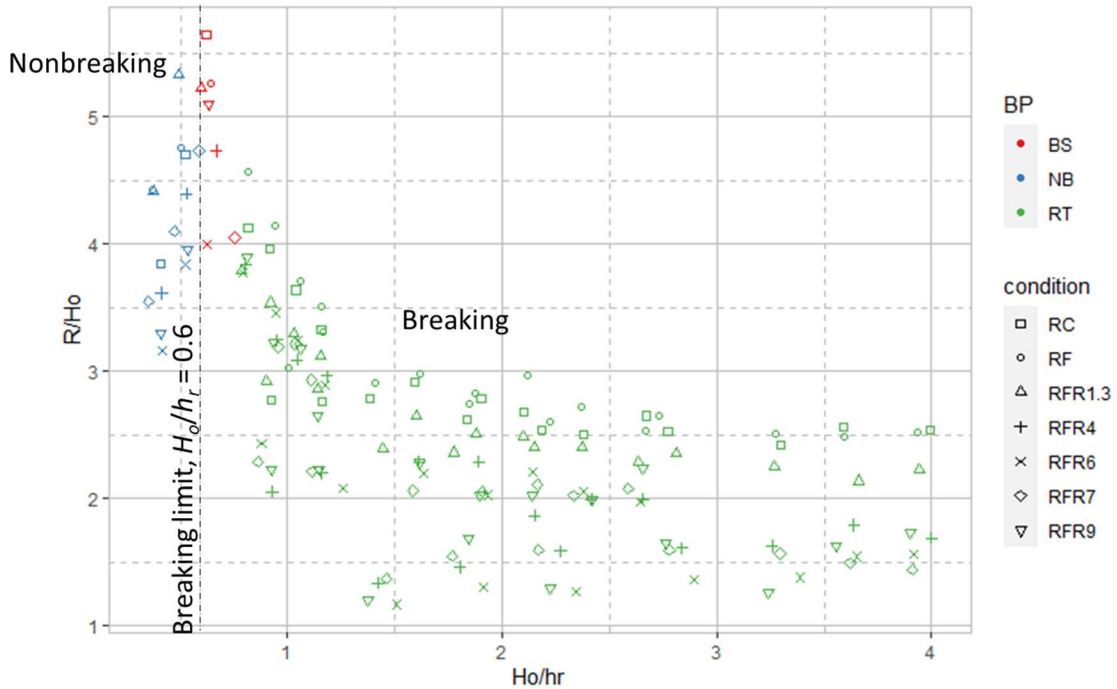
Figure 7-6 The non-dimensionalised runup (R/H_o) against the incident wave height to reef water depth ratio (H_o/h_r) for $h_r > 0$, BP- breaking point, BS – breaking at final slope, NB – nonbreaking, RT – breaking at reef top, RC – reef-crest, RF – reef-flat without roughness, RFR1.3 – reef-flat with w/K of 1.3, RFR4 – reef-flat with w/K of 4, RFR6 – reef-flat with w/K of 6, RFR7 – reef-flat with w/K of 7 and RFR9 – reef-flat with w/K of 9.

For the comparison of runup (R/H_o), the wave nonlinearity (H_o/h_o) is used to investigate the effect of $h_r = 0$. The runup height is monotonically decreased with decreasing offshore wave heights (H_o) for low water depths (i.e., $h_o = 25$ cm and $h_r = 2$ cm), as shown in Fig. 7-7 and reef-flat with 'k' type roughness. However, in case of 'd' type roughness (RFR1.3), reef-flat (RF) and reef-crest (RC), the runup (R/H_o) is monotonically increased with decreasing offshore wave heights (H_o). When the reef water depth, h_r is zero, except the reef-flat case (RF) all the other cases, the runup (R/H_o) is decreased with decreasing offshore wave heights (H_o).
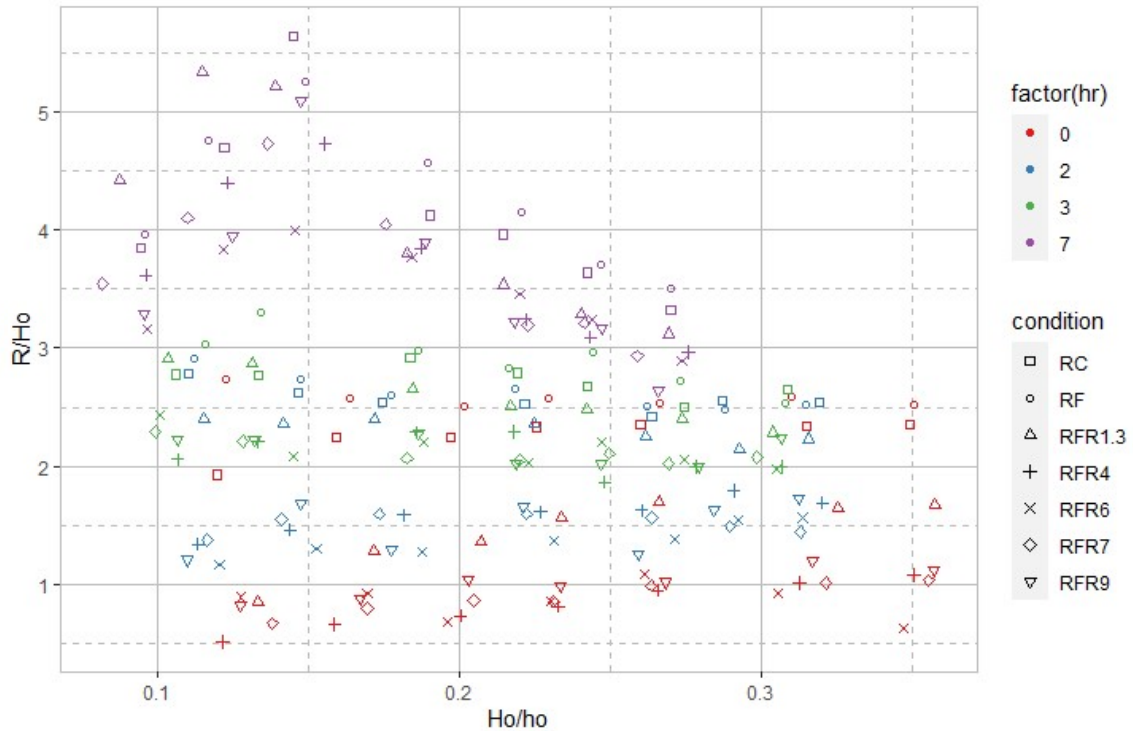
Figure 7-7 The non-dimensionalised runup (R/H_o) against the incident wave height to offshore water depth ratio (H_o/h_o) for all reef water depths, h_r. RC – reef-crest, RF – reef-flat without roughness, RFR1.3 – reef-flat with w/K of 1.3, RFR4 – reef-flat with w/K of 4, RFR6 – reef-flat with w/K of 6, RFR7 – reef-flat with w/K of 7 and RFR9 – reef-flat with w/K of 9.

The runup reduction by reef crest as compared to the reef flat was observed up to 31% and higher runup reduction was seen in shallow depths. In deep reef water depths, there was no reduction could be observed, and some cases runup with reef crest was higher than in the case of the reef flat. In reef flat with w/K was 1.3 (i.e., dense roughness) and in shallow depths, runup was reduced up to 66%. Nevertheless, the runup has been increased up to 10% in deep water for dense roughness case due to the resonance factor. For immediate roughness case (i.e., $4 < w/K < 9$), the runup reduction was recorded between 3% to 81%. The highest runup reduction was observed in shallow water depths.
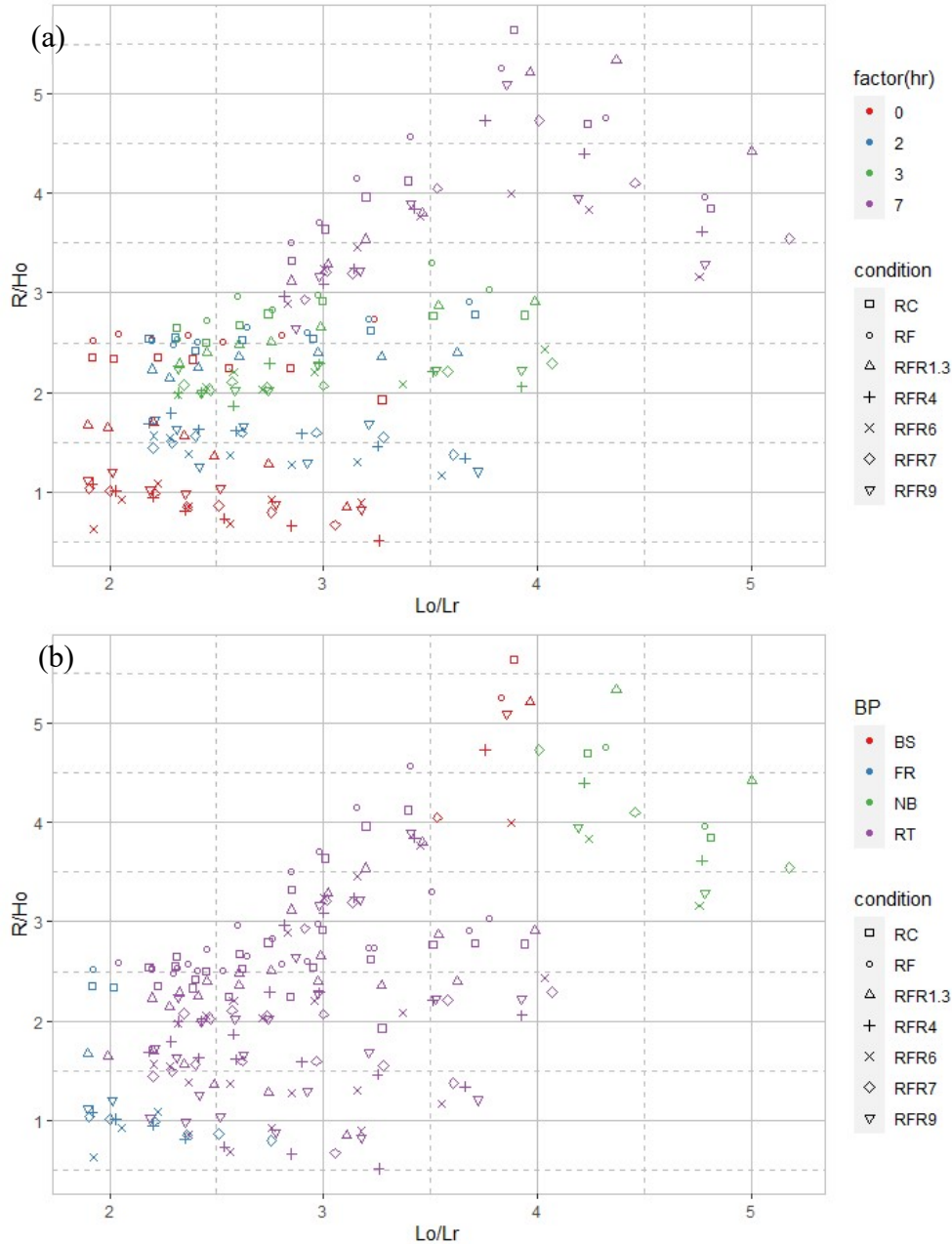
Figure 7-8 The non-dimensionalised runup (R/H_o) against the incident wavelength to reef-flat width ratio (L_o/L_r) for all reef water depths, h_r. RC – reef-crest, RF – reef-flat without roughness, RFR1.3 – reef-flat with w/K of 1.3, RFR4 – reef-flat with w/K of 4, RFR6 – reef-flat with w/K of 6, RFR7 – reef-flat with w/K of 7 and RFR9 – reef-flat with w/K of 9 in the aspect of; (a) reef water depth, (b) breaking point (BP). BS – breaking at final slope, FR – breaking at fore-reef slope, NB – nonbreaking, RT – breaking at reef top.

The reason for the runup increment in low wave heights with reef-flat is the resonance factor, as shown in Fig. 7-8. As the incident wavelength reached four times of reef-flat width ($L_o = 4L_r$), the runup heights (R/H_o) tends to dominate. However, with sufficiently low reef water depths (h_r) and the bottom roughness (especially 'k' type roughness), the resonance factor is getting reduced. In the 'd' type roughness case, the frictional drag (viscous drag) dominates over the pressure drag (form drag). In contrast, for a 'k' type roughness, the pressure drag is considerable (Leonardi et al., 2007), which ultimately dissipates the energy of a wave travelling on shallow depths.

The nonbreaking waves were observed for the incident wavelength is greater than four times of reef-flat width ($L_o > 4L_r$) and more considerable reef water depths (h_r). Therefore, the narrow reef-flat width (L_r) causes less energy dissipation while allowing waves to propagate without breaking. When $L_o = 4L_r$, the wave height amplifies at the resonance stage and exceed the stable wave height at a certain depth. This causes surge breaking (bore type). For $L_o < 4L_r$ progressive and growing waves are generated due to reflection by the final slope at large reef water depths (h_r) which may break as spilling breakers at the reef flat. At shallow reef water depths (h_r), the turbulent bores were observed which were progressive and dissipative, result in lesser runup due to energy dissipation by bottom roughness. Highly nonlinear waves (high H_o/h_o) at very shallow reef water depths (h_r) break at fore-reef slope as surging breaking cause weak propagation on the reef-flat and lesser runup. Therefore, a reef-crest system having sufficiently large reef width and shallow reef water depth with intermediate roughness could effectively dissipate tsunami energy. Otherwise, the tsunami wave may amplify in the coral reef platform causing massive damage to the surrounding area. However, the runup reduction by coral reef roughness was not so significant as in the case of forest model (see Section 5.3 and 6.3.2). This may be due to the frontal area density (A) which obstruct the flow is comparatively higher in forest model than reef canopy model. As a result, the pressure drag is considerable in the forest model, enabling dissipating energy cause lesser runup.

The non-dimensionalised runup (R/h_r) against the surf-similarity, $\xi = s_2/(H_o/h_r)$ is plotted in Fig. 7-9 for reef water depth, $h_r > 0$. The upper bound of the runup results can be identified as the reef-crest (RC), reef-flat (RF) and reef-flat with 'd' type roughness

(RFR1.3). It can be seen that the runup (R/h_r) is decreased with increasing surf-similarity parameter of the final slope, $\xi = s_2/(H_o/h_r)$. Yao et al. (2018) have used both fore-reef slope and final slope as 1/6, and a reef-flat width and height of 9.6 m and 35 cm, with a combination of five incident wave heights (H_o from 4 cm to 12 cm), and five water depths (h_o from 35 cm to 45 cm) corresponded to the reef water depths (h_r from 0 to 10 cm) in their experimental investigations. The present experimental results of runup with reef-flat and the results of reef-flat conducted by Yao et al. (2018) were used to derive an empirical equation using multiple linear regression analysis incorporating the parameters of final slope (s_2), reef water depth (h_r) and offshore wave heights (H_o).

$$\frac{R}{h_r} = C_8 s_2^{(C_9 \ln \xi_2 + C_{10})} \left(\frac{h_r}{H_o}\right)^{(C_{11} \ln s_2 + C_{12})} \tag{7-2}$$
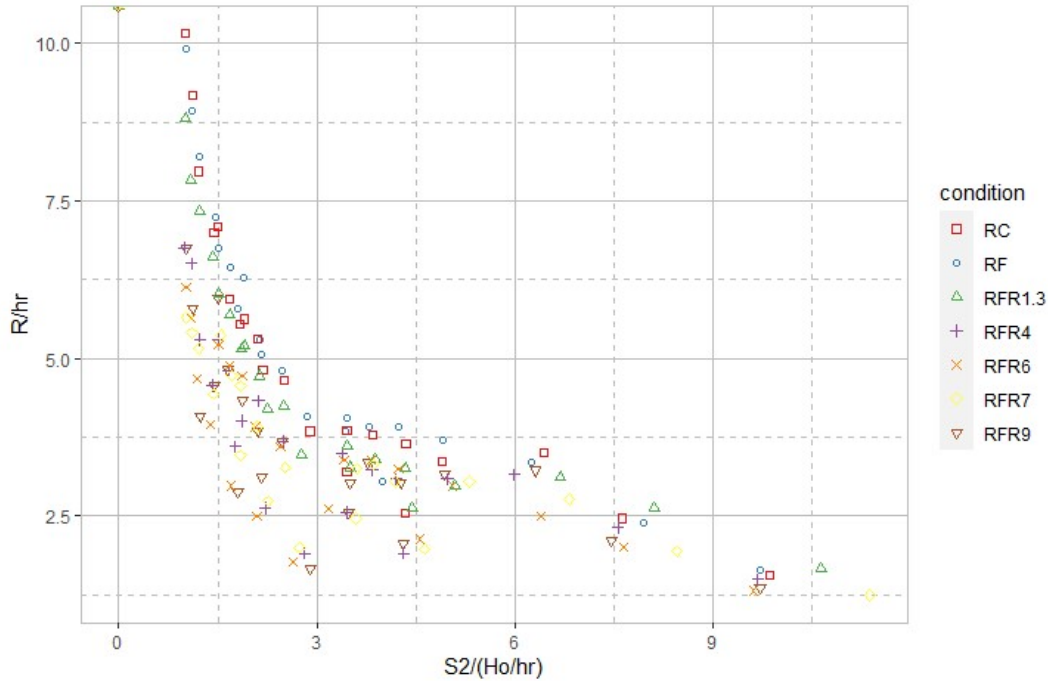
Figure 7-9 The non-dimensionalised runup (R/h_r) against the surf-similarity parameter, $\xi = s_2/(H_o/h_r)$ for reef water depths, $h_r > 0$. RC – reef-crest, RF – reef-flat without roughness, RFR1.3 – reef-flat with w/K of 1.3, RFR4 – reef-flat with w/K of 4, RFR6 – reef-flat with w/K of 6, RFR7 – reef-flat with w/K of 7 and RFR9 – reef-flat with w/K of 9.

The empirical coefficients of C_8, C_9, C_{10}, C_{11}, and C_{12}, were found as 1.475, -1.317, -2.462, -0.416 and -1.28, respectively. The total observations were 41 and the statistical

measures of mean absolute error (MAE), the root-mean-square (RMSE), scatter index (SCI), correlation coefficient (R^2) and agreement index (C_R) were found as 0.233, 0.092, 0.025, 0.981 and 0.995, respectively. The statistical measures show that the correlation between the experiments and the calculated by the proposed Eq. (7-2) is high. It is observed that even the proposed empirical equation does not include the parameters of reef-flat width (L_r) and foreshore slope (s_1), the equation predicts reasonably well for the experimental laboratory results. The proposed empirical solution is shown goodness of fit with experimental data as almost all the data lies within a 20% error range as in Fig. 7-10. Hence the proposed empirical equation can be used to apply for estimating solitary wave runup on a reef-flat without the coral roughness condition.
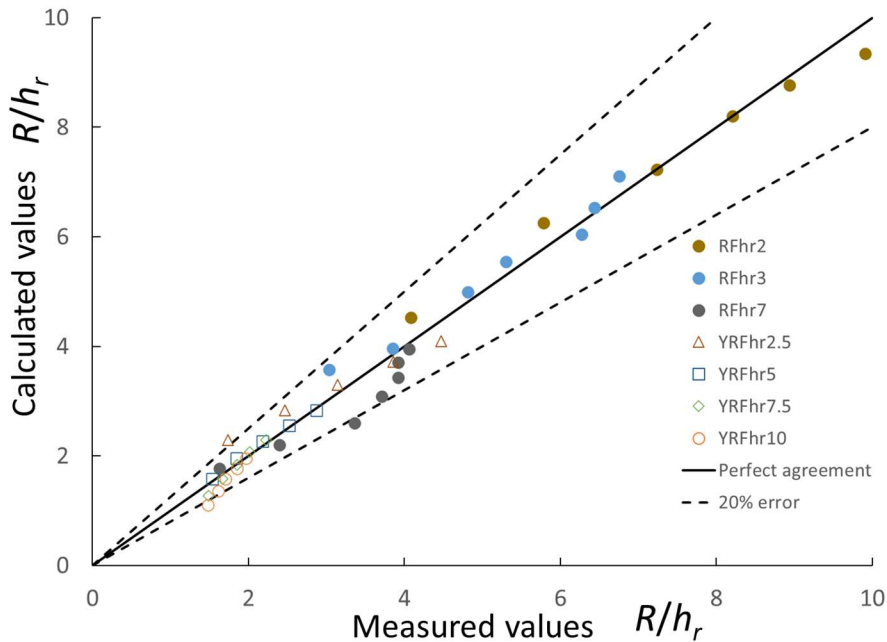
Figure 7-10 Comparison of measured values and calculated values by Eq. (7-2) for the maximum runup (R/h_r) and reef water depth h_r>0. RFhr2, RFhr3 and RFhr7 are present experimental results for reef-flat with reef water depth, 2, 3 and 7 cm, respectively. YRFhr2.5, YRFhr5, YRFhr7.5 and YRFhr10 are results from Yao et al. (2018) for reef-flat with reef water depth 2.5, 5, 7.5 and 10 cm, respectively.

7.3.3   Wave transformation along the Reef-lagoon

The water surface elevation corresponding to initial wave height (H_o) and transmitted wave height at the toe of beach slope (H_{bst}), reef-edge (H_{cr}) and at the toe of final slope (H_T),

respectively, are investigated to understand the flow phenomena nearby a coral reef lagoon. Fig. 7-3 shows the non-dimensionalised transmitted wave height (H_{bst}/h_o) concerning wave height to depth ratio (H_o/h_o) for the case of lagoon water depths (h_L) varying from 4 cm to 14 cm corresponded to still water depth (h_o) change from 20 cm to 30 cm.
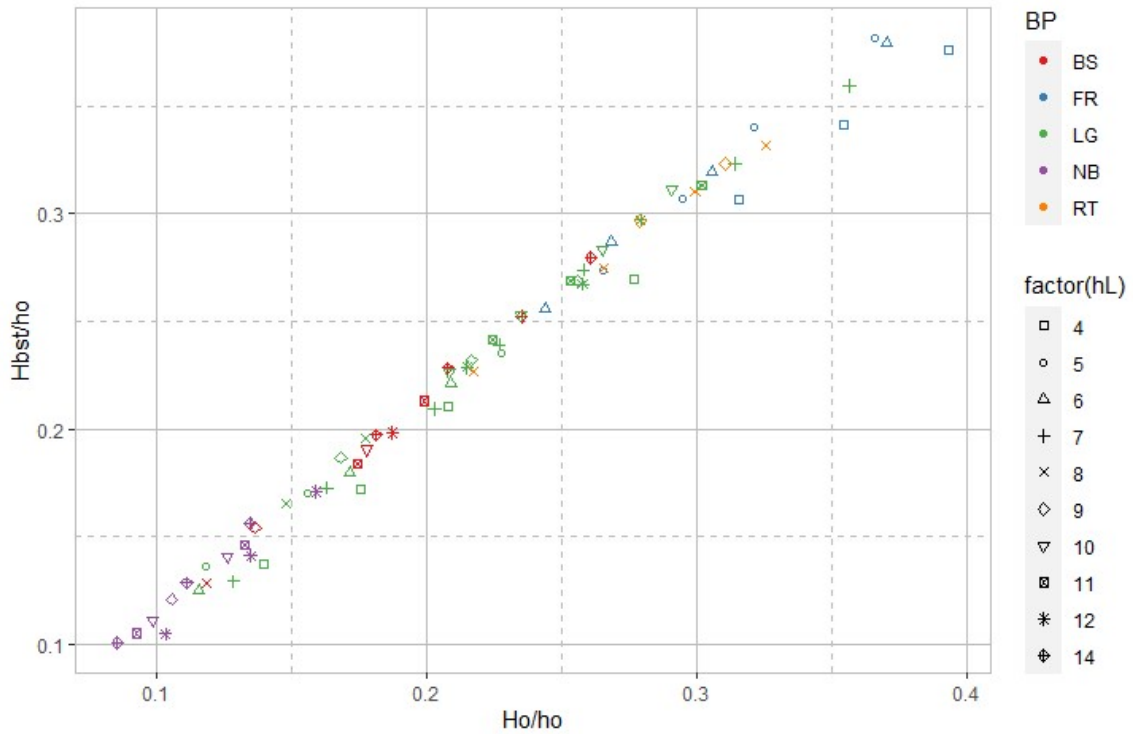
Figure 7-11 The transmitted wave height at toe of beach slope over water depth ratio (H_{bst}/h_o) against the incident wave height to water depth ratio (H_o/h_o) for all lagoon depths h_L (in cm). BP - breaking point, BS – breaking at final slope, FR – breaking at fore-reef slope, LG – breaking at lagoon, NB – nonbreaking, RT – breaking at reef top.

The shoaling of the transmitted wave at beach slope (H_{bst}) concerning the incident wave height (H_o) was within 17% range. As the length of the fore-reef slope is smaller than the incident wavelength (L_o), the waveform becomes pitched-forward, and the shoaling process is not fully evolved in the fore-reef length. Therefore, the leading tip of the incident wave reaches the shore while some part of the waveform remains offshore from the fore reef. Consequently, part of wave energy is transmitted to the reef flat. The waves which break at the reef-lagoon induce wave setup to cause a rise in the water level of reef-lagoon, as shown in Fig. 7-12.

In the case of low water depths (h_o< 23 cm) where reef edge is above the offshore water level, the transmitted wave height at the reef edge (H_{cr}) was significantly reduced compare to the other cases. As the waves propagate, they may either break at the front slope (FR) as shown in Fig. 7-13, and the reflection by fore-reef slope, the part of wave energy is dissipated, and the remaining energy is transmitted into the lagoon. For highly nonlinear waves (higher H_o/h_o) which break at either reef-flat or lagoon inside denoted by RT and LG in Fig. 7-13, due to the wave energy dissipation by depth limited breaking, the transmitted wave heights (H_{cr}) was further reduced. The nonbreaking waves and waves that break at final slope denoted by NB and BS respectively propagated passing the reef ridge with comparatively minimum energy dissipation compared to the cases of nonbreaking waves (NB) and the waves that break at the landward slope (BS).
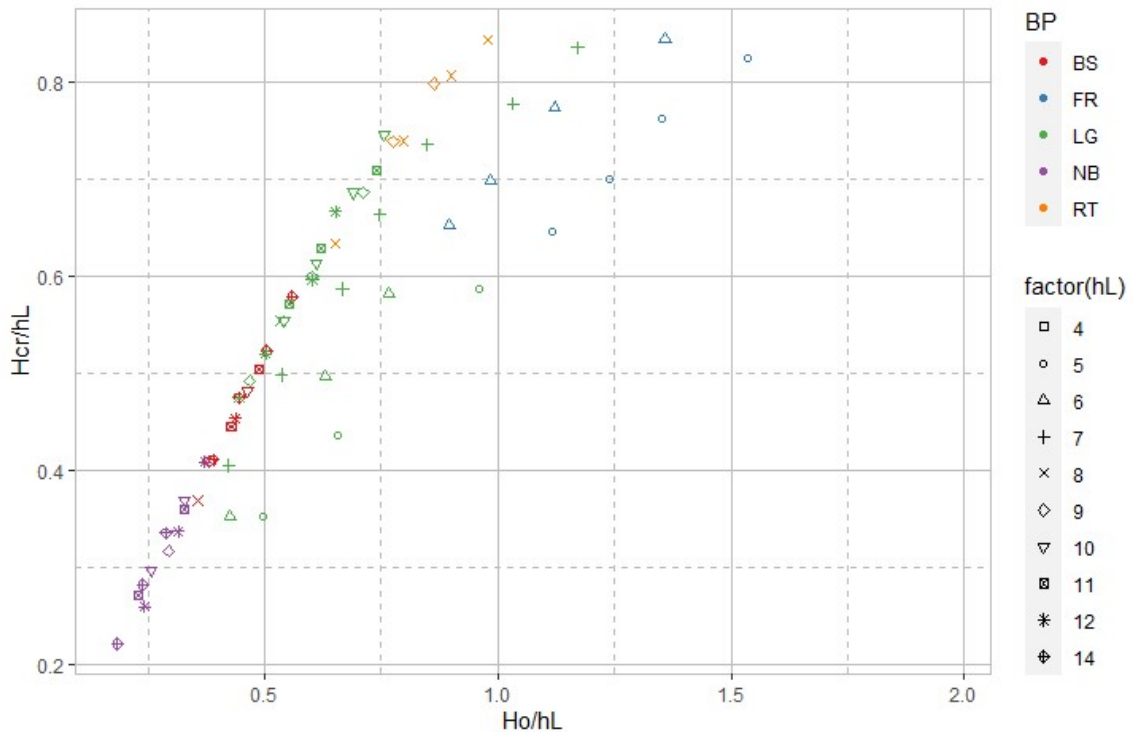
Figure 7-12 The transmitted wave height at reef edge over lagoon depth ratio (H_{cr}/h_L) against the incident wave height to lagoon depth ratio (H_o/h_L) for all lagoon depths h_L (in cm). BP - breaking point, BS – breaking at final slope, FR – breaking at fore-reef slope, LG – breaking at lagoon, NB – nonbreaking, RT – breaking at reef top.

The wave transformation results provided by wave gauge G4 near the toe of final beach slope are shown in Fig. 7-13.
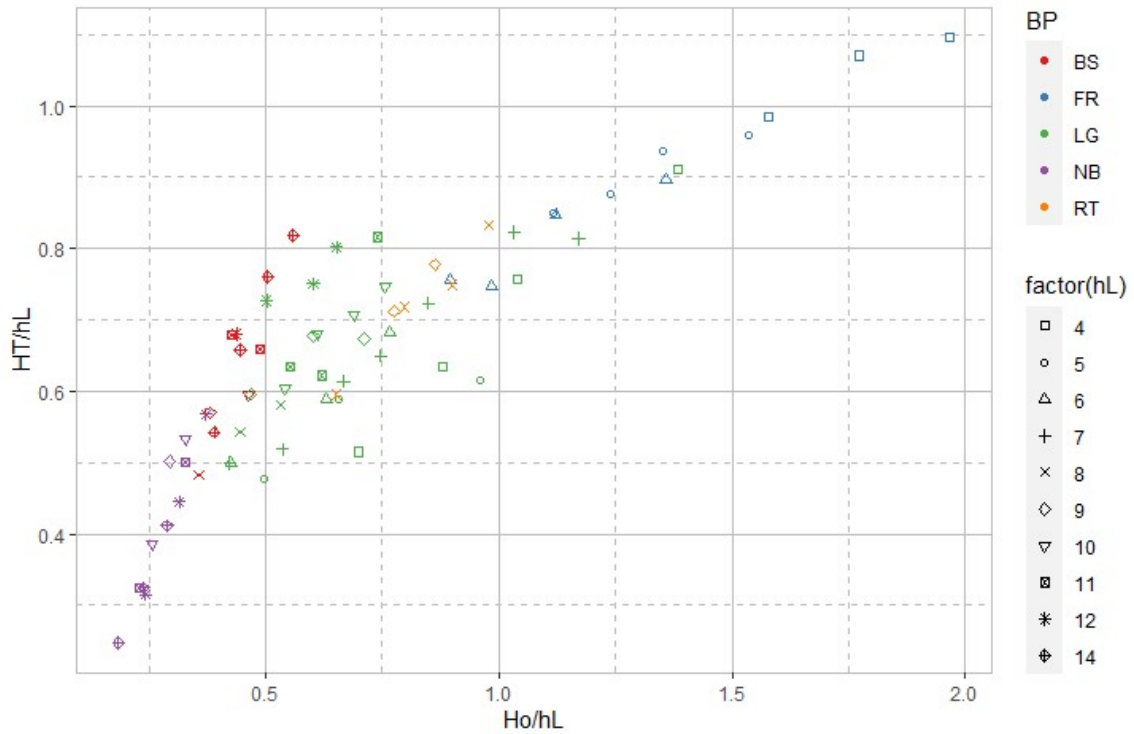
Figure 7-13 The transmitted wave height at toe of final slope over lagoon depth ratio (H_T/h_L) against the incident wave height to lagoon depth ratio (H_o/h_L) for all lagoon depths h_L (in cm). BP - breaking point, BS – breaking at final slope, FR – breaking at fore-reef slope, LG – breaking at lagoon, NB – nonbreaking, RT – breaking at reef-top.

The waves that break at reef-flat, lagoon inside and fore-reef slope (denoted by RT, LG and FR in Fig. 7-5) show a significant reduction in wave heights due to energy dissipation by bottom friction and the turbulence. The waves that break at final slope were observed as surge breaking (bore type), and the waves that break at lagoon inside were observed as spilling breaking. The transmitted wave height was higher than the incident waves for low offshore incident wave heights (H_o) on high water depths (h_L) indicating an amplification.

The breaking criterion for present experimental conditions with reef-lagoon was found as 0.37. When the incident wave height to reef water depth ratio (H_o/h_r) was greater than 0.37, waves either break at the final slope of 1/4 or reef-lagoon or fore-reef slope. For H_o/h_r

< 0.37, the waves propagate throughout the coral reef system without any breaking. The wave breaking ratio for reef-lagoon has deviated with the theoretical breaking criterion as well as in the case of reef-flat (see Section 7.3.1) which is lesser. This is probably due to the force breaking induced at the reef-top where water over reef-top is lesser than lagoon water depth (i.e., $h_r < h_L$). In the literature, Nelson (1994) showed that on laboratory experiments or on coral reef platforms that wave breaking ratio can be reduced to 0.55. Hardy and Young (1996) found in the field survey that depth limited wave breaking ratio can be varied as 0.4 to 0.6.

Yao et al. (2018) found that the runup (R/H_o) increased with the increasing width of the lagoon (L_L) and decreasing width of reef top where they conducted their experiments by setting a constant value of the summation of lagoon length and reef top width (i.e., fixed reef flat width). Therefore, it is expected that due to comparatively, higher lagoon water depths cause less dissipative than in the case of reef-flat with shallow water depth.

7.3.4 Wave runup with Reef-lagoon

The results of maximum runup (R/H_o) with reef-lagoon (RL) for the experimental cases shown in Table 7-1, against wave height to lagoon water depth ratio (H_o/h_L) were plotted as shown in Fig. 7-14. The breaking point (BP) was categorized as breaking at the fore-reef slope (FR), breaking at reef-top (RT), breaking at the final slope (BS) and nonbreaking (NB). When the wave height to reef water depth ratio (H_o/h_L) is below the value of 0.37, the waves propagate through the reef without breaking (denoted by NB) as shown in Fig. 7-14. Beyond the value of H_o/h_L of 0.37, the breaking occurred at the final slope (BS), and for higher H_o/h_L the breaking occurred in the reef-top (RT) or at the fore-reef slope (FR). The runup (R/H_o) was increased with H_o/h_L for nonbreaking waves. The highest runup could be observed from the waves which broke at beach slope (BS) as seen in the case of the reef flat. The runup (R/H_o) was decreased with increasing for H_o/h_L for breaking waves except for very shallow water depths of h_o = 20cm corresponded to h_L = 4 cm. Since offshore water depths (h_o) are lower than the height of reef -ridge, which is 23 cm, the presence of a reef-crest board of 3 cm (i.e., h_r = -3 cm) reduce the wave transmission into the lagoon for low offshore wave heights (H_o) by retarding the wave energy by reflection by the fore-reef slope. Nevertheless, for the cases of lagoon depths, h_L = 5, 6 and 7 cm

corresponded to offshore water depth, $h_o = 21$, 22 and 23 cm and water depth over reef top, $h_r = -2$, -1 and 0 cm, the wave reflection by fore-reef slope become less, and the wave energy of incident waves was transmitted with the shoaling at the reef top.
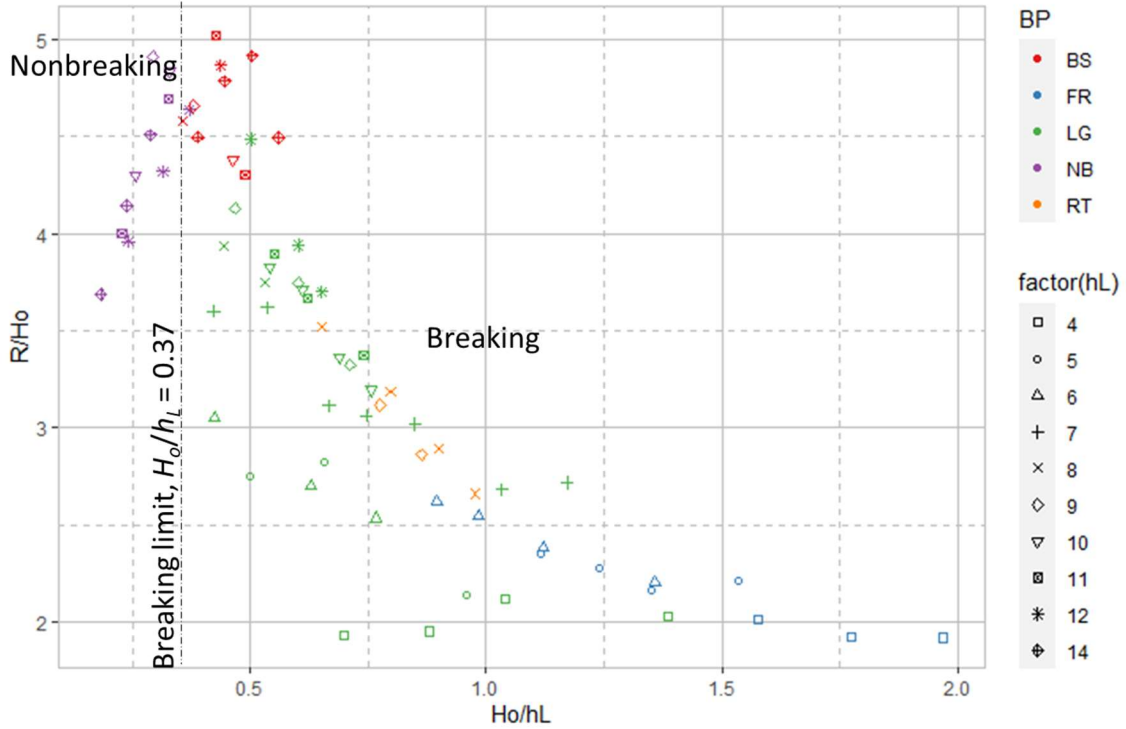
Figure 7-14 The non-dimensionalised runup height (R/H_o) against the incident wave height to lagoon depth ratio (H_o/h_L) for all lagoon depths h_L (in cm). BP - breaking point, BS – breaking at final slope, FR – breaking at fore-reef slope, LG – breaking at lagoon, NB – nonbreaking, RT – breaking at reef.

The runup height is monotonically decreased with decreasing offshore wave heights (H_o) for low water depths (i.e., $h_o = 25$ cm and $h_r = 2$ cm), as shown in Fig. 7-7 and reef-flat with 'k' type roughness. However, in case of 'd' type roughness (RFR1.3), reef-flat (RF) and reef-crest (RC), the runup (R/H_o) is monotonically increased with decreasing offshore wave heights (H_o). When the reef water depth, h_r is zero, except the reef-flat case (RF) all the other cases, the runup (R/H_o) is decreased with decreasing offshore wave heights (H_o). The reason for the runup increment in low wave heights with reef-lagoon is caused by the resonance factor, as shown in Fig. 7-15. As the incident wavelength reached

four times of reef-flat width ($L_o = 4L_r$), the runup heights (R/H_o) tends to be increased. However, with sufficiently low lagoon water depths (h_L), the resonance factor is getting reduced.
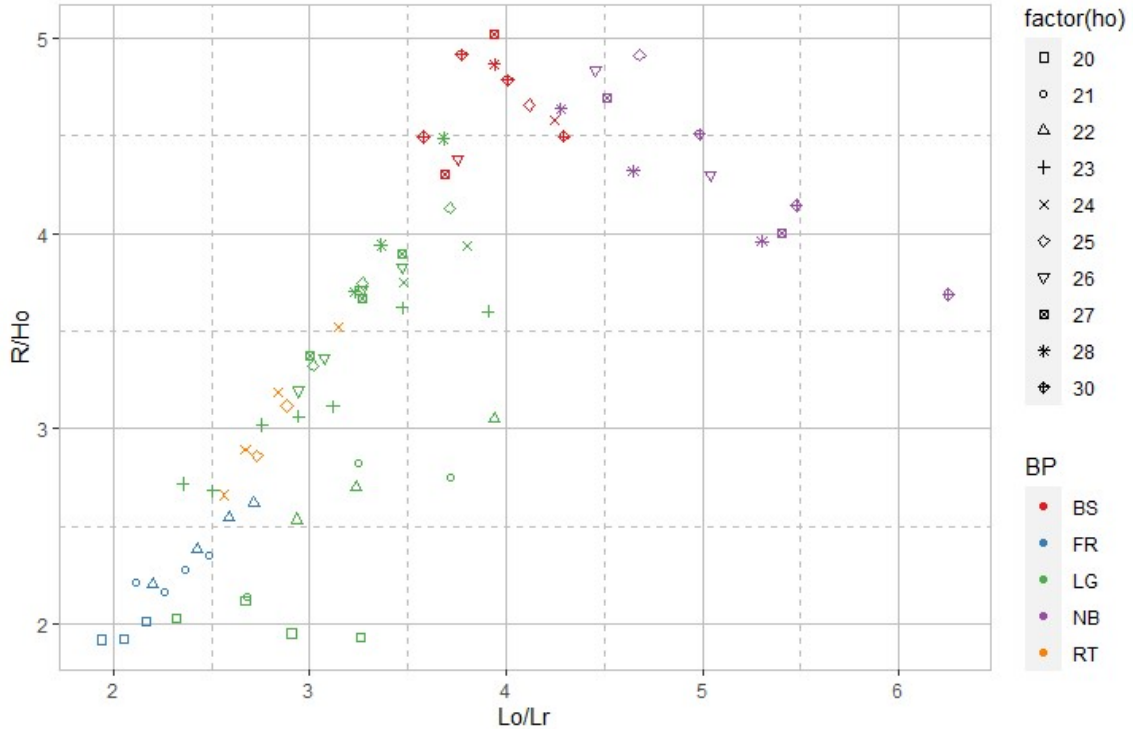
Figure 7-15 The non-dimensionalised runup height (R/H_o) against the incident wavelength to cross-shore distance of reef-lagoon (L_o/L_r) for all lagoon depths h_L (in cm). BP - breaking point, BS – breaking at final slope, FR – breaking at fore-reef slope, LG – breaking at lagoon, NB – nonbreaking, RT – breaking at reef.

The nonbreaking waves were observed with deformed wave shape for the incident wavelength is greater than four times of reef-flat width ($L_o > 4L_r$) and high lagoon water depths (h_L). Therefore, the narrow reef-lagoon width (L_r) causes less energy dissipation while allowing waves with no breaking. When $L_o = 4L_r$, the wave height amplifies at the resonance stage and exceed the stable wave height at a certain depth and resulted in surge breaking (bore type) similar to the reef-flat case (see Section 7.3.2). For $L_o < 4L_r$ progressive and growing waves are generated due to reflection by the final slope at large lagoon water depths (h_L) which may break as spilling breakers at the reef-lagoon. At shallow reef water depths (h_r), the turbulent bores were observed which were progressive

and dissipative, result in lesser runup due to energy dissipation by turbulence. Highly nonlinear waves (high H_o/h_o) at very shallow reef water depths (h_r) break at fore-reef slope as surging breaking cause weak propagation on the reef-lagoon and resulted in the lesser runup. Therefore, a reef-lagoon system consists of sufficiently large reef width and shallow reef water depth and emerged reef-top could effectively dissipate tsunami energy.

The non-dimensionalised runup (R/h_L) against the surf-similarity, $\xi = s_2/(H_o/h_L)$ is plotted in Fig. 7-16 for all lagoon water depth, h_L.
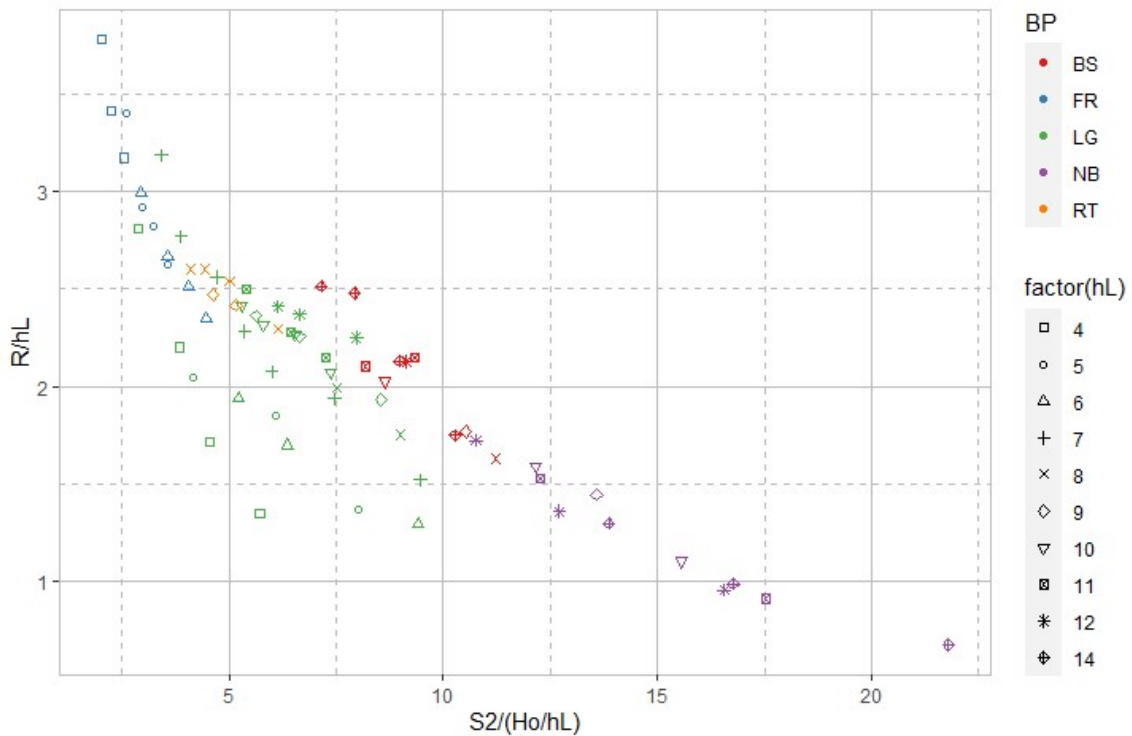
Figure 7-16 The non-dimensionalised runup height (R/h_L) against the the surf-similarity parameter, $\xi = s_2/(H_o/h_L)$ for reef lagoon depths, h_L. BP - breaking point, BS – breaking at final slope, FR – breaking at fore-reef slope, LG – breaking at lagoon, NB – nonbreaking, RT – breaking at reef.

Yao et al. (2018) have used both fore-reef slope and final slope as 1/6, and a reef-lagoon width and depth of 9.6 m and 35 cm. They have conducted four lagoon widths (L_L = 6.4 m, 4.8 m, 3.2 m and 1.6 m) corresponded to the reef top width of 3.2 m, 4.8 m, 6.4 m and 8 m, with a combination of five incident wave heights (H_o from 4 cm to 12 cm), and three lagoon water depths (h_L from 35 cm to 45 cm) corresponded to the reef water depths

(h_r from 0 to 5 cm) in their experimental investigations. The present experimental results of runup with reef-flat and the results of reef-flat conducted by Yao et al. (2018) were used to derive an empirical equation for $h_r > 0$ and breaking waves, using multiple linear regression analysis incorporating the parameters of final slope (s_2), lagoon water depth (h_L) and offshore wave heights (H_o).

$$\frac{R}{h_L} = \left(C_{13} + C_{14}\frac{h_L}{H_o}\right) s_2^{(C_{15} \ln s_2 + C_{16})} \left(\frac{H_o}{h_L}\right)^{(C_{17} \ln s_2 + C_{18})} \tag{7-3}$$

The empirical coefficients of C_{13}, C_{14}, C_{15}, C_{16}, C_{17} and C_{18}, were found as 4.928, -0.429, -2.309, -2.843, 1.133 and 1.828, respectively. The total observations were 67 and the statistical measures of mean absolute error (MAE), the root-mean-square (RMSE), scatter index (SCI), correlation coefficient (R^2) and agreement index (C_R) were found as 0.086, 0.013, 0.01, 0.985 and 0.996, respectively. The statistical measures show that the correlation between the experiments and the calculated by the proposed Eq. (7-3) is high. It is observed that even the proposed empirical equation does not include the parameters of reef-flat width (L_r) and foreshore slope (s_1), the equation predicts reasonably well for the experimental laboratory results of breaking waves on reef lagoon. The proposed empirical solution is shown goodness of fit with experimental data as almost all the data lies within a 20% error range as in Fig. 7-17. Hence the proposed empirical equation can be used to apply for estimating breaking solitary wave runup on a reef-lagoon.

The runup of reef lagoon compared with the cases of reef crest and reef flat with and without roughness as shown in Fig. 7-18 for each offshore water depths (h_o) of 23, 25, 26 and 30 cm corresponded to water depth above reef flat, h_r (reef top in case of the lagoon) as illustrated in Fig. 7-1. The maximum runup on a reef lagoon was 5% to 59% higher than all the cases of reef flat case at same reef water depths (h_r), still water depth (h_o) and wave height (H_o) except weakly nonlinear waves on large water depths ($h_o = 30$ and $H_o/h_o < 0.19$). As the lagoon is deeper, it could exert less dissipation by bottom friction on the travelling waves compared to the shallower reef flat. On the other hand, nonbreaking waves on reef lagoon may subject to less reflection due to the presence of a deep channel and not excite as reef flat to create a standing wave. Reef flat cause early breaking than the reef lagoon due to frictional dissipation induced by the shallow depths. Therefore, it is

anticipated that a reef lagoon may cause intensified damage by the tsunami than the reef flat.
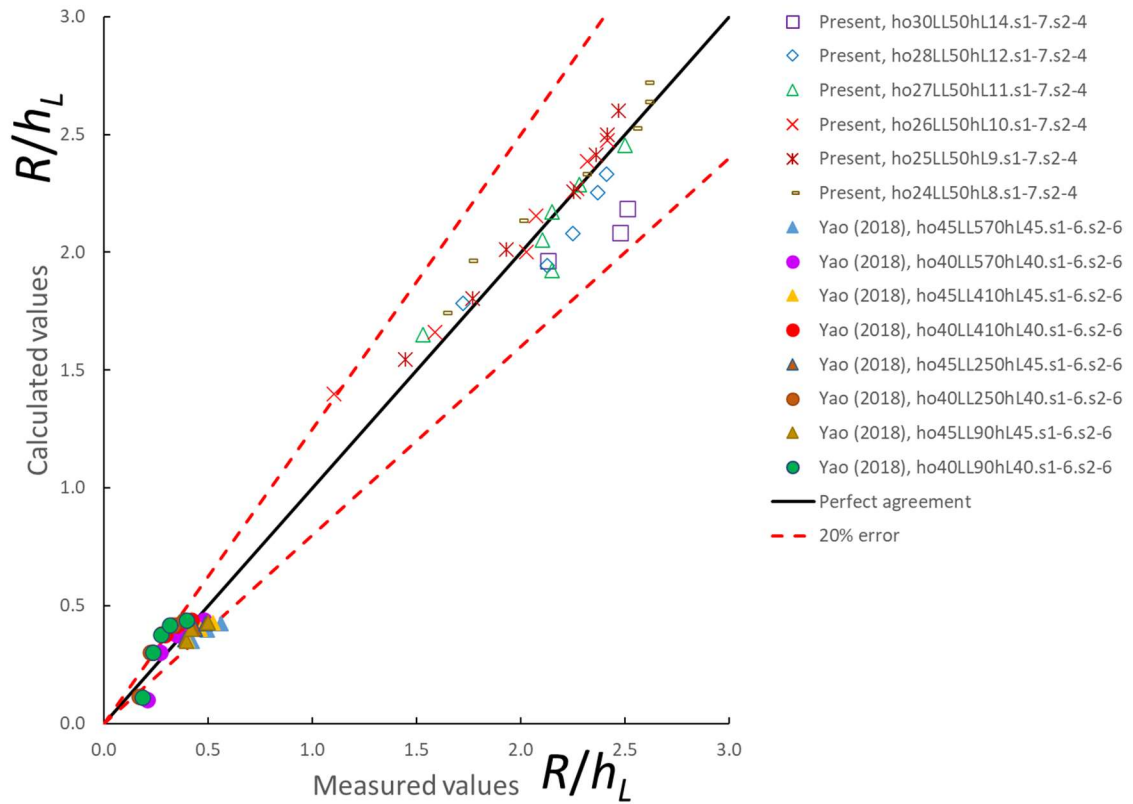
Figure 7-17 The comparison of non-dimensionalised runup height (R/h_L) between the measured values and calculated values by Eq. (7-3) for breaking waves on reef lagoon. Open plots denote present experimental results and closed plots denote experimental results of Yao et al. (2018). Solid line shows the prefect agreement, and the broken line shows the 20% error range. The parameters, h_o, L_L, h_L, s_1 and s_2 define offshore water depth, cross-shore distance of lagoon, lagoon depth, fore reef slope and final slope, respectively.
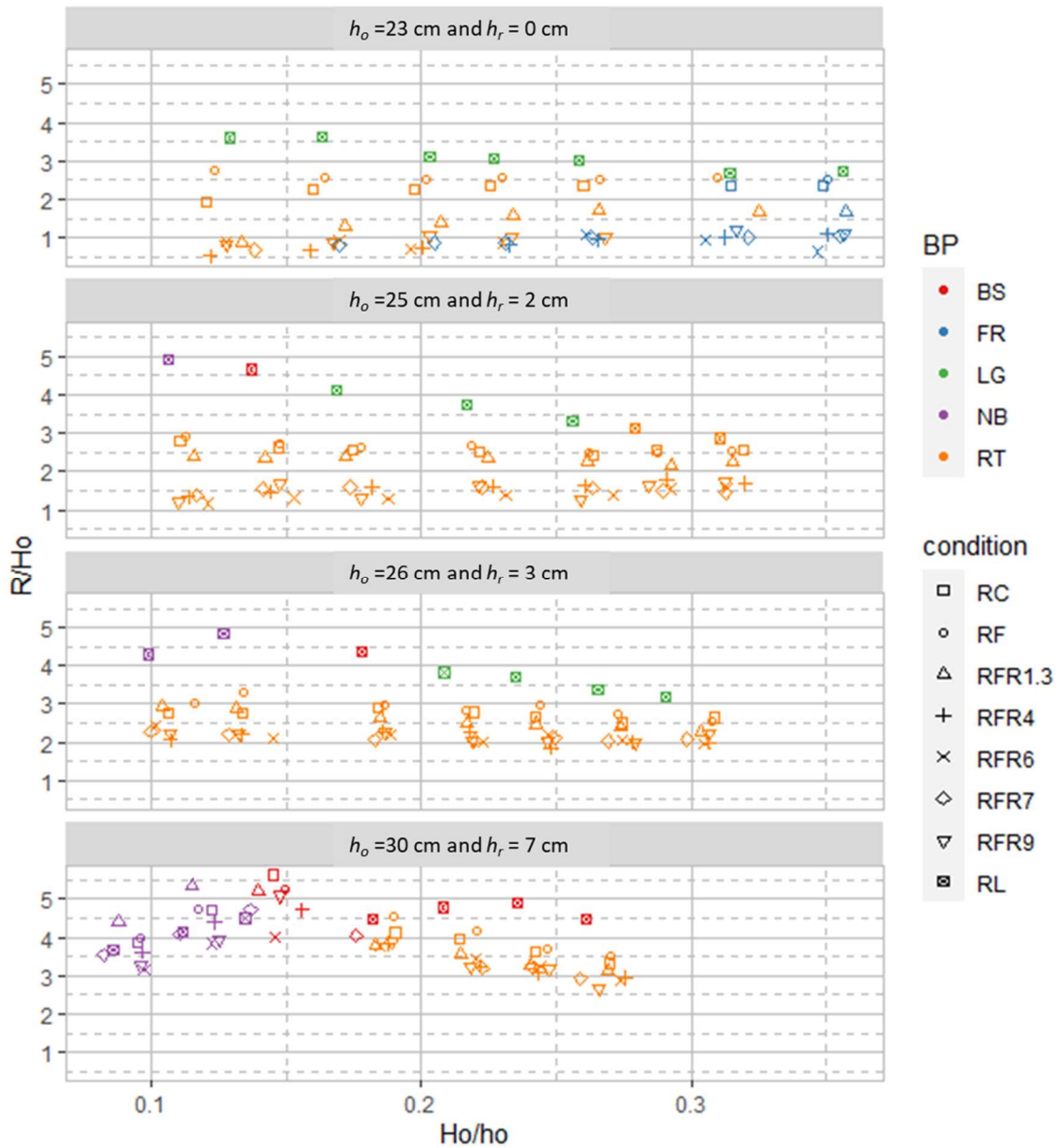
Figure 7-18 Comparison of maximum runup (R/H_o) against the wave height to depth ratio (H_o/h_o) for the cases; reef crest (RC), reef flat without roughness (RF), reef-flat with w/K of 1.3 (RFR1.3), reef-flat with w/K of 4 (RFR4), reef-flat with w/K of 6 (RFR6), reef-flat with w/K of 7 (RFR7), reef-flat with w/K of 9 (RFR9) and reef lagoon (RL) and the offshore water depths (h_o) of 23, 25, 26 and 30 cm. BP - breaking point, BS – breaking at final slope, FR – breaking at fore-reef slope, LG – breaking at lagoon, NB – nonbreaking, RT – breaking at reef.

7.4   Conclusion

A total of 266 laboratory experiments were conducted, covering eight types of bottom bathymetry configurations of coral reef systems which include the reef crest, reef lagoon and reef flat with and without roughness. To understand the physics of tsunami, the transformation and run-up of a tsunami-like solitary wave over coral reef system were investigated. The effects of different wave characteristics by changing wave height and water depths and reef morphology factors such as reef water depth and roughness were analyzed. Rectangular strips at regular intervals were used to represent the coral reef roughness as to simplify the geometry and hence to examine the effect of dense roughness ('d' type roughness) and intermediate roughness ('k' type roughness).

The surging breaking at the fore-reef slope and landward slope, the spilling breaking and turbulent bores at reef flat and nonbreaking waves were observed. The wave transmission characteristics and the wave breaking criterion were investigated. The depth limited breaking criteria was found as 0.6 for reef flat and 0.37 for reef lagoon. The maximum runup on a reef lagoon was 5% to 59% higher than the reef flat case except for weakly nonlinear waves on deep water. Reef flat width was found as the dominant parameter where resonance happens when the incident wavelength approach to four times of reef flat width. The runup results (runup over incident wave height) for large reef water depth, monotonically decrease with increasing wave height to reef water depth ratio and decreasing incident wavelength to reef flat width ratio for breaking waves. The runup increases with increasing wave height to reef water depth ratio and decreasing wavelength to reef flat width ratio for nonbreaking waves. Narrow reef flat widths found to be less effective as it allows the wave to propagate to the inland with minimum energy dissipation. However, for shallow water depths and with bottom roughness, the increment effect of runup is effectively reduced. The runup reduction by reef crest as compared to the reef flat was observed up to 31% and higher runup reduction was seen in shallow depths. In reef flat with dense roughness ('d' type) and shallow depths, runup was reduced up to 66%. In deep reef water depths, there was no reduction could be observed, and some cases runup with reef crest and reef flat with dense roughness was higher than in the case of the reef flat due to the resonance factor. For intermediate roughness case ('k' type), the runup

reduction was recorded between 3% to 81%. The highest runup reduction was observed in shallow water depths. The difference between the runup reduction by changing 'k' type roughness was found less significant. Empirical equations were proposed to predict the solitary wave runup over reef flat and reef lagoon by using the present experimental results and previous research work. The wave height to reef water depth ratio and the beach slope was found to be the most useful parameters to describe the runup. Depending on the reef water depth, reef flat width and the incident wave height, the resonant wave, progressive and growing and progressive and dissipative could be observed.

It is worthy of acknowledging that the reef geometry and tsunami wave are more complex than the present simplified model studied in the laboratory. The application of the empirical equations and the conclusions made in this study should be used with utmost care for tsunami hazard assessment.

.

Chapter 8

Conclusions & Recommendations

8.1   Summary

A statistical and geospatial analysis was conducted for coastal lagoons in Sri Lanka that affected by tsunami using collected field surveying data, statistical data, DEM data and land use data. The spatial variability of the settlement, forest and lagoon mouth was discussed. Influence by existing coast protective structures, drainage structures and the connection to the sea was investigated. The physical dimensions such as beach slope, dune height, barrier length, lagoon length in cross-shore and longshore direction and the area, and the measured tsunami heights during post-tsunami field surveys were investigated and how such parameters affect the damage ratio was illustrated. Limitations of the study were presented, and hence the laboratory experiments were conducted for detail investigations on tsunami runup.

The maximum vertical runup on the landward slope was measured for estimating energy reduction by tsunami-like solitary wave against the change of incident wave characteristics and the bathymetry profiles with and without roughness. The idealized bathymetry profile was changed as the plane slope, compound slope, sand dune coastal lagoon model, reef crest, reef lagoon and reef flat. The forest model of emergent rigid type was used to investigate effect for a forest on a sloping beach and sand dune coastal lagoon with forest. The coral reef roughness was modelled as rectangular strips at regular intervals to represent 'd' type and 'k' type roughness. The surface wave elevation and the maximum runup were used to analyse the effect of the aforementioned cases. The effectiveness in runup reduction and wave height attenuation regarding the forest and coral reef roughness case is explained. The wave breaking characteristics were also discussed. Empirical formulas were proposed and found good agreement with both present experimental conditions as well as previous research work. The tests of the reliability of the proposed equations included the agreement index (C_R), the correlation coefficient (R^2), the mean absolute error (MAE), the root-mean-square error (RMSE), and the scattering index (SCI).

The derived empirical equation can be used to estimate the tsunami runup behind the sand dune coastal lagoon and coral reef system in one horizontal dimension as an approximate and initial estimate. It can also be employed to verify numerical models. The equation is deduced from laboratory data where the energy dissipation might not scale well due to boundary layer dissipation and wave breaking. The refraction, diffraction and resonance effects are ignored in the present experimental conditions.

It is noteworthy to acknowledge that other than constraints in physical space, producing tsunami-like solitary wave in laboratory scale, the forest width, the diameter of the tree trunks, the coral reef roughness and setting the onshore slope, faced some technical complexities. Because of that fact, it is recommended for additional studies, including numerical modelling, to assess further the influence of properties in a coastal zone against the tsunami runup in a precise form. Past field survey and historical data information are also crucial in calibrating the numerical model. Nonetheless, the results of the present study may prove beneficial for the initial estimate, coastal landscape designs and understand the fundamental phenomena in Eco-DRR projects for coastal lagoons, coral reefs, and tree planting.

8.2   Direction of future research

The equation derived for maximum runup with forest model, sand dune coastal lagoon model, reef-flat-crest-lagoon model can be extended to understand the real generated tsunami effect. Present experiments have been carried out in fixed bed conditions and in one horizontal dimension. Therefore, it is recommended to conduct large scale laboratory experiments under movable bed conditions and three-dimensional laboratory modelling to investigate the combined refraction and diffraction phenomena in addition to the erosion. Additional numerical simulations which verify the present results can be used to assess the influence of properties in a coastal zone against the real tsunami conditions. Wave energy dissipation which associated with breaking needs to be quantified in order to simulate actual flow conditions. Past field survey and historical data in addition to laboratory experiments are also crucial in calibrating the numerical model.

References

Alongi, D.M., 2008. Mangrove forests: Resilience, protection from tsunamis, and responses to global climate change. Estuar. Coast. Shelf Sci. https://doi.org/10.1016/j.ecss.2007.08.024

Ammon, C.J., Ji, C., Thio, H.K., Robinson, D., Ni, S., Hjorleifsdottir, V., Kanamori, H., Lay, T., Das, S., Helmberger, D., Ichinose, G., Polet, J., Wald, D., 2005. Rupture process of the 2004 Sumatra-Andaman earthquake. Science (80-.). https://doi.org/10.1126/science.1112260

Applied Technology Council, Federal Emergency Management Agency (FEMA), 2012. Guidelines for Design of Structures for Vertical Evacuation from Tsunamis. Second Edition. FEMA P-646 Publ. https://doi.org/10.1061/40978(313)7

Baird, A.H., Campbell, S.J., Anggoro, A.W., Ardiwijaya, R.L., Fadli, N., Herdiana, Y., Kartawijaya, T., Mahyiddin, D., Mukminin, A., Pardede, S.T., Pratchett, M.S., Rudi, E., Siregar, A.M., 2005. Acehnese reefs in the wake of the Asian tsunami. Curr. Biol. 15, 1926–1930. https://doi.org/10.1016/j.cub.2005.09.036

Baldock, T.E., Cox, D., Maddux, T., Killian, J., Fayler, L., 2009. Kinematics of breaking tsunami wavefronts: A data set from large scale laboratory experiments. Coast. Eng. 56, 506–516. https://doi.org/10.1016/j.coastaleng.2008.10.011

Baldock, T.E., Peiris, D., Hogg, A.J., 2012. Overtopping of solitary waves and solitary bores on a plane beach. Proc. R. Soc. A Math. Phys. Eng. Sci. 468, 3494-3516. https://doi.org/10.1098/rspa.2011.0729

Barbier, E.B., 2016. The Protective Value of Estuarine and Coastal Ecosystem Services in a Wealth Accounting Framework. Environ. Resour. Econ. https://doi.org/10.1007/s10640-015-9931-z

Basco, D.R., 2006. Seawall Impacts on Adjacent Beaches : Separating Fact from Fiction. J. Coast. Res. si39 (Proceedings 8th Int. Coast. Symp. https://doi.org/10.2307/25741675

Battjes, J.A., 1974. Surf Similarity. Proc. 14th ASCE Coast. Engng. Conf. (Copenhagen, Denmark) 1, 466–480. https://doi.org/10.9753/icce.v14.26

Borthwick, A.G.L., Ford, M., Weston, B.P., Taylor, P.H., Stansby, P.K., 2006. Solitary wave transformation, breaking and run-up at a beach. Proc. Inst. Civ. Eng. - Marit. Eng. 159, 97–105. https://doi.org/10.1680/maen.2006.159.3.97

Boussinesq, J., 1872, The´orie des ondes et des remous qui se propagent le long d'un canal rectangulaire horizontal, en communiquant au liquid contenu dans ce canal des vitesses sensiblement pareilles de la surface au fond, J. Math. Pures Appl. 2nd Series, 17, 55– 108.

Bowen, A.J., Inman, D.L., Simmons, V.P., 1968. Wave 'set-down' and set-Up. J. Geophys. Res. 73, 2569–2577. https://doi.org/10.1029/JB073i008p02569

Buckley, M.L., Lowe, R.J., Hansen, J.E., Van Dongeren, A.R., 2016. Wave Setup over a Fringing Reef with Large Bottom Roughness. J. Phys. Oceanogr. 46, 2317–2333. https://doi.org/10.1175/JPO-D-15-0148.1

Camfield, F.E., Street, R.L., 1969. Shoaling of Solitary Waves on Small Slopes. J. Waterw. Harb. Div.

Carrier, G.F., Greenspan, H.P., 1958. Water waves of finite amplitude on a sloping beach. J. Fluid Mech. 4, 97–109. https://doi.org/10.1017/S0022112058000331

Chan, I.C., Liu, P.L.F., 2012. On the runup of long waves on a plane beach. J. Geophys. Res.

Ocean. 117, n/a-n/a. https://doi.org/10.1029/2012JC007994

Chang, Y.H., Hwang, K.S., Hwung, H.H., 2009. Large-scale laboratory measurements of solitary wave inundation on a 1:20 slope. Coast. Eng. 56, 1022-1034. https://doi.org/10.1016/j.coastaleng.2009.06.008

Chang, C.W., Liu, P.L.F., 2019. Long waves dissipation and harmonic generation by coastal vegetation. Appl. Ocean Res. https://doi.org/10.1016/j.apor.2018.10.001

Chatenoux, B., Peduzzi, P., 2007. Impacts from the 2004 Indian Ocean Tsunami: Analysing the potential protecting role of environmental features. Nat. Hazards 40, 289–304. https://doi.org/10.1007/s11069-006-0015-9

Chen, Q., Zhao, H., 2012. Theoretical Models for Wave Energy Dissipation Caused by Vegetation. J. Eng. Mech. 138, 221–229. https://doi.org/10.1061/(ASCE)EM.1943-7889.0000318

Cheriton, O.M., Storlazzi, C.D., Rosenberger, K.J., 2016. Observations of wave transformation over a fringing coral reef and the importance of low-frequency waves and offshore water levels to runup, overwash, and coastal flooding. J. Geophys. Res. Ocean. 121, 3121–3140. https://doi.org/10.1002/2015JC011231

Chindapol, N., Kaandorp, J.A., Cronemberger, C., Mass, T., Genin, A., 2013. Modelling Growth and Form of the Scleractinian Coral Pocillopora verrucosa and the Influence of Hydrodynamics. PLoS Comput. Biol. 9, 1002849. https://doi.org/10.1371/journal.pcbi.1002849

Choi, B.H., Hong, S.J., Pelinovsky, E., 2006. Distribution of runup heights of the December 26, 2004 tsunami in the Indian Ocean. Geophys. Res. Lett. 33, 2–5. https://doi.org/10.1029/2006GL025867

Cochard, R., 2011. The 2004 tsunami in Aceh and Southern Thailand: coastal ecosystem services, damages and resilience. Tsunami Threat. Technol.

Cochard, R., Ranamukhaarachchi, S.L., Shivakoti, G.P., Shipin, O. V., Edwards, P.J., Seeland, K.T., 2008. The 2004 tsunami in Aceh and Southern Thailand: A review on coastal ecosystems, wave hazards and vulnerability. Perspect. Plant Ecol. Evol. Syst. 10, 3–40. https://doi.org/10.1016/J.PPEES.2007.11.001

Contreras-López, M., Winckler, P., Sepúlveda, I., Andaur-Álvarez, A., Cortés-Molina, F., Guerrero, C.J., Mizobe, C.E., Igualt, F., Breuer, W., Beyá, J.F., Vergara, H., Figueroa-Sterquel, R., 2016. Field Survey of the 2015 Chile Tsunami with Emphasis on Coastal Wetland and Conservation Areas. Pure Appl. Geophys. 173, 349–367. https://doi.org/10.1007/s00024-015-1235-2

Dahdouh-Guebas, F., Hettiarachchi, S., Lo Seen, D., Batelaan, O., Sooriyarachchi, S., Jayatissa, L.P., Koedam, N., 2005a. Transitions in ancient inland freshwater resource management in Sri Lanka affect biota and human populations in and around coastal lagoons. Curr. Biol. 15, 579–586. https://doi.org/10.1016/j.cub.2005.01.053

Dahdouh-Guebas, F., Jayatissa, L.P., Di Nitto, D., Bosire, J.O., Lo Seen, D., Koedam, N., 2005b. How effective were mangroves as a defence against the recent tsunami? Curr. Biol. 15, R443–R447. https://doi.org/10.1016/J.CUB.2005.06.008

Dalrymple, R.A., Hwang, P., 1984. Wave diffraction due to areas of energy dissipation. Waterw. Port Coast. Ocean Eng. https://doi.org/10.1061/(ASCE)0733-950X(1984)110

DCS. 2007. Reports on census of buildings and people affected by the tsunami – 2004. Sri Lanka:

Department of Census and Statistics. Available from: www.statististics.gov.lk. [access date 2020.03.25]

Dean, R.G., Bender, C.J., 2006. Static wave setup with emphasis on damping effects by vegetation and bottom friction. Coast. Eng. 53, 149–156. https://doi.org/10.1016/j.coastaleng.2005.10.005

Dean, R.G., Walton, T.L., 2017. Wave Setup, in: Handbook of Coastal and Ocean Engineering: Expanded Edition. World Scientific Publishing Co. Pte. Ltd., pp. 21–43. https://doi.org/10.1142/9789813204027_0002

Dengler, L., Preuss, J., 2003. Mitigation lessons from the July 17, 1998 Papua New Guinea tsunami, Pure and Applied Geophysics. Birkhäuser-Verlag. https://doi.org/10.1007/s00024-003-2417-x

Didenkulova, I.I., Kurkin, A.A., Pelinovsky, E.N., 2007. Run-up of solitary waves on slopes with different profiles. Izv. - Atmos. Ocean Phys. 43, 384–390. https://doi.org/10.1134/S0001433807030139

Fenton, J., 1972. A ninth-order solution for the solitary wave. J. Fluid Mech. 53, 257–271. https://doi.org/10.1017/S002211207200014X

Fernando, H.J.S., McCulley, J.L., Mendis, S.G., Perera, K., 2005. Coral poaching worsens tsunami destruction in Sri Lanka. Eos, Trans. Am. Geophys. Union 86, 301. https://doi.org/10.1029/2005eo330002

Ford, M., Becker, J.M., Merrifield, M.A., Song, Y.T., 2014. Marshall Islands Fringing Reef and Atoll Lagoon Observations of the Tohoku Tsunami. Pure Appl. Geophys. 171, 3351–3363. https://doi.org/10.1007/s00024-013-0757-8

Fuchs, H., Hager, W.H., 2015. Solitary Impulse Wave Transformation to Overland Flow. J. Waterw. Port, Coastal, Ocean Eng. 141, 04015004. https://doi.org/10.1061/(ASCE)WW.1943-5460.0000294

Fuentes, M.A., Ruiz, J.A., Cisternas, A., 2013. A theoretical model of tsunami runup in Chile based on a simple bathymetry. Geophys. J. Int. 196, 986-995. https://doi.org/10.1093/gji/ggt426

Fuhrman, D.R., Madsen, P. A., 2008. Surf Similarity and Solitary Wave Runup. J. Waterw. Port, Coastal, Ocean Eng. 134, 195–198. https://doi.org/10.1061/(ASCE)0733-950X(2008)134:3(195)

Gawehn, M., van Dongeren, A., van Rooijen, A., Storlazzi, C.D., Cheriton, O.M., Reniers, A., 2016. Identification and classification of very low frequency waves on a coral reef flat. J. Geophys. Res. Ocean. 121, 7560–7574. https://doi.org/10.1002/2016JC011834

GEBCO DEM data 2019 version. available from https://download.gebco.net [access date 2020.01.14]

Gedan, K.B., Kirwan, M.L., Wolanski, E., Barbier, E.B., Silliman, B.R., 2011. The present and future role of coastal wetland vegetation in protecting shorelines: Answering recent challenges to the paradigm. Clim. Change 106, 7–29. https://doi.org/10.1007/s10584-010-0003-7

Gelfenbaum, G., Apotsos, A., Stevens, A.W., Jaffe, B., 2011. Effects of fringing reefs on tsunami inundation: American Samoa. Earth-Science Rev. https://doi.org/10.1016/j.earscirev.2010.12.005

Goring, D.G., 1979. Tsunamis: the propagation of long waves onto a shelf. PhD Thesis.

California Institute of Technology.

Gourlay, M.R., 1996a. Wave set-up on coral reefs. 1. Set-up and wave-generated flow on an idealised two dimensional horizontal reef. Coast. Eng. 27, 161–193. https://doi.org/10.1016/0378-3839(96)00008-7

Gourlay, M.R., 1996b. Wave set-up on coral reefs. 2. Set-up on reefs with various profiles. Coast. Eng. 28, 17–55. https://doi.org/10.1016/0378-3839(96)00009-9

Gourlay, M.R., Colleter, G., 2005. Wave-generated flow on coral reefs - An analysis for two-dimensional horizontal reef-tops with steep faces. Coast. Eng. 52, 353–387. https://doi.org/10.1016/j.coastaleng.2004.11.007

Grilli, S.T., Svendsen, I.A., Subramanya, R., 1997. Breaking Criterion and Characteristics for Solitary Waves on Slopes. J. Waterw. Port, Coastal, Ocean Eng. 123, 102–112. https://doi.org/10.1061/(ASCE)0733-950X(1997)123:3(102)

Hall, J.V.J., Watts, G.M., 1953. Laboratory investigation of the vertical rise of solitary waves on impermeable slopes. Army Coast. Eng. Res. Cent. Washingt. DC 33.

Hardy, T.A., Young, I.R., 1996. Field study of wave attenuation on an offshore coral reef. J. Geophys. Res. C Ocean. 101, 14311–14326. https://doi.org/10.1029/96JC00202

Hayashi, Y., 2008. Extracting the 2004 Indian Ocean tsunami signals from sea surface height data observed by satellite altimetry. J. Geophys. Res. 113, C01001. https://doi.org/10.1029/2007JC004177

Hearn, C.J., 1999. Wave-breaking hydrodynamics within coral reef systems and the effect of changing relative sea level. J. Geophys. Res. Ocean. 104, 30007–30019. https://doi.org/10.1029/1999jc900262

Hsiao, S.C., Hsu, T.W., Lin, T.C., Chang, Y.H., 2008. On the evolution and run-up of breaking solitary waves on a mild sloping beach. Coast. Eng. 55, 975–988. https://doi.org/10.1016/j.coastaleng.2008.03.002

Hughes, S.A., 2004. Estimation of wave run-up on smooth, impermeable slopes using the wave momentum flux parameter. Coast. Eng. 51, 1085-1104. https://doi.org/10.1016/j.coastaleng.2004.07.026

Hunt, I. A., 1959. Design of seawalls and breakwaters, U.S. Corps of Engineers, Lake Survey, Detroit, 49 pp.

Huang, Z., Yao, Y.Y., Sim, S.Y., Yao, Y.Y., 2011. Interaction of solitary waves with emergent, rigid vegetation. Ocean Eng. 38, 1080–1088. https://doi.org/10.1016/J.OCEANENG.2011.03.003

Igarashi, Y., Tanaka, N., 2018. Effectiveness of a compound defense system of sea embankment and coastal forest against a tsunami. Ocean Eng. 151, 246–256. https://doi.org/10.1016/j.oceaneng.2018.01.036

Iimura, K., Tanaka, N., 2012. Numerical simulation estimating effects of tree density distribution in coastal forest on tsunami mitigation. Ocean Eng. 54, 223–232. https://doi.org/10.1016/j.oceaneng.2012.07.025

Inoue, S., Wijeyewickrema, A.C., Matsumoto, H., Miura, H., Gunaratna, P., Madurapperuma, M., Sekiguchi, T., 2007. Field survey of tsunami effects in Sri Lanka due to the Sumatra-Andaman earthquake of December 26, 2004. Pure Appl. Geophys. 164, 395–411. https://doi.org/10.1007/s00024-006-0161-8

Iribarren, C.R., Nogales, C.M., 1949. Protection des ports. PIANC Congr. 1949 SII-C4, 31-80.

Irish, J.L., Weiss, R., Yang, Y., Song, Y.K., Zainali, A., Marivela-Colmenarejo, R., 2014. Laboratory experiments of tsunami Run-Up and withdrawal in patchy coastal forest on a steep beach. Nat. Hazards 74, 1933–1949. https://doi.org/10.1007/s11069-014-1286-1

Irtem, E., Gedik, N., Kabdasli, M.S., Yasa, N.E., 2009. Coastal forest effects on tsunami run-up heights. Ocean Eng. https://doi.org/10.1016/j.oceaneng.2008.11.007

Ismail, H., Abd Wahab, A.K., Alias, N.E., 2012. Determination of mangrove forest performance in reducing tsunami run-up using physical models. Nat. Hazards 63, 939–963. https://doi.org/10.1007/s11069-012-0200-y

Jaramillo, S., Pawlak, G., 2011. AUV-based bed roughness mapping over a tropical reef. Coral Reefs 30, 11–23. https://doi.org/10.1007/s00338-011-0731-9

Jarvis A., H.I. Reuter, A. Nelson, E. Guevara, 2008, Hole-filled seamless SRTM data V4, International Centre for Tropical Agriculture (CIAT), available from http://srtm.csi.cgiar.org. [access date 2020.03.26]

Kajiura, K., 1965. The leading wave of a tsunami. Deep Sea Res. Oceanogr. Abstr. 12, 599–600. https://doi.org/10.1016/0011-7471(65)90572-3

Kajiura, K. 1984. Runup of solitary wave on a slope—Investigation of the effects of wave breaking and bottom friction. [In Japanese.] Report of the Tsunami Hazards Mitigation Laboratory. Sendai, Japan: Tohoku University

Kaplan, K., 1955. Generalized laboratory study of tsunami run-up. Army Coast. Eng. Res. Cent. Washingt. DC 60.

Kânoğlu, U., Synolakis, C.E., 1998. Long wave runup on piecewise linear topographies. J. Fluid Mech. 374, 1–28. https://doi.org/10.1017/S0022112098002468

Keller, J.B., Keller, H.B., 1964. Water wave run-up on a beach. Off. Nav. Res. Dep. Navy 40.

Kerr, A.M., Baird, A.H., 2007. Natural Barriers to Natural Disasters. Bioscience 57, 102–103. https://doi.org/10.1641/B570202

Kimiwada, Y., Tanaka, N., Zaha, T., 2020. Differences in effectiveness of a hybrid tsunami defense system comprising an embankment, moat, and forest in submerged, emergent, or combined conditions. Ocean Eng. 208, 107457. https://doi.org/10.1016/j.oceaneng.2020.107457

Kirby, J.T., 2017. Recent advances in nearshore wave, circulation, and sediment transport modeling. J. Mar. Res. 75, 263–300. https://doi.org/10.1357/002224017821836824

Kishi, T., Saeki, H., 1967. The Shoaling, Breaking and Runup of the Solitary Wave on Impermeable Rough Slopes. American Society of Civil Engineers (ASCE), 322–348. https://doi.org/10.1061/9780872620087.021

Kjerfve, B., 1994. Coastal Lagoon Processes. Elsevier Sci. 2, 1689–1699. https://doi.org/10.1017/CBO9781107415324.004

Kobayashi, N., Karjadi, E.A., 1994. Surf‐Similarity Parameter for Breaking Solitary‐Wave Runup. J. Waterw. Port, Coastal, Ocean Eng. 120, 645−650. https://doi.org/10.1061/(ASCE)0733-950X(1994)120:6(645)

Kunkel, C.M., Hallberg, R.W., Oppenheimer, M., 2006. Coral reefs reduce tsunami impact in model simulations. Geophys. Res. Lett. 33, L23612. https://doi.org/10.1029/2006GL027892

Laitone, E. V., 1960. The second approximation to cnoidal and solitary waves. J. Fluid Mech. 9, 430–444. https://doi.org/10.1017/S0022112060001201

Larsen, B.E., Fuhrman, D.R., 2019. Full-scale CFD simulation of tsunamis. Part 1: Model validation and run-up. Coast. Eng. 151, 22–41. https://doi.org/10.1016/j.coastaleng.2019.04.012

Leelawat, N., Suppasri, A., Murao, O., Imamura, F., 2016. A Study on the Influential Factors on Building Damage in Sri Lanka During the 2004 Indian Ocean Tsunami, in: Journal of Earthquake and Tsunami. World Scientific Publishing Co. Pte Ltd. https://doi.org/10.1142/S1793431116400017

Leonardi, S., Orlandi, P., Antonia, R.A., 2007. Properties of d- and k-type roughness in a turbulent channel flow. Phys. Fluids 19, 125101. https://doi.org/10.1063/1.2821908

Leonardi, S., Orlandi, P., Smalley, R.J., Djenidi, L., Antonia, R.A., 2003. Direct numerical simulations of turbulent channel flow with transverse square bars on one wall. J. Fluid Mech. 229–238. https://doi.org/10.1017/S0022112003005500

Li, Y., Raichlen, F., 2001. Solitary wave runup on plane slopes. J. Waterw. Port, Coastal, Ocean Eng. 127, 33–44. https://doi.org/10.1061/(ASCE)0733-950X(2001)127:1(33)

Liu, P.L.F., Lynett, P., Fernando, H., Jaffe, B.E., Fritz, H., Higman, B., Morton, R., Goff, J., Synolakis, C., 2005. Observations by the International Tsunami Survey Team in Sri Lanka. Science (80-.). 308, 1595. https://doi.org/10.1126/science.1110730

Lo, H.Y., Park, Y.S., Liu, P.L.F., 2013. On the run-up and back-wash processes of single and double solitary waves - An experimental study. Coast. Eng. https://doi.org/10.1016/j.coastaleng.2013.05.001

Longuet-Higgins, M.S., Stewart, R.W., 1964. Radiation stresses in ~vater waves; with applications a physical discussion,. Deep Sea Res. 11, 529–562.

Longuet-Higgins, M.S., Stewart, R.W., 1962. Radiation stresses and mass transport in surface gravity waves with application to `surf beats'. J. Fluid Mech. 13, 481–504.

Lowe, R.J., 2005. Oscillatory flow through submerged canopies: 1. Velocity structure. J. Geophys. Res. 110, C10016. https://doi.org/10.1029/2004JC002788

Madsen, P.A., Fuhrman, D.R., Schäffer, H.A., 2008. On the solitary wave paradigm for tsunamis. J. Geophys. Res. Ocean. 113, C12012. https://doi.org/10.1029/2008JC004932

Madsen, P.A., Fuhrman, D.R., Schäffer, H.A., 2008. On the solitary wave paradigm for tsunamis. J. Geophys. Res. Ocean. 113, C12012. https://doi.org/10.1029/2008JC004932

Madsen, P.A., Schäffer, H.A., 2010. Analytical solutions for tsunami runup on a plane beach: Single waves, N-waves and transient waves. J. Fluid Mech. 645, 27–57. https://doi.org/10.1017/S0022112009992485

Martin, D., Bertasi, F., Colangelo, M.A., de Vries, M., Frost, M., Hawkins, S.J., Macpherson, E., Moschella, P.S., Satta, M.P., Thompson, R.C., Ceccherelli, V.U., 2005. Ecological impact of coastal defence structures on sediment and mobile fauna: Evaluating and forecasting consequences of unavoidable modifications of native habitats. Coast. Eng. 52, 1027–1051. https://doi.org/10.1016/j.coastaleng.2005.09.006

Mascarenhas, A., Jayakumar, S., 2008. An environmental perspective of the post-tsunami scenario along the coast of Tamil Nadu, India: Role of sand dunes and forests. J. Environ. Manage. 89, 24–34. https://doi.org/10.1016/j.jenvman.2007.01.053

Massel, S.R.R., Furukawa, K., Brinkman, R.M.M., 1999. Surface wave propagation in mangrove forests. Fluid Dyn. Res. 24, 219–249. https://doi.org/10.1016/S0169-5983(98)00024-0

Mayer, R.H., Kriebel, D.L., 1994. Wave Runup on Composite-Slope and Concave Beaches, in: Coastal Engineering 1994. American Society of Civil Engineers, New York, NY, pp. 2325–2339. https://doi.org/10.1061/9780784400890.169

Mazda, Y., Magi, M., Kogo, M., Phan Nguyen Hong, 1997. Mangroves as a coastal protection from waves in the Tong King Delta, Vietnam. Mangroves Salt Marshes 1, 127–135. https://doi.org/10.1023/A:1009928003700

McCowan, J., 1894. XXXIX. On the highest wave of permanent type. London, Edinburgh, Dublin Philos. Mag. J. Sci. 38, 351–358. https://doi.org/10.1080/14786449408620643

Mei, C.C., Chan, I.C., Liu, P.L.F., 2014. Waves of intermediate length through an array of vertical cylinders. Environ. Fluid Mech. 14, 235–261. https://doi.org/10.1007/s10652-013-9308-1

Mendez, F.J., Losada, I.J., 2004. An empirical model to estimate the propagation of random breaking and nonbreaking waves over vegetation fields. Coast. Eng. 51, 103–118. https://doi.org/10.1016/j.coastaleng.2003.11.003

Miura, H. Wijeyewickrema, A. C., Inoue, S. (2005): Evaluation of Tsunami Damage in the Eastern Part of Sri Lanka Due to the 2004 Sumatra Earthquake Using Remote Sensing Technique. 3rd International Workshop on Remote Sensing for Post-Disaster Response, 12-13 Sep. 2005, Chiba, Japan.

Mizoguchi, Y., Vinodh, T. L. C., Tanaka, N. ,2018, Concept for coastal lagoon categorization based on its function in disaster risk reduction, Proceedings of 12th International Conference on ISE, Tokyo, Japan

Monismith, S.G., 2007. Hydrodynamics of Coral Reefs. Annu. Rev. Fluid Mech. 39, 37–55. https://doi.org/10.1146/annurev.fluid.38.050304.092125

Mullarney, J.C., Henderson, S.M., 2018. Flows Within Marine Vegetation Canopies, in: Advances in Coastal Hydraulics. pp. 1–46. https://doi.org/10.1142/9789813231283_0001

Munk, W.H., 1949. The solitary wave theory and its application to surf problems. Ann. N. Y. Acad. Sci. 51, 376–424. https://doi.org/10.1111/j.1749-6632.1949.tb27281.x

Nakaza, E., Tsukayama, S., Hino, M., 1991. Bore-Like Surf Beat on Reef Coasts, in: Coastal Engineering 1990. American Society of Civil Engineers, New York, NY, pp. 743–756. https://doi.org/10.1061/9780872627765.059

National Geophysical Data Center / World Data Service: NCEI/WDS Global Historical Tsunami Database. NOAA National Centers for Environmental Information. doi:10.7289/V5PN93H7 [access date 2020.01.14]

Nelson, R.C., 1994. Depth limited design wave heights in very flat regions. Coast. Eng. 23, 43–59. https://doi.org/10.1016/0378-3839(94)90014-0

Nepf, H.M., 2012. Hydrodynamics of vegetated channels. J. Hydraul. Res. 50, 262–279. https://doi.org/10.1080/00221686.2012.696559

Nunes, V., Pawlak, G., 2008. Observations of Bed Roughness of a Coral Reef. J. Coast. Res. 2, 39–50. https://doi.org/10.2112/05-0616.1

Nwogu, O., Demirbilek, Z., 2010. Infragravity Wave Motions and Runup over Shallow Fringing Reefs. J. Waterw. Port, Coastal, Ocean Eng. 136, 295–305.

https://doi.org/10.1061/(asce)ww.1943-5460.0000050

Park, H., Cox, D.T., Petroff, C.M., 2015. An empirical solution for tsunami run-up on compound slopes. Nat. Hazards 76, 1727–1743. https://doi.org/10.1007/s11069-014-1568-7

Pedersen, G., Gjevik, B., 1983. Run-up of solitary waves. J. Fluid Mech. 135, 283–299. https://doi.org/10.1017/S0022112083003080

Pedersen, G.K., Lindstrøm, E., Bertelsen, A.F., Jensen, A., Laskovski, D., Sælevik, G., 2013. Runup and boundary layers on sloping beaches. Phys. Fluids 25, 012102. https://doi.org/10.1063/1.4773327

Peiris, N., Pomonis, A., 2005. December 26, 2004 Indian Ocean Tsunami: vulnerability functions for loss estimation in Sri Lanka. World Scientific Pub Co Pte Lt, pp. 411–416. https://doi.org/10.1142/9789812701602_0045

Pelinovsky, E.N., Mazova, R.K., 1992. Exact analytical solutions of nonlinear problems of tsunami wave run-up on slopes with different profiles. Nat. Hazards 6, 227–249. https://doi.org/10.1007/BF00129510

Peregrine, D.H., 1983. Breaking Waves on Beaches. Annu. Rev. Fluid Mech. 15, 149–178. https://doi.org/10.1146/annurev.fl.15.010183.001053

Perry, A.E., Schofield, W.H., Joubert, P.N., 1969. Rough wall turbulent boundary layers. J. Fluid Mech. 37, 383–413. https://doi.org/10.1017/S0022112069000619

Pomeroy, A., Lowe, R., Symonds, G., Van Dongeren, A., Moore, C., 2012. The dynamics of infragravity wave transformation over a fringing reef. J. Geophys. Res. Ocean. 117. https://doi.org/10.1029/2012JC008310

Pomonis, A., Rossetto, T., Peiris, N., Wilkinson, S., Del Re, D., Koo, R., Manlapig, K.R., Gallocher, S., 2006. The Indian Ocean Tsunami of 26 December 2004: Mission Findings in Sri Lanka and Thailand.

Pujara, N., Liu, P.L.F., Yeh, H., 2015. The swash of solitary waves on a plane beach: Flow evolution, bed shear stress and run-up. J. Fluid Mech. 779, 556–597. https://doi.org/10.1017/jfm.2015.435

Quiroga, P.D., Cheung, K.F., 2013. Laboratory study of solitary-wave transformation over bed-form roughness on fringing reefs. Coast. Eng. 80, 35–48. https://doi.org/10.1016/j.coastaleng.2013.05.002

Rabinovich, A.B., Thomson, R.E., 2007. The 26 December 2004 Sumatra Tsunami: Analysis of tide gauge data from the World Ocean Part 1. Indian ocean and South Africa, in: Pure and Applied Geophysics. Springer, pp. 261–308. https://doi.org/10.1007/s00024-006-0164-5

Raby, A., Macabuag, J., Pomonis, A., Wilkinson, S., Rossetto, T., 2015. Implications of the 2011 Great East Japan Tsunami on sea defence design. Int. J. Disaster Risk Reduct. 14, 332–346. https://doi.org/10.1016/j.ijdrr.2015.08.009

Raupach, M.R., 1992. Drag and drag partition on rough surfaces. Boundary-Layer Meteorol. 60, 375–395. https://doi.org/10.1007/BF00155203

Renaud, F.G., Sudmeier-Rieux, K., Estrella, M., 2013. The role of ecosystems in disaster risk reduction. United Nations University Press.

Robertson, B., Hall, K., Zytner, R., Nistor, I., 2013. Breaking Waves: Review of Characteristic Relationships. Coast. Eng. J. 55, 1350002. https://doi.org/10.1142/S0578563413500022

Roeber, V., Yamazaki, Y., Cheung, K.F., 2010. Resonance and impact of the 2009 Samoa

tsunami around Tutuila, American Samoa. Geophys. Res. Lett. 37, n/a-n/a. https://doi.org/10.1029/2010GL044419

Rossetto, T., Peiris, N., Pomonis, A., Wilkinson, S.M., Del Re, D., Koo, R., Gallocher, S., 2007. The Indian Ocean tsunami of December 26, 2004: Observations in Sri Lanka and Thailand. Nat. Hazards 42, 105–124. https://doi.org/10.1007/s11069-006-9064-3

Saeki, H., Hanayasu, S., Ozaki, A., Takagi, K., 1971. The Shoaling and Run-Up Height of the Solitary Wave. Coast. Eng. Japan 14, 25–42. https://doi.org/10.1080/05785634.1971.11924124

Sælevik, G., Jensen, A., Pedersen, G., 2013. Runup of solitary waves on a straight and a composite beach. Coast. Eng. 77, 40–48. https://doi.org/10.1016/J.COASTALENG.2013.02.007

Samarakoon, M.B., Tanaka, N., Iimura, K., 2013. Improvement of effectiveness of existing Casuarina equisetifolia forests in mitigating tsunami damage. J. Environ. Manage. 114, 105–114. https://doi.org/10.1016/j.jenvman.2012.10.050

Satyanarayana, B., Van der Stocken, T., Rans, G., Kodikara, K.A.S., Ronsmans, G., Jayatissa, L.P., Husain, M.L., Koedam, N., Dahdouh-Guebas, F., 2017. Island-wide coastal vulnerability assessment of Sri Lanka reveals that sand dunes, planted trees and natural vegetation may play a role as potential barriers against ocean surges. Glob. Ecol. Conserv. 12, 144–157. https://doi.org/10.1016/j.gecco.2017.10.001

Shuto, N., 2019. Tsunami hazard mitigation. Proc. Japan Acad. Ser. B 95, 151–164. https://doi.org/10.2183/pjab.95.012

Shuto, N., 1987. The Effectiveness and Limit of Tsunami Control Forests. Coast. Eng. Japan 30, 143–153. https://doi.org/10.1080/05785634.1987.11924470

Shuto, N., 1967. Run-Up of Long Waves on a Sloping Beach. Coast. Eng. Japan 10, 23–38. https://doi.org/10.1080/05785634.1967.11924053

Silva, E. I. L., Katupotha, J., Amarasinghe, O., Manthrithilake, Herath, Ariyaratne, Ranjith, 2013. Lagoons of Sri Lanka: from the origins to the present. IWMI Books, Reports H046256, International Water Management Institute.

Smith, L., Jensen, A., Pedersen, G., 2017. Investigation of breaking and non-breaking solitary waves and measurements of swash zone dynamics on a 5° beach. Coast. Eng. 120, 38-46. https://doi.org/10.1016/j.coastaleng.2016.11.004

Sriram, V., Didenkulova, I., Sergeeva, A., Schimmels, S., 2016. Tsunami evolution and run-up in a large scale experimental facility. Coast. Eng. 111, 1–12. https://doi.org/10.1016/j.coastaleng.2015.11.006

Stockdon, H.F., Holman, R.A., Howd, P.A., Sallenger, A.H., 2006. Empirical parameterization of setup, swash, and runup. Coast. Eng. 53, 573–588. https://doi.org/10.1016/j.coastaleng.2005.12.005

Stoesser, T., Kim, S.J., Diplas, P., 2010. Turbulent Flow through Idealized Emergent Vegetation. J. Hydraul. Eng. 136, 1003–1017. https://doi.org/10.1061/(ASCE)HY.1943-7900.0000153

Strusínska-Correia, A., Husrin, S., Oumeraci, H., 2013. Tsunami damping by mangrove forest: A laboratory study using parameterized trees. Nat. Hazards Earth Syst. Sci. 13, 483–503. https://doi.org/10.5194/nhess-13-483-2013

Sumer, B.M., Jensen, P.M., Sørensen, L.B., Fredsøe, J., Liu, P.L.F., Carstensen, S., 2010. Coherent structures in wave boundary layers. Part 2. Solitary motion. J. Fluid Mech. 646,

207–231. https://doi.org/10.1017/S0022112009992837

Suppasri, A., Shuto, N., Imamura, F., Koshimura, S., Mas, E., Yalciner, A.C., 2013. Lessons Learned from the 2011 Great East Japan Tsunami: Performance of Tsunami Countermeasures, Coastal Buildings, and Tsunami Evacuation in Japan. Pure Appl. Geophys. 170, 993–1018. https://doi.org/10.1007/s00024-012-0511-7

Synolakis, C.E., 1988. Are solitary waves the limiting waves in long wave runup? Coast. Eng. 219–233.

Synolakis, C.E., 1987. The runup of solitary waves. J. Fluid Mech. 185, 523–545. https://doi.org/10.1017/S002211208700329X

Synolakis, C.E., Okal, E., Bernard, E., Synolakis C. Okal, E.B.E., 2005. The Megatsunami of December 26 , 2004. Natl. Acad. Eng. Publ. 35, 26–35.

Tait, R.J., 1972. Wave set-up on coral reefs. J. Geophys. Res. 77, 2207–2211. https://doi.org/10.1029/jc077i012p02207

Takayama, T., Kamiyama, Y., Kikuchi, O., 1977. Wave Transformation on a Reef, Technical Note of the Port and Harbour Research Institute, Ministry of Transport, Japan, 278, 32p. (in Japanese).

Tanaka, N., 2009. Vegetation bioshields for tsunami mitigation: Review of effectiveness, limitations, construction, and sustainable management. Landsc. Ecol. Eng. https://doi.org/10.1007/s11355-008-0058-z

Tanaka, N., Jinadasa, K.B.S.N., Mowjood, M.I.M., Fasly, M.S.M., 2011. Coastal vegetation planting projects for tsunami disaster mitigation: Effectiveness evaluation of new establishments. Landsc. Ecol. Eng. 7, 127–135. https://doi.org/10.1007/s11355-010-0122-3

Tanaka, N., Nandasena, N.A.K., Jinadasa, K.B.S.N., Sasaki, Y., Tanimoto, K., Mowjood, M.I.M., 2009. Developing effective vegetation bioshield for tsunami protection. Civ. Eng. Environ. Syst. https://doi.org/10.1080/10286600802435850

Tanaka, N., Sasaki, Y., Mowjood, M.I.M., Jinadasa, K.B.S.N., Homchuen, S., 2007. Coastal vegetation structures and their functions in tsunami protection: Experience of the recent Indian Ocean tsunami. Landsc. Ecol. Eng. 3, 33–45. https://doi.org/10.1007/s11355-006-0013-9

Tanaka, N., Sasaki, Y., Mowjood, M.I.M.M., 2007. Effects of sand dune and vegetation in the coastal area of Sri Lanka at the Indian Ocean Tsunami, in: Advances in Geosciences. World Scientific Publishing Co., pp. 149–159. https://doi.org/10.1142/9789812708915_0015

Tanaka, N., Sato, H., Igarashi, Y., Kimiwada, Y., Torita, H., 2018. Effective tree distribution and stand structures in a forest for tsunami mitigation considering the different tree-breaking patterns of tree species. J. Environ. Manage. 223, 925–935. https://doi.org/10.1016/j.jenvman.2018.07.006

Tanaka, N., Yagisawa, J., Yasuda, S., 2013. Breaking pattern and critical breaking condition of Japanese pine trees on coastal sand dunes in huge tsunami caused by Great East Japan Earthquake. Nat. Hazards. https://doi.org/10.1007/s11069-012-0373-4

Tanino, Y., Nepf, H.M., 2008. Laboratory Investigation of Mean Drag in a Random Array of Rigid, Emergent Cylinders. J. Hydraul. Eng. 134, 34–41. https://doi.org/10.1061/(asce)0733-9429(2008)134:1(34)

Temmerman, S., Meire, P., Bouma, T.J., Herman, P.M.J., Ysebaert, T., De Vriend, H.J., 2013. Ecosystem-based coastal defence in the face of global change. Nature.

https://doi.org/10.1038/nature12859

Thuy, N.B., Tanimoto, K., Tanaka, N., Harada, K., Iimura, K., 2009. Effect of open gap in coastal forest on tsunami run-up-investigations by experiment and numerical simulation. Ocean Eng. 36, 1258–1269. https://doi.org/10.1016/j.oceaneng.2009.07.006

Vinodh, T.L.C., Tanaka, N., 2020. A unified runup formula for solitary waves on a plane beach. Ocean Eng. 216, 108038. https://doi.org/10.1016/j.oceaneng.2020.108038

Vinodh, T. L. C., Tanaka, N., 2019, Review of existing coastal defence system in Sri Lanka against tsunami, Proceedings of the special session on Coastal and Lagoon Environment, 7th ACEPS2019, 84-91, 17th October 2019, Galle, Sri Lanka.

Vinodh, T.L.C., Tanaka, N., Takemura, T., 2019, Experimental study of runup reduction of solitary wave by emergent rigid vegetation on a slope, Journal of JSCE, Ser. B1 (Hydraulic Engineering), 75, 2, I_703-I_708.

Vinodh, T.L.C., Tanaka, N., 2018a, Experimental study on the energy reduction of a solitary wave using a sand dune-coastal lagoon system, Journal of JSCE, Ser. B1 (Hydraulic Engineering), 74, 5, I_1231-I_1236. https://doi.org/10.2208/jscejhe.74.5_I_1231

Vinodh, T.L.C., Tanaka, N., 2018b, Experimental study on the energy reduction of a solitary wave using a sand dune-coastal lagoon system, Proceedings of 12th International Conference on ISE, Tokyo, Japan

Vinodh, T.L.C., Tanaka, N., 2018c, Experimental study on the energy reduction of a solitary wave using a sand dune-coastal lagoon system, Proceedings of 9th International Conference on ICSBE, 466, 111- 119

Wijetunge, J.J., 2014. A deterministic analysis of tsunami hazard and risk for the southwest coast of Sri Lanka. Cont. Shelf Res. 79, 23–35. https://doi.org/10.1016/j.csr.2013.09.009

Wijetunge, J.J., 2009a. Field measurements and numerical simulations of the 2004 tsunami impact on the south coast of Sri Lanka. Ocean Eng. 36, 960–973. https://doi.org/10.1016/j.oceaneng.2009.06.002

Wijetunge, J.J., 2009b. Field measurements and numerical simulations of the 2004 tsunami impact on the east coast of Sri Lanka. Pure Appl. Geophys. 166, 593–622. https://doi.org/10.1007/s00024-009-0458-5

Wijetunge, J.J., 2006. Tsunami on 26 December 2004: Spatial Distribution of Tsunami Height and the Extent of Inundation in Sri Lanka. Sci. Tsunami Hazards 24, 225–239.

Willmott, C.J., 1981. On the validation of models. Phys. Geogr. 2, 184–194. https://doi.org/10.1080/02723646.1981.10642213

Wu, Y.-T., Liu, P.L.-F., Hwang, K.-S., Hwung, H.-H., 2018. Runup of Laboratory-Generated Breaking Solitary and Periodic Waves on a Uniform Slope. J. Waterw. Port, Coastal, Ocean Eng. 144, 04018023. https://doi.org/10.1061/(ASCE)WW.1943-5460.0000476

Yanagisawa, H., Koshimura, S., Goto, K., Miyagi, T., Imamura, F., Ruangrassamee, A., Tanavud, C., 2009. The reduction effects of mangrove forest on a tsunami based on field surveys at Pakarang Cape, Thailand and numerical analysis. Estuar. Coast. Shelf Sci. 81, 27–37. https://doi.org/10.1016/j.ecss.2008.10.001

Yang, Y., Irish, J.L., Weiss, R., 2017. Impact of Patchy Vegetation on Tsunami Dynamics. J. Waterw. Port, Coastal, Ocean Eng. https://doi.org/10.1061/(asce)ww.1943-5460.0000380

Yao, Y., Du, R., Jiang, C., Tang, Z., Yuan, W., 2015. Experimental Study of Reduction of

Solitary Wave Run-Up by Emergent Rigid Vegetation on a Beach. J. Earthq. Tsunami. https://doi.org/10.1142/S1793431115400035

Yao, Y., He, F., Tang, Z., Liu, Z., 2018. A study of tsunami-like solitary wave transformation and run-up over fringing reefs. Ocean Eng. 149, 142–155. https://doi.org/10.1016/j.oceaneng.2017.12.020

Yasuda, T., Ueyama, H., Mase, H., 2020. Empirical Estimation of Wave Height Over Reef Based on Boussinesq Wave Model, in: APAC 2019. Springer Singapore, pp. 175–181. https://doi.org/10.1007/978-981-15-0291-0_25

Zaha, T., Tanaka, N., Kimiwada, Y., 2019. Flume experiments on optimal arrangement of hybrid defense system comprising an embankment, moat, and emergent vegetation to mitigate inundating tsunami current. Ocean Eng. 173, 45–57. https://doi.org/10.1016/j.oceaneng.2018.12.054

Zhu, L., Chen, Q., 2017. Attenuation of Nonlinear Waves by Rigid Vegetation: Comparison of Different Wave Theories. J. Waterw. Port, Coastal, Ocean Eng. 143, 04017029. https://doi.org/10.1061/(asce)ww.1943-5460.0000415